Histone Post-translational Modifications in the Brain of the Senescence-accelerated Prone 8 Mouse

WANG, Chunmei

A Thesis Submitted in Partial Fulfillment of

the Requirements for the Degree of

Doctor of Philosophy

in

Biology

The Chinese University of Hong Kong

August 2009

ProQuest LLC.
789 East Eisenhower Parkway
P.O. Box 1346
Ann Arbor, MI 48106 - 1346

Thesis committee:

Supervisor: Professor NGAI Sai Ming

(Department of Biology, the Chinese University of Hong Kong)

Internal examiner: Professor FUNG Ming Chiu

(Department of Biology, the Chinese University of Hong Kong)

Internal examiner: Professor GE Wei

(Department of Biology, the Chinese University of Hong Kong)

External examiner: Professor ZHU Guang

(Department of Biochemistry, the Hong Kong University of Science & Technology)

Declaration

I, Wang Chun Mei, declare that this thesis represents my own work, except where due acknowledgement is made and that it has not been previously included in a thesis, dissertation or report submitted to this university or to any other institution for degree, diploma or other qualifications.

Signed _____

WANG CHUN MEI

Abstract of thesis entitled:

Histone Post-translational Modifications in the Brain of the Senescence-accelerated Prone 8 Mouse

Submitted by WANG Chun Mei

for the degree of Doctor of Philosophy

at the Chinese University of Hong Kong in August 2009

Nowadays, many countries including China are experiencing aging populations. Aging has become the major risk factor for many diseases, such as neurodegenerative disease. The studies on the role of epigenetics in the aging process have grown tremendously in recent years. However, no systematic investigations have provided the information on histone post-translational modifications (PTMs) in aged brain and the roles of histone PTMs in brain aging are still unknown.

In this study, the brain of senescence accelerated mouse prone 8 (SAMP8) mice model was adopted to investigate PTMs state (especially methylation patterns) of core histones (H2A, H2B, H3 and H4). Seven methylated sites (H3K24, H3K27, H3K36, H3K79, H3R128, H4K20 and H2A R89) were detected by tandem matrix-assisted laser desorption/ionization time-of-flight mass spectrometry (MALDI-TOF/TOF MS) analysis. The methylation of H3K27 and H3K36 demonstrated a modulating relationship and methylated H3K27 might contribute to the hypermethylation state and gene repression in aged brain. Western blotting results showed that mono-methylated H4K20 decreased during SAMP8 mice aging

and di-methylated H3K79 decreased in the brain of 12-month-old SAMP8 mice compared with age-matched senescence accelerated-resistant mouse (SAMR1) control. Di-methylated H3K79 could express in neuron cells of cerebral cortex and hippocampus. Whereas, the number of H3K79 methylation negative cells was higher in the cortex of 12-month old SAMP8 mice than that of age-matched control SAMR1 mice. Chromatin immunoprecipitation (ChIP) result indicated homeodomain transcription factor Pbx1 isoform 1 (Pbx1), transcription factors and transcriptional regulator proteins, such as T-box isoform 20, TetR family precursor BAZ2B and ribosomal protein, were recruited to methylated H3K79 site. Therefore, a model of methylated H3K79 on gene transcriptional regulation was proposed. Furthermore, the consequences of decreased H3K79 methylation in Neuro-2a (N2a) cells were investigated via transfection with *Dot1* (**d**isruptor **o**f **t**elomeric silencing) siRNA. After transfection, N2a cells displayed shorter neurite and less dendrite. Proteomic change in the N2a cells provided convincing evidence for the multi-function of decreased H3K79 methylation on transcriptional regulation, protein translation and folding, stress response and DNA breaks repair, which would contribute to brain dysfunction during neurodegenerative disease or aging.

This study gave a new insight into the link between histone PTMs and brain aging. It could provide the experimental evidence for future studies and help us to better understand aging or neurodegenerative disease at epigenetic level. Furthermore, it could benefit for setting up the strategies for epigenetic therapy to neurodegenerative disease.

摘要

現在，包括中國在內的許多國家都面臨著人口老齡化的問題。衰老已經成為許多疾病的主要危險因素，例如神經衰退性疾病。近年來，表觀遺傳學在衰老過程中的研究增長迅速。可是，目前並沒有衰老過程中腦組織組蛋白轉錄後修飾的系統性研究，而且組蛋白轉錄後修飾在腦衰老過程中的機理也不清楚。

本研究，採用快速衰老亞系 8 小鼠(SAMP8)作為研究對象，對其腦組織中的核心組蛋白轉錄後的修飾（主要是甲基化修飾）進行了研究。運用基質輔助雷射解吸附飛行時間質譜（MALDI TOF/TOF MS），在 12 月大小的 SAMP8 小鼠腦中發現了 7 個甲基化位點，它們分別是位於組蛋白 H3 上的第 24, 27, 36 和 79 位的賴氨酸，第 128 位的精氨酸，位於組蛋白 H4 上的第 20 位的賴氨酸和位於組蛋白 H2A 上的第 89 位的精氨酸。其中，位於組蛋白 H3 上的第 27 和 36 位的賴氨酸的甲基化呈現相互調節現象。組蛋白 H3 上第 27 賴氨酸的甲基化可能會造成衰老腦組織中組蛋白高度甲基化狀態進而抑制基因的表達。蛋白免疫印跡實驗結果顯示，組蛋白 H4 第 20 位的賴氨酸的單（mono-）甲基化程度在快速衰老亞系 8 老鼠的衰老進程中顯著減少；組蛋白 H3 第 79 位的賴氨酸雙（di-）甲基化的程度低於同年齡的抗快速衰老亞系 1（SAMR1）小鼠。免疫組化結果顯示大部分組蛋白 H3 第 79 位的賴氨酸雙（di-）甲基化的陽性信號分佈在大腦皮層和海馬的神經細胞內。但是在快速衰老亞系 8 老鼠大腦皮層的其陽性細胞數目要少於抗快速衰老亞系 1 的對照小鼠。染色體免疫共沉澱結果顯示 Pbx1，轉錄因子和轉錄調節蛋白可以集聚到甲基化的組蛋白 H3 第 79 位賴氨酸附近。根據這一結果，本研究建立了一個組蛋白 H3 第 79 位的賴氨酸甲基化如

何調節基因轉錄表達的模型。本實驗還通過運用 RNA 干預技術抑制小鼠腦神經瘤細胞（Neuro-2a）中 *Dot1* 基因的表達，降低細胞中組蛋白 H3 第 79 位的賴氨酸甲基化程度，並對這種變化為神經細胞帶來的影響進行了深入地研究。小鼠腦神經瘤細胞在轉染後細胞形態發生變化，細胞的軸突變短，樹突變少。蛋白質組學的研究結果顯示組蛋白 H3 第 79 位的賴氨酸甲基化程度的降低可以影響細胞基因的轉錄表達，蛋白質的翻譯和折疊，脅迫反應和去氧核糖核酸的斷裂修復，而這些變化可以引起神經衰退性疾病或衰老過程中腦組織的功能失調。

本實驗對組蛋白轉錄後的修飾與腦組織衰老的關係提供了新的見解。它不但為以後的研究提供了實驗依據，使我們在表觀遺傳表達水平上對衰老和神經衰退性疾病有了更深入的瞭解，並可為最終制定治療措施做出貢獻。

Acknowledgements

For me, the four-year Ph.D study was the most arduous but enjoyable time in my life. Without even one of the following people, this thesis would not be completed. Here, I would like to express my sincere gratitude to them.

First of all, I must heartfelt thank to Prof. NGAI Sai Ming, my supervisor, for his patient guidance, encouragement and support for my project. He provides me the opportunity to do research in histone post translational modifications. During the period of fulfilling this project, it was so great to learn the new and advanced techniques on molecular biotechnology, bioinformatics and proteomics from him, and I appreciated the opportunity to work on MALDI-TOF/TOF mass spectrometer, HPLC, peptide synthesizer, and so on in his lab. During my Ph.D study, Prof. Ngai not only gave me a good training in the techniques, but also taught me the way of learning and thinking independently, which are very important for a scientific researcher. So I am indebted to Prof. NGAI, not only for his patient guidance and continuous encouragement throughout my study, but also for his invaluable suggestions and critical comments on the preparation of this thesis.

I am obliged to Prof. FUNG Ming Chiu and Prof. GE Wei for their guidance and invaluable suggestions and appraisal for the improvement of my project. I also would like to express my faithful gratitude to Professor ZHU Guang in the department of Biochemistry, The Hong Kong University of Science & Technology, my external examiner, for his constructive suggestions and comments on my studies and this thesis.

I would like to thank Prof YEW Tai Wei in department of Anatomy, for providing me the animal model. Without this animal model, my studies cannot be carried out on time. And I also thank the staff in his lab for the preparing brain samples.

I appreciated the valuable generous assistance and technical support for Ms TSAI Sau Na Helen, Mr LAU Kwok Wing Wilson, Mr KWOK Wai Kwan Freddie and Mr TANG Cho On Thomas, technicians in biology department; Mrs Yeung Yeo Geok Yen, technician in MBT. Thanks are also given to every current and past labmates in EG08 laboratories (Zhong Mingqi, Ester, Jason, Karen, Xiaoyu, Shao Jianlin and Wu tao) and my friends in the department of biology for their friendliness, supports and sharing the moments of being working together.

Last but not the least, I am deeply grateful to my family for their eternal love, understanding, care, and support.

Table of contents

General abbreviations

2DE	Two-dimensional gel electrophoresis
AD	Alzheimer's disease
APP	Amyloid precursor protein
BAZ2B	Bromodomain adjacent to zinc finger domain 2b
BLAST	Basic local alignment search tool
bp	Base pair
cDNA	Complementary DNA
ChIP	Chromatin immunoprecipitation
CID	Collision induced dissociation
cm	Centimeter
Da	Dalton
DNA	Deoxyribonucleic acid
dNTP	Deoxyribonucleoside triphosphate
Dot1	Disruptor of telomeric silencing
DSB	Double strand break
eIFs	Eukaryotic translation initiation factors
ES	Embryonic stem
FBP-1	Far upstream element binding protein 1
FTMS	Fourier transform mass spectrometry
g	Microgram
HAT	Histone acetyltransferase
HDAC	Histone deacetylase
ICAT	Isotope coded affinity tag
IEF	Isoelectric focusing
IPG	Immobilized pH gradient
iTRAQ	Multiplexed isobaric tagging technology
K	Lysine

LC	Liquid chromatography
MALDI	Matrix assisted laser desorption ionization
mg	Milligram
MH^+	Monoisotopic peptide mass
ml	Milliliter
MLL1	Mixed lineage leukemia 1
mm	Millimeter
mM	Millimole
MS	Mass spectrometry
MS/MS	Tandem mass spectrometry
MW	Molecular weight
N2a	Neuro-2a
NAC	Nascent polypeptide-associated complex
NAP1L1	Nucleosome assembly protein 1-like 1
NAP1L2	Nucleosome assembly protein 1-like 2
NER	Nucleotide excision repair
OD	Optical density
PCNA	Proliferating cell nuclear antigen
PCR	Polymerase chain reaction
PKA	Protein kinase
PMF	Peptide mass finger printing
PR-HPLC	Reversed-phase high performance liquid chromatography
PTM	Post translational modification
R	Arginine
ROS	Reactive oxygen species
RT-PCR	Reverse transcriptase PCR
S	Serine
S/N	Signal to noise
SAM	Senescence accelerated mouse

SAMP8	Senescence accelerated mouse prone 8
SAMR1	Senescence accelerated resistant mouse 1
SDS-PAGE	Sodium dodecyl sulfate polyacrylamide gel electrophoresis
SET	Suppressor of variegation, enhancer of zeste and trithorax
siRNA	Small interfering RNA
SOD	Superoxide dismutase
SS	Shear stress
T	Threonine
Tbx20	T-box isoform 20
TOF	Time-of-flight
UV	Ultraviolet
v	Volume
V	Voltage
Vh	Voltage hour
µl	Microliter
µM	Micromole

Abbreviations of chemicals

ACN	Acetonitrile
BSA	Bovine serum albumin
CHAPS	3-[(3-cholamidopropyl)dimethylammonio]-1-propanesulfonate
DAB	3, 3'-Diaminobenzidine
DMEM	Dulbecco's modified eagle medium
DMSO	Dimethyl sulfoxide
dNTP	Deoxyribonucleoside triphosphate
DTT	Dithiothreitol
FBS	Fetal bovine serum
H_2SO_4	Sulfuric acid
HE	Hematoxylin and Eosin
$K_3Fe(CN)_6$	Potassium ferricyanide
MTT	3-(4,5-Dimethylthiazol-2-yl)-2,5-diphenyltetrazolium bromide
Na_2CO_3	Sodium carbonate
$Na_2S_2O_3$	Sodium thiosulfate
$NaHSO_3$	Sodium bisulfite
NH_4HCO_3	Ammonium bicarbonate
PBS	Phosphate buffered saline
PFA	Paraformaldehyde
PMSF	Phenylmethylsulfonyl fluoride
PMSF	Phenylmethylsulfonyl fluoride
SOD	Superoxide dismutase
TCA	Trichloroacetic acid
TFA	Trifluoroacetic acid

List of tables

List of figures

Chapter 1 Literature Review

1.1 Histone

1.1.1 Introduction

Histones are a group of small, water-soluble proteins and contain large amounts of basic amino acids, particularly lysine (K) and arginine (R). They were firstly discovered in the nucleus of avian red blood cells in 1884 by Albrecht Kossel, a German physiologist (Kossel, 1929). The word "histone" came from the German "Histon" which means "of unknown origin". Histones are the chief protein components of chromatin in the nuclei of eukaryotic cells and certain Archaea, but not in bacteria. In mammals, they are abundant in the thymus and pancreas. Before the early 1990s, histones were usually dismissed as merely packing material for nuclear DNA. During the early 1990s, the regulatory functions of histones were discovered (Grunstein, 1992).

1.1.2 Classes

There exist five major classes of histone: linker H1 (H5), H2A, H2B, H3 and H4. Among these histones, H2A, H2B, H3 and H4 are called core histones. Each two of them assemble to form an octamer, which outside is wrapped by 147 base pairs of DNA to form the basic repeating units of chromatin in eukaryotes-nucleosome

(Luger, 1997). Histone H1 was the linker histone that could bind the nucleosome and lock the DNA into place to form higher order structure (Daniel and Farkas, 1996). Histone H5 performed the same function as histone H1, and replaced H1 in certain cells (Ramakrishnan *et al*., 1993). Molecular weight, the number of amino acids and basic amino acids of histone proteins were summarized in Table 1.1.

Table 1.1 Summary of histone proteins

Type	M.W.(KDa)	Number of amino acids	Approx. content of basic amino acids
H1/H	17-28	200-265	27% lysine, 2% arginine
H2A	13.9	129-155	11% lysine, 9% arginine
H2B	13.8	121-148	16% lysine, 6% arginine
H3	15.3	135	10% lysine, 15% arginine
H4	11.3	102	11% lysine, 4% arginine

1.1.3 Structure

All the core histones are highly conserved through evolution. They are relatively similar in a 'helix-turn-helix-turn-helix' motif structure, which allows positively charged amino acids of histone to bind tightly to the negative charges of DNA. Each of core histones has a relevant globular domain and a flexible N-terminal tail. The globular domain mediates histone–histone interactions within the octamer. The 20-35

residue N-terminal tails can protrude from the nucleosome octamer. Besides N-terminal tails, histone H2A also has an additional ~37 amino acid carboxy-terminal domain that protrudes from the nucleosome. These histone 'tails' did not contribute significantly to the structure of individual nucleosomes nor to their stability, but they play an essential role in controlling the folding of nucleosomal arrays into higher order structures and were subjected to the post translational modifications (PTMs) (Peterson and Laniel, 2004).

1.1.4 Histone variant

The existence of primary structure variants of the nucleosomal histones had long been known (Patthy and Smith, 1973; Patthy and Smith, 1975). Histone variants were nonallelic isoforms of the major histones. They had their own unique feature which was different from others in same class whereas histones in same class had similar amino acid sequence homology and core structure (Pusarla and Bhargava, 2005). The "bulk" histones were encoded by genes belonging to multicopy, intronless families that were transcribed into non-polyadenylated mRNA, while histone variants were encoded by genes located outside the canonical histone gene cluster, mostly in single copies and with introns. They were constitutively expressed into polyadenylated mRNA (Pusarla and Bhargava, 2005). The different histone variants might specifically interact with high mobility group proteins to form potentially transcribable chromatin structures, or histone variants might differ in the

strength of the histone-histone interactions which they were involved in and affect nucleosome stability and unfolding and could potentially regulate various nuclear functions such as transcription, gene silencing, chromosome segregation, replication, repair and recombination.

H2A is one kind of histones with the largest number of variants and is differentiated by their C-terminal sequence and genome localization (Mariño-Ramírez *et al.*, 2005). Its variants included H2AZ and H2AX, which were found in most eukaryotes, as well as H2A.Bbd and MacroH2A, which were only found in vertebrates. High levels of macroH2A, a variant of H2A were contained in mammalian inactive X-chromosomes (Chadwick and Willard, 2002). Compared with normal H2A, macroH2A was almost three times larger. H2AZ could replace major H2A and reduce the stability of nucleosome. Histone variant H2AX was found more abundant and played important role in DNA breakage repair as well as V(D)J recombination which benefit for the diversity of immunoglobulin (Redon *et al.*, 2002). Moreover, H2AX was found to involve in the mediation of cell cycle checkpoint (Kastan and Bartek, 2004).

Histone H2B was markedly deficient in variants. The sperm-specific H2B in sea urchins had a long N-terminal tail that is highly charged, which was different from the major H2B subtypes (Strickland *et al.*, 1977). H2B variants had specialized biological functions in chromatin compaction and transcription repression, particularly during gametogenes (Poccia and Green, 1992).

Histone H3 variants included H3.3, centromeric H3 (CenH3) (Ahmad and

Henikoff, 2002a; Malik and Henikoff, 2003) and a mammalian testis-specific H3 variant-H3.4 (Witt *et al.*, 1996). H3.3 was expressed throughout the cell cycle and often localized in transcriptionally active regions of the chromosome (Ahmad and Henikoff, 2002b). CenH3 was a conserved essential centromeres binding protein, and mediated the chromosome segregation in eukaryotes (Orthaus *et al.*, 2008).

Histone H4 is one of the slowest evolving proteins, and there appears to be no known sequence variants of histone H4. H4 genes were constitutively expressed throughout the cell cycle and encoded proteins that were identical in sequence to the major H4 (Akhmanova *et al.*, 1996). The reason for a lack of sequence variants is not clear.

1.2 Histone post-translational modifications (PTMs)

Post-translational modification is the modification of a protein after its translation which is the later steps in protein biosynthesis. Proteins could be modified by attaching other biochemical molecules such as acetate group, methyl group phosphate group. It is also could be modified by changing one amino acid to another amino acid even by change the structure of amino acid such as the disulfide bridge's formation between amino acids. The modification of proteins could extend their functions in different biology process.

1.2.1 Histone PTMs types and sites

Histone protein is an important case of PTMs. The study of histone PTMs began in 1964 with the identification of ε-metyllysine in acid hydrolysates of calf thymus histones by Murray (Murray, 1964). Later, the report of the modifications in the core histones was extended to include phoshorylation (Keinsmith *et al.*, 1966; Ord and stocken, 1967), acetylation (Gershey *et al.*, 1968; Vidali *et al.*, 1968), ADP-ribosylation (Ueda *et al.*, 1975), Carbonylation, deimination (Hagiwara *et al.*, 2002), ubiquitylation (Shiio and Eisenman, 2003) and proline isomerization (Nelson, 2006). The overview of different classes of modification identified on histones was listed on the table 1.2.

Now, there are at least eight different classes of covalent modifications involving more than 60 distinct modification sites within the major core histones characterized to date, and most PTMs sites are found primarily on the residues of the core histones whose N-terminal tails protrude from the nucleosome. Nevertheless, some PTMs could be found in their globular domains, such as methylation on the hisotne H3 lysine 79 (H3K79) (Fig 1.1). Studies in yeast and mammals have identified conserved modifications at defined amino acid residues of histones as well as non-conserved modifications at some other sites. For example, acetylated H4K5, H4K8, H4K12 and H4K16 were commonly detected in humans, fly and yeast. Acetylated H3K9 and H3K27 could only be found be in budding yeast whereas their methylated form only be detected in chicken erythrocytes (Marvin *et al.*, 1990; Zhang *et al.*, 2002; Kurdistani *et al.*, 2004).

Table 1.2 Overview of different classes of modification identified on histones

Histone post-translational modifications	Residues Modified
Acetylation	K-ac
Methylation (lysines)	K-me1 K-me2 K-me3
Methylation (arginines)	R-me1 R-me2 R-me2
Phosphorylation	S-ph T-ph
Ubiquitylation	K-ub
Sumoylation	K-su
ADP ribosylation	E-ar
Deimination	R > Cit

Fig 1.1 Post-translational modifications of human nucleosomal histones. The modifications include acetylation (ac), methylation (me), phosphorylation (ph) and ubiquitination (ub1). Most of the known histone modifications occur on the N-terminal tails of histones, with the exceptions, such as ubiquitination of the C-terminal tails of H2A and H2B and acetylation and methylation of the globular domain of H3 at K56 and K79, respectively. Globular domains of each core histone are represented as colored ovals (Bhaumik *et al.*, 2007).

1.2.2 Histone modification enzymes

Histone PTMs were catalyzed by a specific enzyme at a specific site and resulted in unique functions. Enzyme complexes might prefer for the specific histones (Lee *et al.*, 2005); and the proteins that associate with the enzyme may affect its selection of residue to modify (Metzger *et al.*, 2005) or the degree of methylation (mono-, di-, or tri-) at a specific site (Steward *et al.*, 2006).

Until now, histone modification enzymes have been identified for acetylation (Sterner and Berger, 2000), methylation (Zhang and Reinberg, 2001), phosphorylation (Nowak and Corces, 2004), deimination (Cuthbert *et al.*, 2004; Wang *et al.*, 2004), ubiquitination (Shilatifard, 2006), sumoylation (Nathan *et al.*, 2006), ADP-ribosylation (Hassa *et al.*, 2006) , proline isomerization (Nelson *et al.*, 2006), and demethylation (Shi *et al.*, 2004).

1.2.3 Histone code

Histone PTMs could be involved in many biological processes such as gene regulation, DNA damage response and chromosome condensation or relaxation. Distinct histone modifications on one or more tails might act sequentially or in combination. Based on the finding of histone lysine acetylation worked in a dosage compensation process, the concept of a histone code was firstly introduced by Turner (Turner, 1993). Later it was named by Allis in 2000 (Strahl and Allis, 2000). The

content of the hypothesis includes four parts: 1) Specific tail modifications and / or their combinations constitute the histone code that determines the transcriptional state of the genes; 2) Modifications on the same or different histone tails may be interdependent; 3) Binary switches-neighboring modifications act together; 4) Modification of cassettes-residues in linear strings of densely modifiable sites can have different biological readouts, depending on their modification state.

The histone code was investigated by Dion's group in 2005 (Dion *et al.*, 2005). An acetylation code with the combination of four lysine residues (K5, K8, K12 and K16) of the histone H4 tail in budding yeast was tested. Their results shed significant light on the explanation of histone code hypothesis. They constructed all combinations in which one, two, or three of the four histone lysine residues were changed to arginine, and then measured genome-wide changes in gene expression by using DNA microarray. The results revealed that the mutation of lysine 16 induced specific transcriptional consequences (affecting approximately 100 genes). However, the mutation of lysines 5, 8, and 12 induced gene expression change with nonspecific and cumulative effects. Increased transcription was correlated with an increase in the total number of mutations (affecting approximately 1,200 genes), which indicated that acetylation of histone H4 was interpreted by two mechanisms: a specific mechanism for lysine 16 and a nonspecific, cumulative mechanism for lysines 5, 8, and 12.

Now, histone code has become an important research part of the epigenetic code together with DNA methylation modifications and RNA interference. Aberrant

patterns of histone modifications in cancer have been well investigated, which will be crucial parameters in cancer diagnosis and prognosis and help to develop novel strategies for epigenetic therapy in a near future (Herranz and Esteller, 2007; Smith *et al.*, 2007). Moreover, the functions of histone modification in DNA repair processes and the combination of modification sites have become as specific marker for different DNA repair pathway (Escargueil *et al.*, 2008).

1.2.4 How is the histone code read?

Histone code is an epigenetic code which changes gene expression without altering DNA sequence. Their molecular mechanisms were generalized into 'cis' mechanisms and 'trans' mechanisms (Wang *et al.*, 2007). They proposed that Cis mechanisms could alter intra- and inter-nucleosomal contaction via changes of steric or charge interactions and Trans mechanisms utilize non-histone 'readers' that bind to specific histone modification sites and lead to diversity functions. For example, histone acetylation could unfold chromatin via neutralization of the basic charges of lysines and induce transcriptional activation (Kouzarides, 2007). By using recombinant nucleosomal arrays, researchers found that acetylated H4K16 could inhibit the formation of higher order chromatin and induce transcriptional silencing (Shogren-Knaak *et al.*, 2006; Shogren-Knaak and Peterson, 2006). Phosphorylation was another modification that might have important consequences for chromatin

compaction via charge changes. To 'trans' mechanisms, the reader proteins were recruited to specific modification sites or provide an adaptor function. They contained specific interacting domains: bromodomain, chromodomain or tudor domain. For example, inhibitor of growth (ING) proteins could recognize H3K4 methylation, heterochromatin protein 1 (HP1) could recognize methylated H3K9 and methyalted H3K27 is recognized by polycomb proteins (Wang *et al*., 2007).

Actually, there has the third mechanism to interpret the histone code. It is the cross-talk between different modifications on the same histone tail or on different histone tails. By cross-talking, the status of one histone modification could regulate that of other modifications. For example, H3K9me3 could be recognized by heterochromatin protein 1 and mediate the formation of heterochromatin. However, phosphorylated H3S10 which is catalyzed by aurora B kinase leaded to the release of HP1 from heterochromatin and keep the tri-methylated state of H3K9 for the proper chromosome segregation during mitosis (Fischle *et al*., 2005). Another experiment showed that the methylation of H3K4 and H3K79 required the ubiquitylation of H2B lysine 123 (Wang *et al*., 2007).

1.3 The function of histone PTMs

1.3.1 Establishment of global chromatin environments

There are two different types of chromatin environments in the genome, silent

heterochromatin and active euchromatin, which are the condensation and relaxation states of chromatin. Chromatin condensation was observed at mitosis and apoptotic cell death, whereas chromatin relaxation was prepared for gene replication, damage repair, recombination and transcription (Ito, 2007). The covalent modifications on histone tails had showed their important roles in genome state controlling. Acetylation, phosphorylation and methylation played a critical role in dynamic condensation/relaxation. Addition of acetyl groups to histones reduced the attractive force between positively charged histone proteins and the negatively charged DNA phosphate backbone, resulting in a more relaxed and accessible chromatin structure. The presence of methylation at H3K9 could maintain heterochromatin state, and constitutive heterochromatin could typically be identified by H3K27 monomethylation, and the trimethylation of H3K9 and H4K20 (Gelato and Fischle, 2008). Actively transcription euchromatin had high levels of acetylated H3K9 and H3K16, and the occurrence of trimethylated at H3K4, H3K36, and H3K79 (Kouzarides, 2007). Moreover, histone modifications, di-methylated H3K9 and H3K4, tri-methylated H3K27, mono-methylated H4K20 and general deacetylation of histones were the indicators of inactive X chromosome (Brinkman *et al*., 2006).

1.3.2 Gene transcription regulation

Histone modifications could not only control the eukaryotic genomes state, but also were distributed in distinct localized patterns within the upstream region, the

core promoter, the 5' end of the open reading frame (ORF) and the 3'end of the ORF. The location of a modification was tightly regulated and was crucial for its effect on transcription (Li *et al*., 2007).

The idea of a function in transcription was considered as early as the 1960s. Acetylation was the first discovered histone modification type which was linked with active transcription. The researchers demonstrated that histone acetylation could reduce their efficacy as inhibitors of transcription, and thought that this might imply a dynamic and reversible mechanism for activation as well as repression of RNA synthesis (Allfrey *et al*., 1964). In 1996, two studies showed that histone acetylases and deacetylases were, in fact, well-known transcriptional regulators (Brownell *et al*., 1996; Taunton 1996). These studies provided the first clear connection between histone acetylation and transcriptional regulation. Phosphorylation of histone H3 was found to cooperate with acetylation in transcriptional activation (Barratt *et al*., 1994).

Among the modifications, acetylation, phosphorylation and unbiquitination had been implicated in activation whereas sumoylation, deimination, and proline isomerization had been implicated in repression (Kouzarides, 2007). But sometimes, any modification had the potential to activate or repress under different conditions including the histone (for example, H3 versus H4), the lysine acceptor (for example, H3K4 versus H3K9), the histone location (for example, whether bound to a coding versus noncoding region of a gene), and other contextual influences. In general, lysine methylation at H3K9, H3K27, and H4K20 was associated with transcriptional repression, whereas methylation at H3K4, H3K36, and H3K79 was associated with

transcriptional activation. Interestingly, the positive effect of methylation at H3K36 was found when it was on the coding region, while the negative effect was observed when in the promoter (Carrozza *et al.*, 2005). The same phenomenon could also be found on methylation at H3K9 (vakoc *et al.*, 2005).

1.3.3 Histone modifications in response to DNA damage

DNA damage can be caused by both extrinsic agents (chemical agents, UV radiation and ionizing radiation) and intrinsic agents (reactive oxygen species and endogenous alkylating agents), or result from collapsed DNA replication forks and from oxidative destruction of deoxyribose residues. Genomic instability and cancer initiation could be induced if the repair of DNA lesions is unsuccessful. Now it has been widely accepted that histone modifications have important roles in response to DNA damage and DNA repair. The modifications not only signal the presence of damage, but provide an essential function by acting as a landing platform for necessary repair/signaling proteins (Altaf *et al.*, 2007).

In many species, such as mammals, *Xenopus laevis*, *Drosophila melanogaster, and Saccharomyces cerevisiae*, the phosphorylation of serine residue in the global domain of H2AX (serine 139 in mammals and serine 129 in yeast) was one of the first events in response to DNA damage (Altaf *et al.*, 2007). H2AX deleted or H2AX–S139A mutated cells were sensitized to ionizing radiation (IR) or camptothecin and genomic instability (Celeste *et al.*, 2002; Bassing *et al.*, 2002).

This modification could not only stabilize the association of different repair proteins at the damaged site, but also recruit cohesins to DNA double strand breaks (DSBs) (Ström *et al.*, 2004; Unal *et al.*, 2004). Besides H2AX, other histone phosphorylation events also take place during DNA damage response. In the presence of DNA damaging agents, yeast H2A serine 122 was phosphorylated and essential for cell survival (Harvey *et al.*, 2005). In addition to the phosphorylation on histone H2A, the phosphorylation at serine 14 of histone H2B and the phosphorylation at serine 1 of histone H4 also undergone in response to DNA damage (Fernandez-Capetillo *et al.*, 2004; Cheung *et al.*, 2005).

Methylation of H3 and H4 also played a crucial role in DNA repair through the association of DNA damage response proteins. Methylated H3K79 played an important role in the checkpoint activation when DNA damages took place at G1 and intra S-phase and mammalian 53BP1 or budding yeast homolog Rad9 could be recruited to the DNA damage sites by the recognition of methylated H3K79 site (Huyen *et al.*, 2004). DSBs could affect the accessibility of 53BP1 to methylated histone H3K79 through the change of higher order chromatin structure (Altaf *et al.*, 2007).

Except for the phoshporylation and methylation, other histone modifications, such as acetylation, are also involved in the DNA repair. Acetylated lysine 56 of histone H3 played an important role in DNA repair and its mutation made the cells sensitive to genotoxic agents (Masumoto *et al.*, 2005). Histone H4 lysine 16-specific deacetylase Sir2 was recruited to the HO lesion during homologous recombinational

repair of double-strand DNA repair (Tamburini and Tyler. 2005), indicating that certain histone modification could induce DNA repair by different pathway.

1.4 Histone PTMs and diseases

An altered pattern of epigenetic modifications, including histone PTMs pattern, is central to many common human diseases. Next, some diseases associated with histone modifications were described.

1.4.1 Histone PTMs and cancer

The disruption of genomic DNA methylation patterns was the first epigenetic abnormality to be described in human cancer ((Fraga and Esteller, 2005). The promoter CpG island hypermethylation of tumor suppressor genes could cause transcriptional repression (Cohen *et al.*, 2008). It was found that histone modifications had the relationship with the repression of tumor suppressor genes by inducing promoter hypermethylation (Fraga and Esteller, 2005). Many studies had explored the mosaic patterns of histone modification in cancer cells. Tumor cells showed less acetylated lysine 16 histone H4 by the MS/MS comparison of histone H4 peptides. This change appeared early and accumulated during the tumorigenic process. The same change could also be found on the trimethylation of H4K20. Therefore, loss of acetylation at histone H4K16 and tri-methylated H4K20 were

regarded as a common hallmark of human cancer (Fraga *et al.*, 2005). Another study also showed that patterns of H3 and H4 were potential predictors of clinical outcome in prostate cancer (Seligson *et al.*, 2005). In this study, two disease subtypes with distinct risks of tumor recurrence in patients with low-grade prostate cancer could be distinguished by differential staining via using antibodies to histone acetylation and dimethylation in histones H3 and H4. This study was the first profile of histone modifications in cancer with prognostic relevance.

Moreover, histone modification enzymes were also found to play the role in the cancer. Histone methyltransferases for H4K20 and for H3K9 could act as tumor-suppressor genes. Suv39h knock-out mice were prone to developing cancer (Peters *et al.*, 2001). HDAC inhibitors became another promising group of agents for the epigenetic therapy of cancer. One of the main therapeutic mechanisms of HDAC inhibitors was their transcriptional reactivation of dormant tumor-suppressor genes, such as p21WAF1 (Mack, 2006). The first drug of this type, suberoylanilide hydroxamic acid (SAHA), had been approved by the FDA for the treatment of cutaneous T-cell lymphoma (Thompson, 2006).

1.4.2 Histone PTMs and inflammation disease

The increasing evidence indicated that histone acetylation played a critical role in the process of regulation of inflammatory genes and histone deacetylase (HDAC) suppressed inflammatory gene expression. During the inflammatory response,

nuclear factor kappaB (NF-kB) could induce histone acetylation and other histone modifications in a temporal manner (Ito *et al.*, 2000; Lee *et al.*, 2006) leading to recruitment of other co-activator and remodeling complexes and the induction of inflammatory gene expression (Ghosh and Karin, 2002). In epithelial cells, NF-kB-induced acetylation happened preferentially on lysine residues 8 and 12 of histone H4 (Ito *et al.*, 2000; Nie *et al.*, 2005). Increased HAT activity and the reduction in HDAC activity were detected in bronchial biopsies from patients with asthma compared with normal airways (Ito *et al.*, 2002). Similar changes were also found in alveolar macrophages obtained by bronchoalveolar lavage from patients with asthma (Cosio *et al.*, 2004). In chronic obstructive pulmonary disease (COPD), there was also a marked reduction in HDAC activity and expression in peripheral lung and alveolar macrophages, resulting in amplification of the inflammatory response. This decrease was correlated with disease severity (Ito *et al.*, 2005; Barnes, 2008). Corticosteroids could less the inflammatory reaction by inhibiting HAT activity and the recruitment of HDAC2 to the activated transcription complex, and then new strategies to control inflammatory reaction in COPD are now developing in clinic by targeting to the activity restoration of HDAC2 enzyme or to mitigate HAT-related signaling (Mroz *et al.*, 2007).

1.4.3 Histone PTMs and diabetes

Globally, diabetes, especially type 2 diabetes, represents a major challenge to

world health. It is a complex multigenic syndrome primarily due to beta-cell dysfunction associated with a variable degree of insulin resistance. The investigations led to a new understanding on the mechanisms of diabetes. Genome wide scans for both type 1 and type 2 diabetes loci indicated that HDACs might play a role in the pathogenesis of diabetes. A significant linkage was observed that HDAC2 and HDAC Sirt2 lie on the chromosome 6q21 of type 1 and 19q13 of type 2, respectively (Concannon *et al.*, 2005; van Tilburg et *al.*, 2003; Betz *et al.*, 1998; Voelter-Mahlknecht *et al.*, 2005). High concentrations of glucose could recruit the histone acetyltransferase p300 to the insulin promoter and induce the hyperacetylation of histone H4 at the insulin promoter (Mosley *et al.*, 2004).

1.5 Histone PTMs and aging

1.5.1 Introduction

Aging is characterized by the progressive functional decline of multiple organs and tissues, eventually culminating in death. Aging process is accompanied by an impairment of the physiological systems. Its damage occurred to molecules (DNA, proteins, and lipids), cells and different organs. Typical changes could be observed during aging process, such as a loss of hearing ability, particularly for higher frequencies; the decline in the ability to taste salt and bitter; the reduction of the thymus gland; increasing levels of antibodies, memory loss, and so on. These

changes are deleterious, universal and thus far irreversible. Many countries including China are experiencing aging populations because of declining birth and mortality rates. The aging problem has already become a global headache.

1.5.2 Mechanisms of aging

A wide variety of theories about the mechanisms of aging have been proposed. However, there is still not a generally accepted theory which can provide well-proven explanation for this universal phenomenon of life. Next, several popular theories were described.

1.5.2.1 The free radical theory

Denham Harman first proposed the free radical theory of aging in1956. The discovery of superoxide dismutase and the existence of H_2O_2 *in vivo* provided solid evidences for this hypothesis and make it popular (McCord and Fridovich, 1969; Chance *et al.*, 1979). Reactive oxygen species (ROS) are ions or very small molecules that include oxygen ions, free radicals, and peroxides. ROSs is produced naturally during normal metabolic process of oxygen and they play important roles in cell signalling. However, during times of environmental stress such as UV exposure or ionizing radiation, ROS level could increase dramatically, which results in significant damage to cell structures. A modified free radical theory was proposed by

Harman in 1972 which emphasized the central role of mitochondria (Harman, 1972). The finding that mitochondria could generate large amount of ROS provided supporting evidence for this theory (Chance *et al.*, 1979). However, other experiment could not give more solid support for this theory (Reviewed in Hamilton *et al.*, 2001; Van Remmen and Richardson, 2001; Bokov *et al.*, 2004).

Reactive oxygen species such as peroxides and aldehydes also played a role in oxidative damage in cells, which was a major contributor to the functional decline that is characteristic of aging (Harman, 1956). Therefore, a modification from the free radical theory to the oxidative stress theory of aging was proposed (Sohal and Weindruch 1996). Study found chronic oxidative stress in cells of aerobic organisms not only under pathological conditions but also under physiological conditions. During aging, the imbalance between prooxidants and antioxidants led to the accumulation of reactive oxygen species in various cellular processes and resulted in the loss of functional efficiency progressively. The researches on oxidative stress in different model organisms during aging had been reviewed (Muller *et al.*, 2007). Transgenic experimental animal models targeting either ROS-generating or ROS-scavenging systems had also been developed in these studies. Studies in a wide range of species had supported the role of ROS in many age-related diseases (Buffenstein *et al.*, 2008).

Nowadays, this theory was widely accepted as a pivotal determinant of both lifespan and health span. However, antioxidants administered as dietary supplements, like vitamins E and C, could not increase maximum lifespan significantly.

Superoxide dismutase (SOD), a special class of antioxidant that neutralizes the chemicals and prevents them from harming cells, could protect against oxidative stress but had little or no effect on life span in *Caenorhabditis elegans* (Doonan *et al.*, 2008). More interestingly, removing SODs from tiny *Caenorhabditis elegans* soil worms made them live longer, which was opposite to the results gotten from mice, flies or yeast (Van Raamsdonk and Hekimi, 2009). Therefore, the role of oxidative stress as a determinant of longevity is still open to question.

1.5.2.2 Mitochondrial theory

Mitochondria has a wide variety of functions, including adenosine triphosphate (ATP) production, ROS generation, calcium homeostasis, apoptotic signalling, and control of energy efficiency. Many evidences were accumulated in support of a role for oxidative damage to the mitochondrial respiratory chain and mitochondrial DNA in the determination of mammalian lifespan (Jang and Remmen, 2009). Mitochondrial DNA (mtDNA) mutations were the sign of apoptosis and could induce cell loss finally. They accumulated with age in a number of tissues and were common in neurodegenerative diseases (Reeve *et al.*, 2008).

The mitochondrial theory of aging was first proposed in 1972 by Denham Harman and was further developed and verified by Miquel (Harman, 1972; Miquel *et al.*, 1980). Mitochondrial theory and free radical theory had a strong connection to each other that they are often discussed together as if mitochondrial theory was one

form or specific development stage of free radical theory. However, the mitochondrial theory concerned far more than free radicals and involved several biological topics, such as genetics, membranes and bioenergetics (Jang and Remmen, 2009). Somatic mutation of mtDNA engendered respiratory chain dysfunction, and enhanced the production of DNA-damaging oxygen radicals. In turn, that was proposed to result in the accumulation of further mtDNA mutations. Finally, a bioenergetic crisis led to overt tissue dysfunction and degeneration (Jacobs, 2003). Today, the free radical theory focusing on mitochondrial as the centre of ROS production is becoming one of the most popular theories of aging (Gruber *et al.*, 2008).

However, Rasmussen's study provided the evidence against the mitochondrial theory (Rasmussen *et al.*, 2003). In his study, no general membrane alterations or changes in the cytochrome contents were observed after comparing quadriceps muscle from healthy humans at age around 70 and 20. At the same time, no age related change was found at central bioenergetic systems, including pyruvate dehydrogenase, tricarboxylic acid cycle, respiratory chain and ATP synthesis. Therefore, the mitochondrial theory of aging remained an attractive hypothesis that needs much more critical experimental evidences before it is verified or falsified (Jacobs, 2003).

1.5.2.3 The telomerase theory

Telomere is a region of repetitive DNA at the end of chromosomes, which protects the end of the chromosome from destruction. Telomere length is predominantly genetically determined, but other factors could also determine the length of telomere, such as age (shorter telomeres in older people), paternal age (longer telomeres in subjects with older fathers at their birth) and sex (shorter telomeres in men). The elevated levels of oxidative stress and inflammation could also lead to telomere shortening (Starr *et al.*, 2008; Savale *et al.*, 2009).

Telomere was first recognized and defined as the functional ends of chromosomes by Muller and McClintock (Muller, 1938; McClintock, 1941). The research found that the amount and length of telomeric DNA in human fibroblasts decreased during aging *in vitro* and possibly *in vivo* (Harley *et al.*, 1990). Telomere shortening was implicated with a broad range of aging tissues and organs in *vivo* (Bird *et al.*, 2003; Campisi, 2001; Kirkwood, 2002). Therefore, telomere attrition has been regarded as an aging biomarker (Bekaert *et al.*, 2005).

1.5.2.4 Misrepair-accumulation theory

This very recent novel theory suggested that aging was the result of the accumulation of misrepair (Wang *et al.*, 2009). Their theory combined the roles of environmental damage, repair, gene regulation, and multicellular structure in the aging process. They said this theory could give the explanation for many phenomena, such as the aging phenotypes, premature aging and the difference of longevity in

different species and is consistent with the point of view of physical theory of complex systems. Normally, misrepair happened during whole life and was regarded as the result of active repair processes which benefited for survival. During aging process, misrepaired structure could not be repaired or restored to the normal undamage state and induced the death eventually. However, this theory needs a plenty of experimental evidences to validate before being widely accepted.

1.5.3 The models on aging research

Saccharomyces cerevisiae, one kind of budding yeast, are often be used as a model for the study of aging due to its unique feature that it could proliferate in both the haploid and diploid states. After several divisions, cells could show morphological changes, slow the rate of cell cycle and loss the capacity of reproduction, which are the features of aging of budding yeast. The observations had shown it's relevance to aging in higher eukaryotes, such as the similarity at metabolism, stress resistance, gene dysregulation and genetic instability (Jazwinski, 2001; Leonardo, 2001).

Many of marine invertebrates, such as bivalves and sea urchins, are the earth's longest lived animals. These animals grow and reproduce throughout their lifespan and there is no apparent functional decline or increase in mortality rate with age. Recently, Bodnar summarized the experimental data on the molecular or cellular changes of marine invertebrates and evaluated their potential as model systems for

aging, and provided direction for future research efforts (Bodnar, 2009). They said studying on these animals might reveal some exceptionally effective defenses against the destructive process of aging and provide valuable information to understand aging process. The researchers had used Teleost fish (*Channa punctatus*) to study the effect of age on brain catalase (CT) activity (Jena *et al.*, 1998).

C. elegans was another powerful model system for aging study due to its genetics, relatively short life span, and ease of propagation of populations of synchronized individuals (Golden and Melov, 2007). Many investigations have been performed and the mutations of some aging related single genes have showed the effect to increase life span of *C. elegans* (Friedman and Johnson, 1988; Johnson, 2002; Kenyon *et al.*, 1993; Kimura *et al.*, 1997).

Murine models were usually used on aging study. Among them, senescence-accelerated mouse (SAM) model was the most popular one. It was established by Takeda as a murine model of accelerated aging (Takeda *et al.*, 1981). SAM prone (SAMP) mice exhibited a shorter life span of about 18 months and early manifestation of various signs of senescence, including decreased activity, hair loss, and lack of hair glossiness, skin coarseness, periphthalmic lesions and cataracts, and increased lordokyphosis of the spine. SAMP strains included SAMP1, SAMP2, SAMP3, SAMP6, SAMP7, SAMP8, SAMP9, SAMP10 and SAMP11. Among them, SAMP8 strain was characterized by age-related learning and memory deficits and was thought to be a good model for aging and neurodegenerative research. It was usually used to investigate the fundamental mechanism of age-related learning and

memory deficits at the gene and protein levels (Butterfield and Poon, 2005).

Cells in culture represented another possible option as an experimental model to explore the mechanisms of aging. Cultured cells represented a simpler situation than the whole organism or even a tissue. They could be obtained from humans and animals of different ages and genetic backgrounds, and could be examined and tested with vary large array of techniques (Kahn and Fraga, 2009). Early-passage euploid fibroblasts from human subjects ranging in age from young to elderly adult are available from the Coriell Institute (http://ccr.coriell.org). The senescent state of these cells could be induced and subjected to a number of aging studies. However, the results gotten from the cultured cells are often questioned whether they could accurately represent or mimic their *in vivo* counterparts.

1.5.4 Brain aging and neurodegenerative diseases

The brain as the centre of the nervous system, is a highly complex organ. During aging, brain showed structural changes, such as neuronal shrinkage and expansion of the ventricular volume, which were caused by the loss of white matter and neuronal loss. At the same time, dendritic loss and age-related modification of synaptic structure could be observed in the aged brain. Aged brain also showed the imbalance between different neurotransmitter systems, such as the loss of dopamine. All the changes accompanied with aging could induce mild changes in cognitive capacity even in cognitively intact humans, including declines in memory and

executive function (Wong, 2002). Therefore, brain aging was regarded as the major risk factor for most common neurodegenerative diseases, such as Alzheimer's disease (AD), Parkinson's disease and Huntington's disease (HD). These three diseases have a common basis as they were linked to the appearance of oligomers and other toxic aggregates consisting of the β-amyloid peptide, α-synuclein, superoxide dismutase, and huntingtin, respectively.

To date, many researches have been performed in an attempt to elucidate the mechanisms of brain aging and the neurodegenerative disease from various aspects. For example, the investigations on mitochondrial dysfunction and oxidative stress in aging and neurodegenerative diseases (Reviewed in Lin and Beal, 2006; Keating, 2008; Yang *et al.*, 2008a). The morphological and biochemical features of apoptosis in aged neurodegenerative brain (Reviewed in Culmsee and Landshamer, 2006; Okouchi *et al.*, 2007; Nakamura and Lipton, 2009). Transcriptional profiling defined a set of genes with reduced or increased expression in aged brain (Lu *et al.*, 2004; Hong *et al.*, 2008; Burger *et al.*, 2008). These genes played central roles in synaptic plasticity, vesicular transport, mitochondrial function, learning and memory formation or stress response, antioxidant and DNA repair. Comparative proteome analysis was also used to identify aging-related brain proteins in brains from mouse model or AD patient (Reed *et al.*, 2009; Schonberger *et al.*, 2001; Yang *et al.*, 2008b). These investigations could provide the clues to elucidate the pathology of brain aging and neurodegenerative diseases. However, the mechanisms of aging and neurodegenerative diseases still remain unknown.

1.5.5 Histone PTMs on aging and neurodegenerative disease

The impact of the genome on aging has been well established. However, nongenomic mechanisms also played the predominant role in aging process and determined longevity. Epigenesis is one kind of nongenomic mechanisms that strongly affects both the aging process and the longevity. To date, most work has focused on two circumstances that can dramatically alter gene expression: DNA methylation and histone post-translational modifications. Genomic global DNA methylation state, which was generally associated with the silencing of gene expression, showed a decrease with age in many species. Histone modification could be associated with both gene activation and repression.

DNA methylation on gene expression regulation during aging had been demonstrated (Conde-Pérezprina *et al.*, 2008; Kim *et al.*, 2009). Many genes were silenced after birth, such as the genes for hemoglobin F (Oneal *et al.*, 2006). This trend accelerated especially after age 25, with increasing numbers of genes silenced as aging. When this silencing affected tumour suppressor genes, an aging person might develop cancer. Silencing of glutathione S-transferases could impair detoxification. Similar mechanisms might silence the genes for DNA repair enzymes, hormone biosynthesis, and enzymes that protect against free radicals, genes responsible for immune surveillance, and so on. In addition to the silencing of many genes, there was also increased expression of genes during aging, such as the smaller

group of oncogenes, genes which were associated with typical diseases of old age, and genes mediating immune responses (Burzynski, 2005; Brink *et al.*, 2009).

Researchers proposed that either the methylation of promoter sequences or the acetylation of histones could involve silencing of the genes during aging process (Burzynski, 2003). Previous investigations indicated that tri-methylaion of histone H4 at lysine 20 increased in kidneys and liver of the old-aged rat (Sarg *et al.*, 2002), while the level of H4 acetylation decreased in the rat brain cortical neurons with age (Piña *et al.*, 1988). Researchers proposed that these modifications could induce chromatin remodelling, which in turn regulate gene expression (Han *et al.*, 2006).

During neurodegeneration, the degree of acetylation balance in brain was greatly impaired (Saha and Pahan, 2006). The inhibition of histone deacetylation not only enhanced the neurotoxicity which was induced by the C-terminal fragments of amyloid precursor protein but also inhibited proliferation and induced apoptosis in neuroblastoma cells (Kim *et al.*, 2004; De Ruijter *et al.*, 2004). At the same time, increased histone acetylation could induce sprouting of dendrites, synapses increase, and benefit for learning behavior and long-term memories (Fischer *et al.*, 2007). All these evidences pointed to transcriptional dysregulation which was governed by histone acetylation and deacetylation state as an important pathologic mechanism of neurodegenerative diseases. Now, HDACs have become an attractive therapeutic target for neurodegenerative diseases associated with learning and memory impairment, which increased the possibility of recovery of long-term memories in patients with dementia (Butler and Bates, 2006; Langley *et al.*, 2005). However,

histone acetylation is transient and could not adequately explain long-lasting transcriptional changes in neurodegenerative diseases (Kim *et al*., 2008). Therefore, it is presumed that other modification types might also play a contributory role in the pathogenesis mechanism of neurodegenerative diseases. Increased monoubiquityl histone H2A and decreased monoubiquityl H2B were found involving in transcriptional repression during HD, and these two ubiquitylation states inhibited methylation of histone H3 at lysine 9 and methylation of histone H3 at lysine 4, respectively (Kim *et al*., 2008). Investigation showed that histone acetylation could affect monoubiquityl histone H2A, whereas monoubiquityl histone H2B regulated histone methylation (Sadri-Vakili *et al*., 2007; Ng *et al*., 2002b; Sun and Allis, 2002). Thus, histone monoubiquitylation provided a potential bridge between histone acetylation and methylation, leading to changes in gene expression in neurodegenerative diseases (Kim *et al*., 2008a). All previous studies indicated that the investigations on histone PTMs involved in gene expression and DNA double breaks repairs during aging could help us better understand the pathologic mechanism of aging and neurodegenerative diseases, and also provide potential targets for the development of therapeutic interventions against these diseases.

As far as I know, no systematic investigations on the histone PTMs patterns (histone code) in the aged brain have been performed and the exact mechanisms of histone PTMs involved in aging and neurodegenerative diseases have not been elucidated yet. Therefore, as a major part of the epigenetics, the researches on histone PTMs will become more important in the fields of neurodevelopment and

neurodegeneration.

1.6 Objectives of this study and its long-term significance

Aging is considered as the greatest risk factor for the development of the neurodegenerative diseases, such as Alzheimer's diseases (AD). Histone post-translational modifications (PTMs) regulation had been demonstrated the linkage to neurological disorders in previous studies. More and more findings were consistent with the growing attention to epigenetic regulation in brain physiology and pathology (Shi, 2007). Aging epigenetics became an emerging discipline that promised exciting discoveries and histone modification maps as aging markers (Fraga and Esteller, 2007). Previous reports indicated that acetylation balance was greatly impaired during neurodegeneration, monoacetylated H4 decreased during aging due to a gradual loss of chromatin structure plasticity. But till now, no systematic investigations on studying the patterns of histone PTMs in the brain upon aging have been performed, and the exact mechanisms of histone PTMs involving in brain aging are still not clear. Therefore, the objectives of this project were listed below:

1. To identify the patterns of histone post-translational modifications of core histone (histone H2A, H2B, H3 and H4), in particular the methylation, in the brain of 12-month-old senescence-accelerated mouse prone 8 (SAMP8) mouse. And to investigate the multi-methylation state in the brain of different age-old SAMP8.

2. To investigate the tissue distribution of H3K79 methylation, its localization in the brain and its corresponding interaction proteins.

3. To study the biological changes in Neuro 2a (N2a) cells in response to the decrease of H3K79 methylation using siRNA profile by silencing *Dot1* (H3K79 methyltransferase gene).

This study will give us a new insight into the linkage between histone PTMs and brain aging and provide the experimental evidences for future studies. I hope this study could help us to understand aging or neurodegenerative disease better at epigenetic level. In future, I hope the platform for the exchange of comprehensive information to the medical practitioners could be established, which will facilitate medical prediction, detection, and prognoses of aging related neurodegenerative diseases and eventually provide the opportunity in the development of new therapeutic targets in order to prevent or cure these age-related diseases.

Chapter 2 Identification of histone methylation multiplicities patterns in the brain of senescence-accelerated prone mouse 8

2.1 Introduction

Eukaryotic DNA is wrapped around the histone complexes and other nuclear proteins composing the chromatin. The N-terminal tails of core histones (H2A, H2B, H3 and H4) are prone to histone post-translational modifications (PTMs), such as methylation, acetylation, phosphorylation and ubiquitination (Bonaldi *et al*., 2004). Some modifications, including acetylation and phosphorylation, are reversible and dynamic; whereas other modifications, such as methylation, are found to be more stable. They are involved in the long-term maintenance of gene expression and methylation normally acts as a long-term epigenetic mark (Cheung and Lau, 2005). Certain histone modifications and/or constellations of modifications act in diverse biological processes (Margueron *et al*., 2005; Roopra *et al*., 2004). Histone acetylation increases the accessibility of nucleosomal DNA through chromatin re-structuring transitions and plays an important role in the modulation events of eukaryotic gene expression. Histone methylation can take part in many biological processes, such as gene regulation and X-chromosome inactivation (Miao and Natarajan, 2005).

An altered pattern of histone modifications is essential to many common human diseases. For instance, loss of acetylation at lysine 16 and tri-methylation at lysine 20

of histone H4 (H4K20) is a common hallmark of human cancer (Fraga *et al.*, 2005). Histone acetylation plays a vital role in the process of inflammatory genes regulation and could mediate the anti-inflammatory effects of corticosteroids in asthma patients (Cosío *et al.*, 2004). Previous studies indicated an indirect linkage between PTMs regulation and neurological disorders. For example, SMCX, a member of the H3K4me3-specific demethylase family, played a role in neuronal cell survival, dendritic development and was involved in X-linked mental retardation (XLMR) (Shi, 2007). During neurodegeneration, the degree of acetylation balance in brain could be greatly impaired (Saha and Pahan, 2006). Tri-methylaion of histone H4 at lysine 20 increased in kidneys and liver of the old-aged rat (Sarg *et al.*, 2002), while the level of H4 acetylation decreased in the rat brain cortical neurons with age (Piña *et al.*, 1988).

Aging is considered as the greatest risk factor for the development of the neurodegenerative diseases, such as Alzheimer's diseases (AD). Function declination and gene expression alternation could be detected in the aging human brain (Blennow *et al.*, 2006; Doudet, 2007). Recently, increasing findings indicated the importance of epigenetic regulation in brain physiology and pathology (Shi, 2007). Aging epigenetics might be an emerging discipline that promises exciting discoveries on the mechanism of brain aging, and histone modification maps might act as the markers of aging (Fraga and Esteller, 2007). But till now, no systematic investigations have described the patterns of histone PTMs in the aged brain, and the underlying mechanisms of histone PTMs involved in aging are unknown.

In this study, the senescence-accelerated mouse (SAM) model was selected. This model was selected from AKR/J strain mice by Takeda and co-workers (1981) as a murine model of accelerated aging (Takeda *et al.*,1981). SAM-prone (SAMP) mice exhibited a shortened life-span (about 18 months) and early manifestation of various signs of senescence. Among all SAM strains, SAMP8 mice were characterized by age-related learning and memory deficits. It exhibited many physiological findings of AD and, therefore, is regarded as an excellent model for studying aging and the early phase of AD. Senescence accelerated-resistant mouse (SAMR1), which genetically resembled SAMP8, showed normal aging characteristics (Yasunobu and Yasuyuki, 1998) and was used as controls in this study.

Combination of the enzymatic digestions (tryspin and glu-c), nano-liquid chromatography (nano-LC) and tandem matrix-assisted laser desorption/ionization time-of-flight mass spectrometry (MALDI-TOF/TOF MS) analysis were employed to detect the histone methylation of core histones (histone H2A, H2B, H3 and H4) in brains of SAMP8. Specific methylations with defined multiplicities were confirmed and the abundance of specific methylation multiplicities was further investigated by Western blotting.

2.2 Materials and Methods

2.2.1 Animal model

3- and 12-month-old senescence-accelerated mice (SAM), including SAMP8 and SAMR1 were housed in an animal room at 23°C with 12-12-h light-dark cycles. Each group included 3 male mice and 3 female mice. The mice were terminated via cervical dislocation. The brain samples were divided into four groups: 3-month-old SAMR1 (R1-3M); 3-month-old SAMP8 (P8-3M); 12-month-old SAMR1 (R1-12M); 12-month-old SAMP8 (P8-12M). The Institutional Animal Care and Use Committee at the Chinese University of Hong Kong approved all animal procedures in this study.

2.2.2 Histone extraction

Core histone proteins were extracted from the mouse brain samples using acid extraction methodology (Janzen *et al*., 2006a) with slight modifications. Briefly, the brain tissue was first homogenized in lysis buffer (10 mM Tris-HCl, pH 7.6, 150 mM NaCl, 1.5 mM $MgCl_2$, 0.05 % NP40, and 1 mM phenylmethylsulfonyl fluoride (PMSF), 50 mM sodium bisulfite ($NaHSO_3$), 45 mM sodium butyrate), and nuclei were obtained by centrifugation (1,500×g for 10 min). For the preparation of histones, nuclei were incubated with 4 volumes of 0.2 N sulfuric acid (H_2SO_4) for 2 h at 4°C.

The supernatant was precipitated with 20 % trichloroacetic acid (TCA) (Final concentration) and followed by centrifugation (12,000×g for 20 min). The obtained pellet was washed with cold acetone and subsequently dissolved in MilliQ water. 2-mercaptoehanol was added into the sample at a final concentration of 0.1 % before lyophilization. The samples were stored at -80°C before analysis. The quantity of histone protein was evaluated using PlusOne^{TM} 2D Quant Kit (GE Healthcare Life Sciences, Sweden).

2.2.3 Reversed–phase high performance liquid chromatography (RP-HPLC)

Approximately 100 μg acid-extracted histone mixture was resuspended in 2 ml 0.1 % trifluoroacetic acid (TFA) in water and directly loaded into a RP-HPLC column (C4 Vydac, 4.6×250 mm;5 μm; Grace Vydac, CA) connected to an Agilent 1100 series with diode array detector (Agilent Technologies, USA). The effluent was monitored at 210 nm. Flow rate was 1 ml/min. The column was firstly washed with solvent A (0.1 % TFA in water) for 10 min before running with a gradient increased solvent B (0.05 % TFA in acetonitrile) from 20% to 38% in 18 min, then from 38 % to 50 % in 24 min. The individual histone was eluted from the column by applying the multistep gradient of solvent B. The fractions were collected every minute. 1 μl of the individually collected histone fraction was spotted on a MALDI plate directly; molecular weight was detected by the linear mode of MALDI-TOF/TOF tandem mass spectrometry system of 4700 proteomics analyzer (Applied Biosystems Inc.,

USA). The remaining fractions were dried by lyophilization for SDS-PAGE gel electrophoresis and protein identification by MALDI-TOF/TOF tandem mass spectrometry analysis.

2.2.4 SDS-PAGE gel electrophoresis

The lyophilized histones mixtures were denatured using Laemmli SDS sample buffer; the denatured samples were loaded onto a 15 % SDS-PAGE gel running at 120 V for 2 h. Gels were stained with Coomassie brilliant blue dye and the protein bands were excised for in-gel protein digestion and MALDI-TOF/TOF tandem mass spectrometry analysis.

2.2.5 In-solution protein digestion

RP-HPLC separated individual histone samples were digested with either trypsin (Promega, USA) or endoproteinase Glu-c (Roche Applied Science, USA) to generate the corresponding peptides for MALDI-TOF/TOF tandem mass spectrometry analysis or nano-LC separation. The reactions were conducted in a final volume of 30 µl according to the manufacturer's protocols. The molar ratio of enzyme to substrate was adjusted to 1:10. Reactions were carried out for 14-16 h at 30°C. 1.5 µl of digested sample was analyzed by MALDI-TOF/TOF tandem mass spectrometry while 20 µl digested sample was subjected to nano-LC separation.

2.2.6 In-gel protein digestion

The protein bands on the SDS-PAGE gel were excised, cut into small pieces, and destained with 50 % acetonitrile (ACN)/ 50 mM ammonium bicarbonate (NH_4HCO_3). The gel slices were digested with 20 ng/ μl trypsin in 50 mM NH_4HCO_3 for 14-16 h at 30°C. The histone peptides were extracted from the gel with 2.5 % TFA in 50 % ACN for MALDI TOF/TOF tandem mass spectrometry analysis.

2.2.7 Nano liquid chromatography (Nano-LC)

Solvent A and solvent B were used as running buffer. Solvent A was 0.05 % TFA and 2 % ACN in water; Solvent B was 0.05 % TFA in 80 % ACN. The digested histone peptides were separated at the gradient of 30 %-80 % solvent B in 30 min by the Nano liquid chromatography (LC) system (LC Packing Inc., USA) using C18 column (Column 1: ID 300 μm Length: 10 cm; Column 2: ID 75 μm, Length: 15 cm, 3 μm, 100 A.). The effluent was monitored at 210 nm using Ultimate^{TM} UV detector. The fractions were collected automatically by probot and analyzed by the MALDI-TOF/TOF tandem mass spectrometry.

2.2.8 MALDI-TOF/TOF tandem mass spectrometry analysis

One microliter of each RP-HPLC fraction or enzyme digested sample was spotted on a MALDI plate followed by 0.5 μl α-cyano-4-hydroxycinamic acid (Sigma, USA). Linear mode of mass spectrometry was used to confirm the molecular weight of the individual histone in each fraction collected from the RP-HPLC. The mass range was acquired from 4000 to 28000 Da and the laser intensity was 4600. Reflector positive ion mode of mass spectrometry was used to detect digested peptides for histone protein identification. Peptides ranged from 500 *m/z* to 3500 *m/z* were acquired, signal intensity of peptides in each spectrum was accumulated with 1500-2500 laser shots at a fixed laser intensity of about 4000-4500. Monoisotopic peptides were detected with a mass tolerance of 30 ppm without smooth. Eight peptides with strong intensities (minimum s/n ratio was 50) were selected as precursor ions for further MS/MS analysis. Ion signals were accumulated with 4000-5000 laser shots at a fixed laser intensity of about 4500-4800. Then histone proteins were further identified by peptide-mass-finger printing (PMF) analysis using GPS Explore™ software v2.0 (Applied Biosystems Inc., CA) and Mascot search engine. NCBI nr protein database was selected and species of mouse was tested. Partial modifications of oxidation on methionine were always taken into account. For phosphorylation analysis, serine (S) and threonine (T) were both selected; Lysine (K) and arginine (R) were selected for methylation analysis and lysine (K) for acetylation analysis. At most one missed cleavage of trypsin /Glu-c digestion was allowed, and a mass tolerance of 50 ppm was used in the database searching. The candidate sequences which include the modification site were confirmed by *de novo*

sequencing.

2.2.9 Western blotting assay

Histone mixture (10 μg) was resolved on 15 % SDS-PAGE gels. The proteins were transferred to a polyvinylidene difluoride membrane (Hybond ECL, Amersham Biosciences Piscataway, USA). The membrane was blocked in 5 % non-fat skimmed milk and was immunoprobed with antibodies specific to mono-, di-, and tri-methyl H4K20 (1:5000) or tri-methyl H3K27, H3K36 (1:1000) (Upstate, Biotechnology, Inc, USA). Alkaline phosphate-conjugated rabbit IgG (Santa Cruz Biotechnology, CA) at 1:3000 dilutions was used as secondary antibody. The signal was detected by the NBT/BCIP tablet (Roche Applied Science, USA). The members were scanned and analyzed by Bio-Rad Quantity One 4.4.0 software (Bio-Rad, USA).

2.2.10 Statistics

All data are expressed as mean ± standard deviation (SD). The data were analyzed by Statistical Package for the Social Science (SPSS) for Windows (version 11.5, Chicago, USA). Student-Newman-Keuls (SNK) test and Least-significant difference (LSD) test of one way analysis of variance (ANOVA) were used to compare the difference among mean values. Statistical significance was accepted at $p<0.05$.

2.3 Results

2.3.1 Preparation of histones

Acid-extracted histone mixtures (see Materials and Methods section) were separated by RP-HPLC with C4 column. The representative chromatogram was shown in Fig.2.1. Six major peaks could be separated by RP-HPLC. The individual histone was identified by linear mode of MALDI TOF MS (Fig.2.2), SDS-PAGE gel electrophoresis and MALDI TOF MS/MS (Fig.2.3a and b). Linker histone H1 (peak 1) was more hydrophilic and was therefore firstly eluted at 25 min after injection which was followed by H2B (peak 2), H2A (peak 3), H4 (peak 4) and finally H2A (peak 5). Peak 6 was resulted from the elution of H3, which indicated that H3 was the most hydrophobic one among the core histone molecules separated. Part of H4 could be co-eluted with H2A which is probably due to their similar hydrophobic ability (Fig.2.2 fraction 36 and Fig.2.3a). Peak 3 and peak 5 were confirmed to be the two variants of H2A (Fig.2.2 fraction 34 and fraction 37).

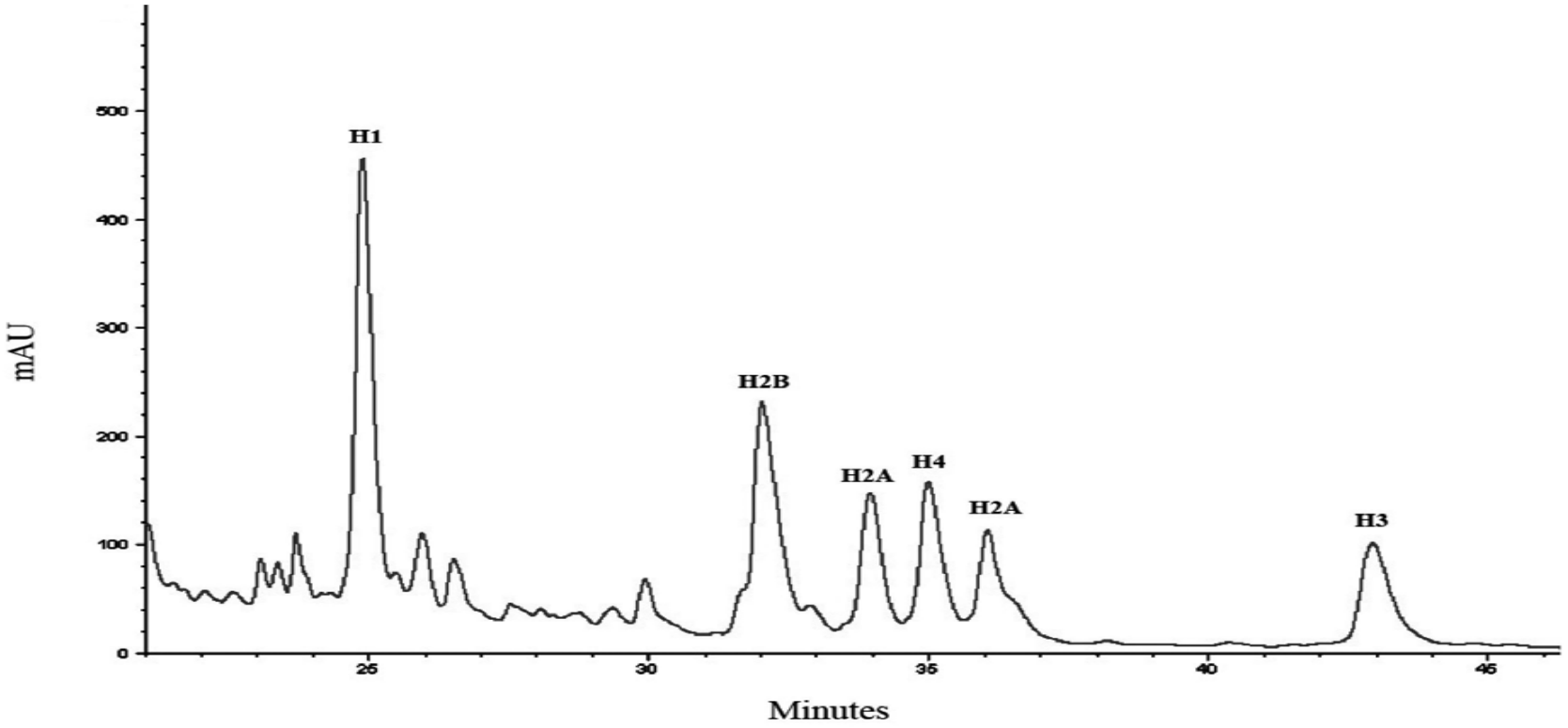

Fig.2.1 Chromatogram of histones separation by RP-HPLC. 100 µg acid extracted histone mixture from SAMP8 mice brain was separated on a C4 reversed-phase column (Scale: absorbance at 210 nm. The detector of RP-HPLC was G1315A diode array detector). The program was run 1 ml per minute starting with solvent A (0.1 % TFA in water) in 10 min before running with a gradient increased from 20 % to 38 % solvent B (0.05 % TFA in acetonitrile) in 18 min, then from 38 % to 50 % solvent B in 24 min. The fractions were collected every minute.

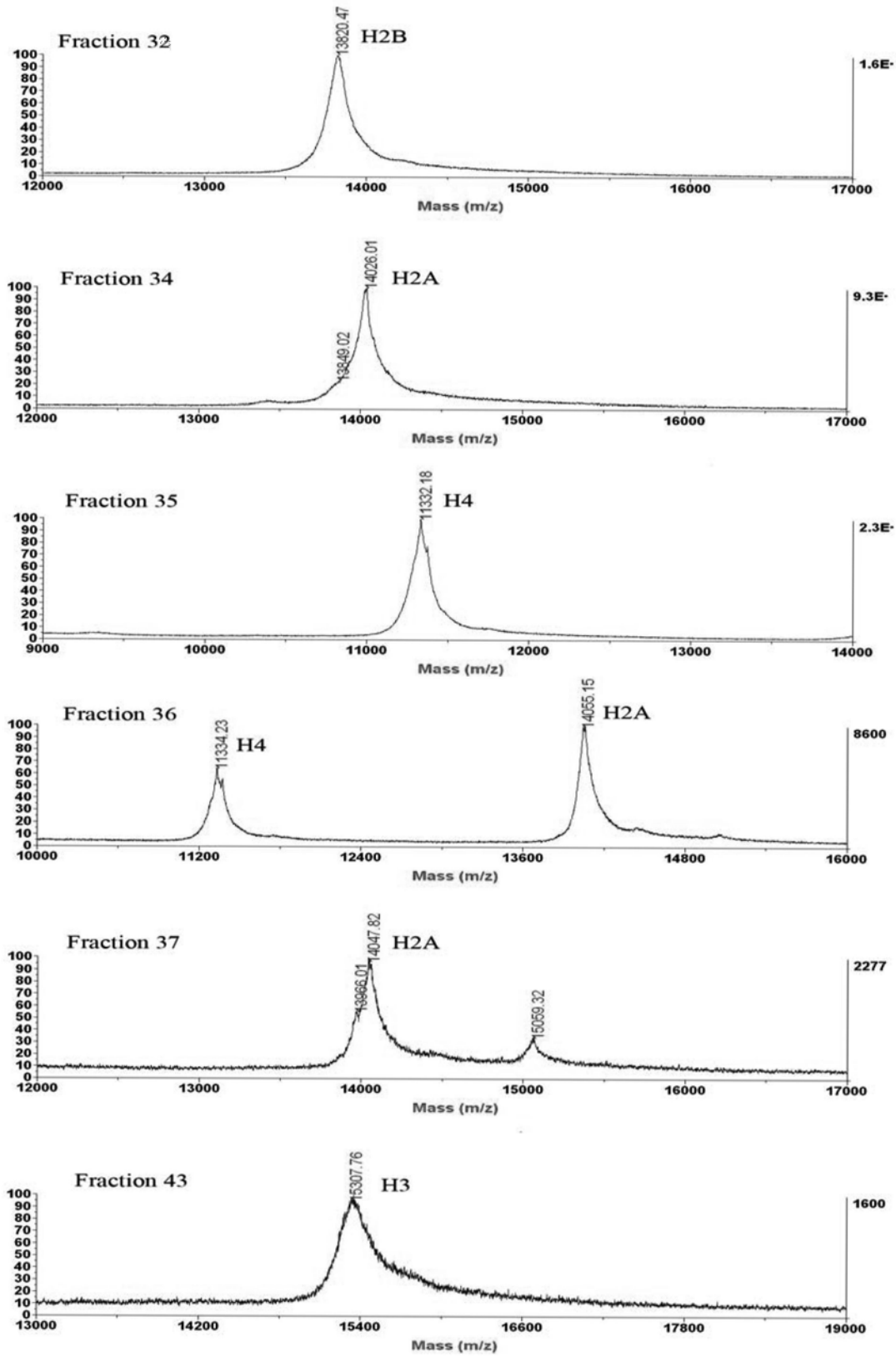

Fig.2.2 Molecular weight detection of histones in HPLC fractions by linear mode of MALDI-TOF/TOF MS.

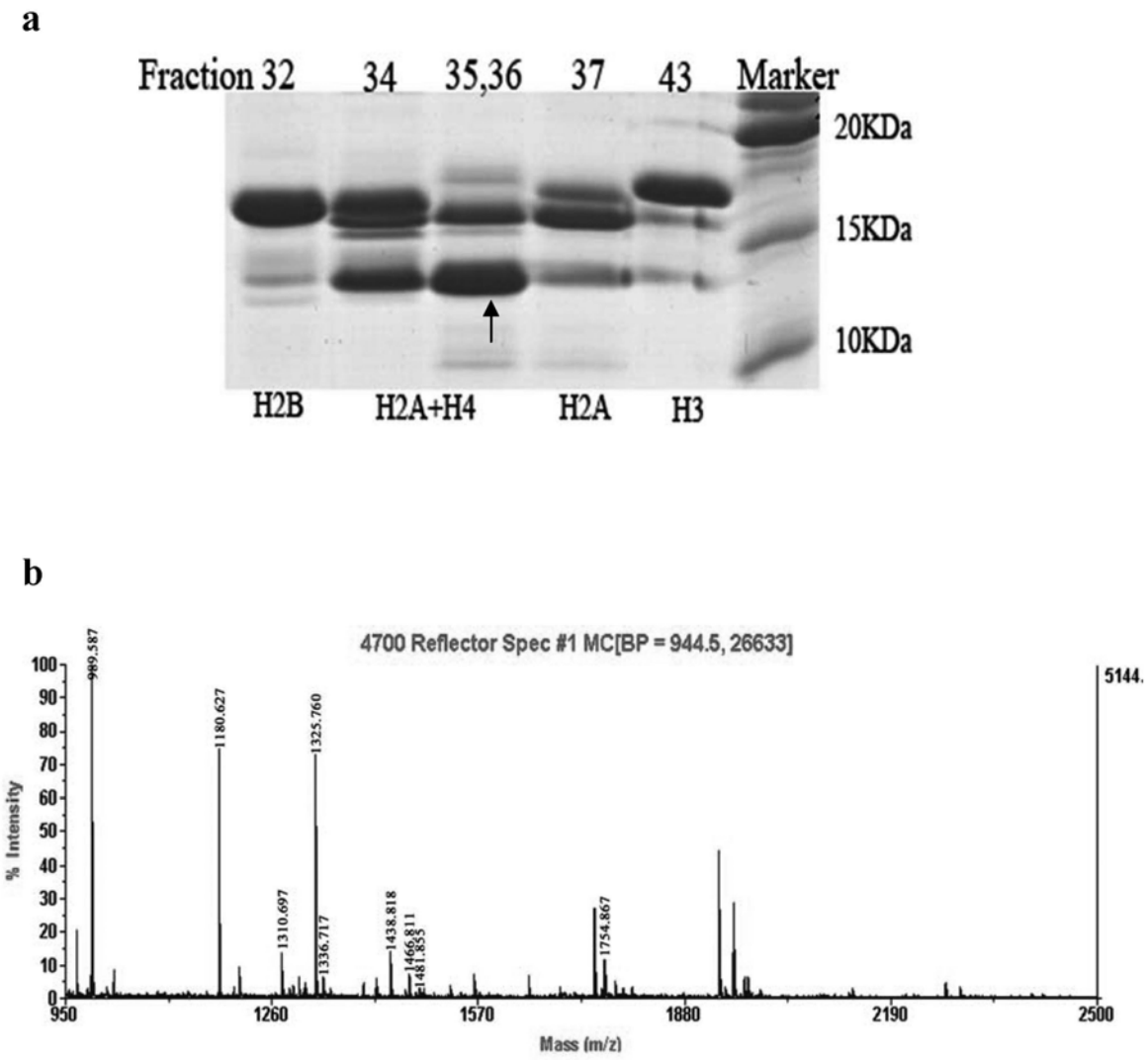

Fig.2.3 Identification of histones in RP-HPLC fractions. Collected fractions were lyophilized and parts of the fractions re-dissolved fraction were run on a 15 % SDS-PAGE gel, stained by Coomassie brilliant blue. **a.** The band was cut off and digested by trypsin for 14-16 h at 30°C after destaining. The peptides were extracted from the gels with 2.5 % TFA in 50 % ACN and identified by the reflector mode of MALDI-TOF/TOF MS. **b.** MS spectrum of the band in **a.** which was indicated by an arrow. Nine labeled peptides were matched with H4 protein.

2.3.2 Identification of post-translational modifications using the combination of nano-LC and MALDI-TOF/TOF MS

After obtaining the purified individual histone molecules, the type and the site of PTMs on individual histone were investigated. The digested histone peptides were firstly separated by nano-LC before mass spectrometric analysis. The procedure of histone PTMs identification was summarized in Fig.2.4. Defined PTMs on the modified histone peptides were identified by calculating monoisotopic mass shift (Δm) in comparison with the theoretical masses of unmodified histone peptide. Peptide fragment ions showed in Fig. 2.5. The calculated mass shift resulted from the specific modifications were listed in Table.2.1. The exact modification site could be confirmed by the mass shift of the particular peptide fragment ions which were obtained from the MALDI-TOF/TOF MS analysis.

Table 2.1 Mass change of some PTMs

Modification	Structure	Monoisotopic mass shift (Δm)
Methylation	$-CH_3$	14.0157
Di-methylation	$-2CH_3$	28.0314
Tri-methylation	$-3CH_3$	42.0471/43.054
Acetylation	$-COCH_3$	42.0106
Phosphorylation	$-H_2PO_4$	79.9963

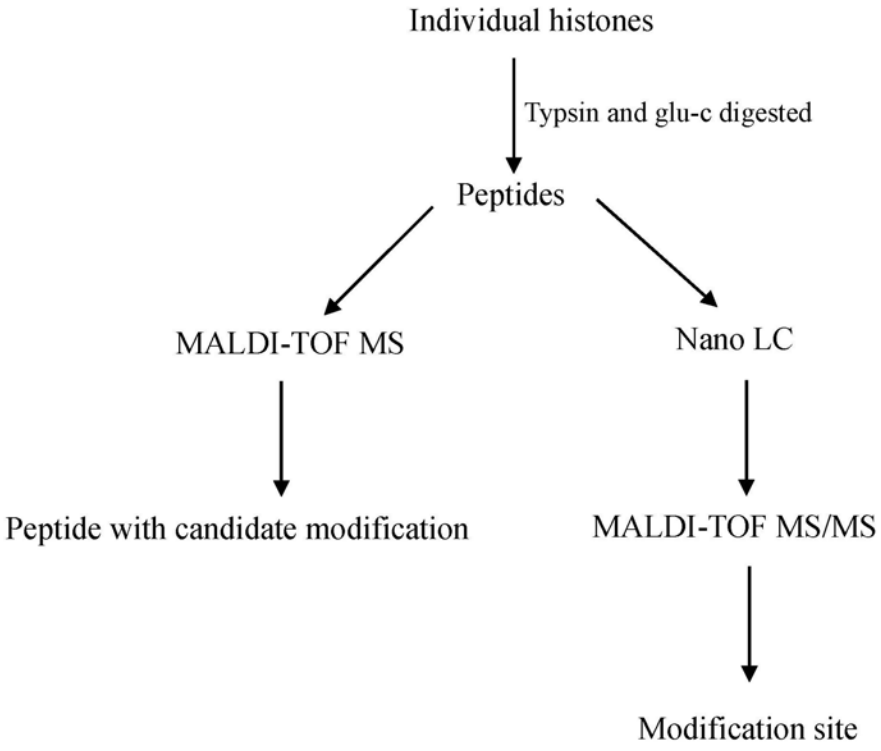

Fig.2.4 Schematic illustration of the analysis of histone PTMs by the combination of nano-LC and MALDI-TOF/TOF MS.

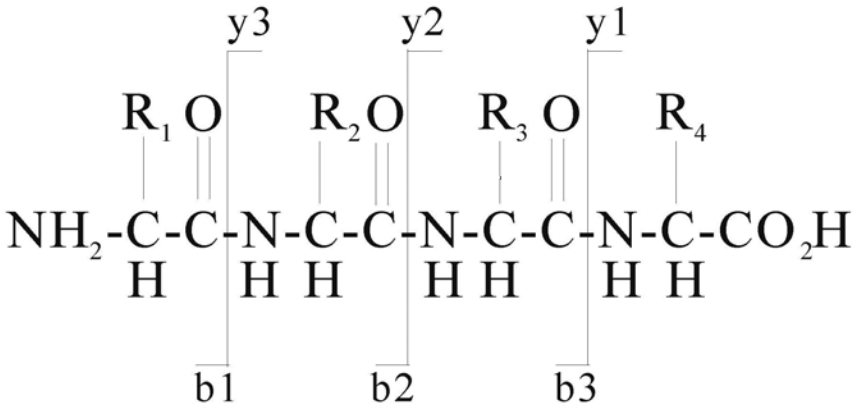

Fig 2.5 Peptide fragment ions. Collision induced dissociation (CID) forms mainly b and y ions and b2-b1= amino acid.

Fig.2.6 demonstrated the detection of histone H3K79 methylation. The peptide mass fingerprints were obtained from trypsin digestion of histone H3 which was isolated from the brain of 12-month-old SAMP8 mice. The peaks at *m/z* 1335.738, 1349.752 and 1363.752, each separated by 14 Da, indicated potential mono- and di-methylation (Fig.2.6a). These three peaks were subjected to further MS/MS analysis. The y-ion series of these three peaks displayed in TOF/TOF CID spectra pinpointed the exact location of methylation site and the corresponding multiplicities (Fig.2.6b). In Fig. 5b, the mass of the first four members of peak series, y1 (175.13), y2 (288.22), y3 (403.25), and y4 (504.30), were the same in all three CID spectra of *m/z* 1335.738, 1349.752 and 1363.752, whereas from y5 ion onwards their masses showed systematic differences of 14 or 28 Da. The first peak at *m/z* 1335.738 was deduced to be the unmodified sequence, ^{73}EIAQDFKTDLR^{83}, and two peptides of *m/z* 1349.752 and *m/z* 1363.752 were the modified peptide sequences with mono- and di-methylation, respectively. The methylation occurred at the 79th amino acid of H3, which was lysine (K79). In the glu-c digested H3 spectrum, the peaks at *m/z* 2322.176, 2336.187 and 2350.192 were observed (Fig.2.6c). The peak at *m/z* 2322.176 confirmed the unmodified sequences to be ^{74}IAQDFKTDLRFQSAAIGALQE^{94}, which included K79 site. The other two peaks were the mono- and di-methylated H3K79 peptides, and the methylation also occurred at the 79th lysine. Previous studies suggested that ubiquitination of H2B on K123 was needed for H3K79 trimethylation in yeast and ubiquitination of H2B on K120 was essential for normal levels of H3K79 dimethylation in humans

(Shahbazian *et al.*, 2005; Zhu *et al.*, 2005). In the aged brain of SAMP8, only mono- and di-methylated H3K79 could be detected and no ubiquitnated H2B peptides were found in the mass spectra.

Through the combination of nano-LC with MALDI-TOF/TOF tandem mass spectrometry analysis, the type, site and the corresponding multiplicities of histone PTMs in the 12-month-old SAMP8 mice brain were detected, and results were summarized in Table 2.2. Most of the modifications, especially methylation, lied on the histone H3. The major sites of methylation were K24, K27, K36, K79 and R128 of histone H3, K20 of histone H4, R89 of histone H2A. The major sites of acetylation were K14, K18 of histone H3 and one phosphorylated site was found at S38 on histone H2B.

In addition to the MS analysis, Western blotting was performed to further confirm and quantify the above identified modifications. Several commercial antibodies, such as anti-methylated H4K20 (mono-, di- and tri-), anti-trimethylated H3K27, H3K36 antibodies were used (Fig.2.7, and Fig.2.8).

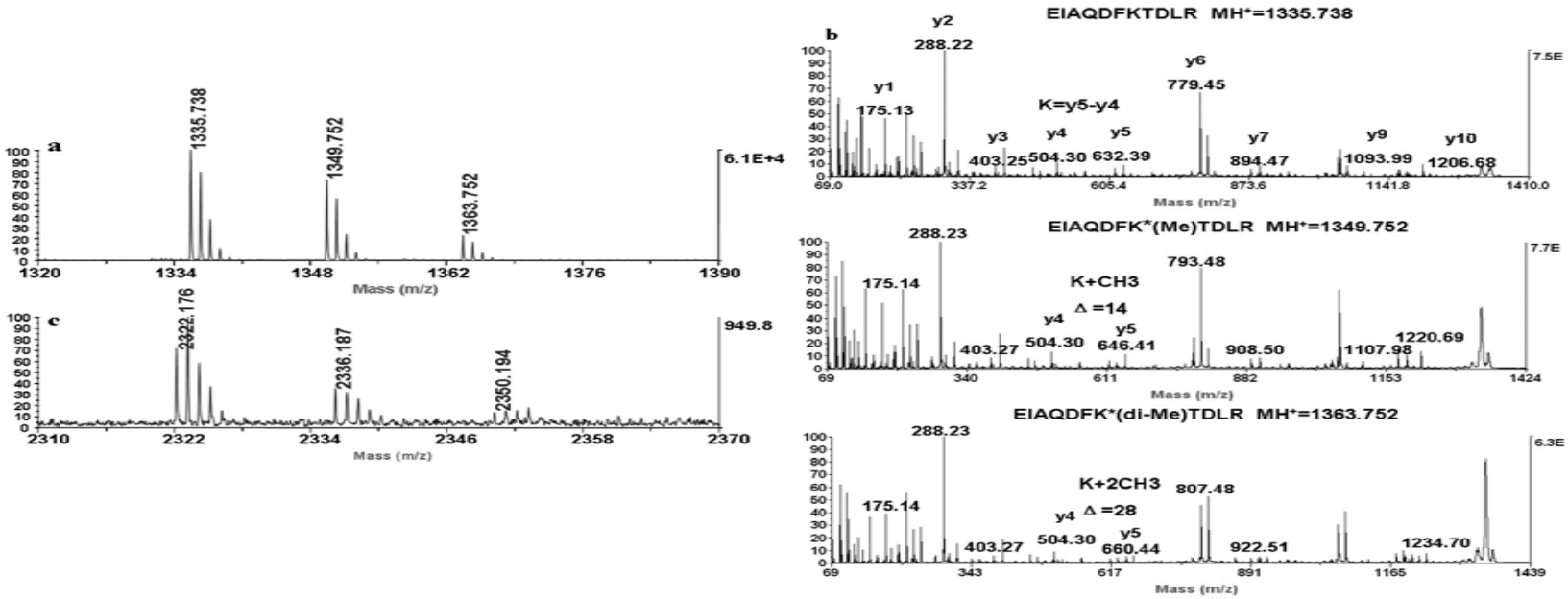

Fig.2.6 Identification of mono- and di-methylated H3K79 by MS. a. Part of trypsin digested H3 MS spectra showed the peaks at *m/z* 1335.738, 1349.752 and 1363.752, each separated by 14 Da, which indicated the potential mono- and di-methylation. **b.** TOF/TOF CID spectra of three peaks. The original peak at *m/z* 1335.738 deduced the peptide ^{73}EIAQDFK*TDLR^{83}. In the TOF/TOF CID spectra of three peaks, the mass of the first four members of peak series, y1 (175.13), y2 (288.22), y3 (403.25), and y4 (504.30) were all the same, whereas from y5 ion (*m/z* 632.39, *m/z* 646.41, *m/z* 660.44) up, they showed systematic differences of 14 or 28Da, which proved that K79 was mono-methylated and di-methylated. **c.** Part of Glu-c digested H3 MS spectra. The first peak at *m/z* 2322.176 deduced the sequence to be ^{74}IAQDFK*TDLRFQSAAIGALQ E^{94}. The *m/z* 2336.187 and 2350.19 corresponded to the addition of one and two methyl group on lysine residues, respectively. All experiments were performed three times.

Table 2.2 Summary of detected histone modifications in the 12-month-old SAMP8 mice

Histone	Modification	Site	Degree	Possible functions	References
H3	Methylation	K24	Mono-	?	-
		K27	Mono-, di- tri-	Transcriptional silencing X inactivation (tri-Me)	Müller *et al*., 2002 ; Plath *et al*., 2003
		K36	Mono-, di- tri-	Transcriptional elongation	Bell *et al*., 2007
		K79	Mono-, di-	Euchromatin Transcriptional elongation DNA repair	Frederiks *et al*., 2008; Wysocki *et al*., 2005
		R128	Mono-	?	-
	Acetylation	K14	-	Transcriptional activation DNA repair	Kurdistani *et al*.,2004; Sanders *et al*., 2004
		K18	-	Transcriptional activation	Kurdistani *et* al.,2004
H4	Methylation	K20	Mono-, di- tri-	Transcriptional silencing (mono-Me) Heterochromatin (tri-Me) Transcriptional activation DNA repair	Yang and Mizzen 2009; Kourmouli *et al*.,2004
H2A	Methylation	R89	Mono-	?	-
H2B	Phosphorylation	S38	-	?	-

Note: ? indicates no function has been reported.

2.3.3 Mono-methylated H4K20 decreased in brain of 12-month-old SAMP8 mice when compared with 3-month-old SAMP8 mice

Previous studies had detected a significant increase of tri-methylated H4K20 in the liver and kidneys of old-aged rats (Sarg *et al*., 2002). In this study, three types of H4K20 methylation (mono-, di- and tri-methylation) could also be found in the brain of 12-month-old SAMP8 mouse (Fig.2.7a). In the brain of the 3, 12-month-old SAMP8 mice and age-matched control SAMR1 mice, tri-methylated H4K20 was found to be the dominant methylation event, followed by the di-methylated K20 whereas the mono-methyl derivative was merely observable. However, tri- and di-methylated forms of H4K20 did not essentially change in both of the brain of young (3-month-old) and old (12-month-old) mouse. While the amount of mono-methylated form decreased significantly in brain of 12-month-old SAMP8 mice when compared with that of 3-month-old SAMP8 mice (Fig.2.7b).

A

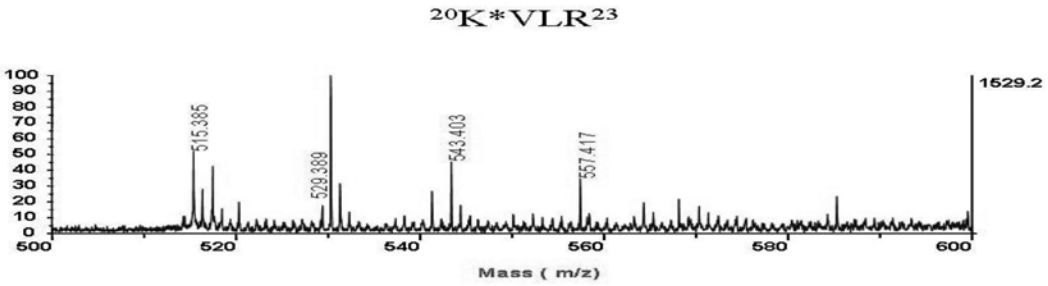

B

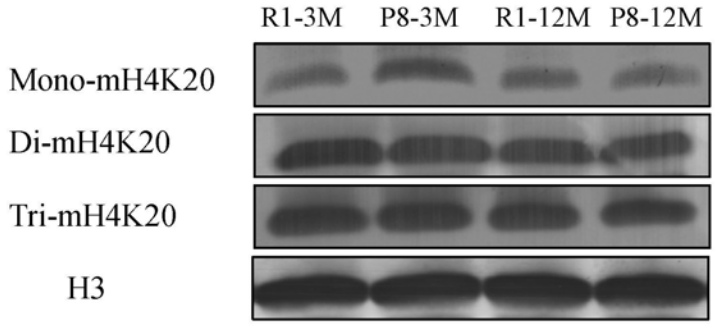

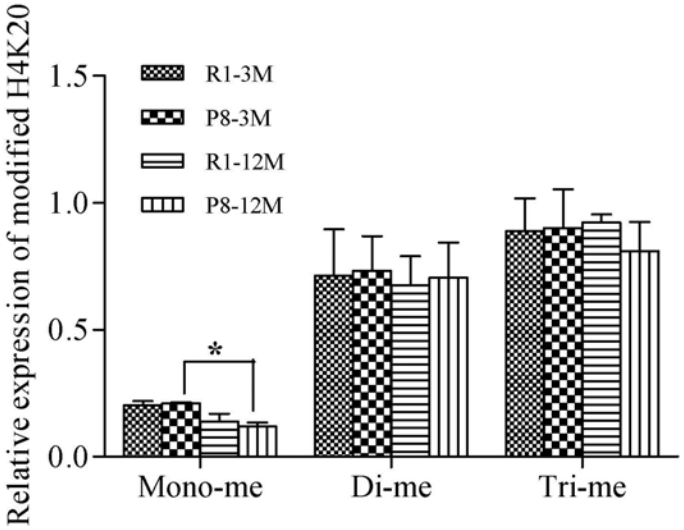

Fig.2.7 Identification and confirmation of H4K20 methylation. a. MALDI-TOF/ TOF MS spectra display of H4 peptide ^{20}KVLR^{23} in typsin digested spectra and subsequent masses of modifications. The peak at *m/z* 515.38 was identified as the peptide ^{20}KVLR^{23}. Other peaks were assigned to be one, two and three methyl groups at the peptides. **b.** The expression of the mono-, di- and tri-methylated H4K20 in the brain of 3- and 12-month-old SAMP8 mice and age-matched mice SAMR1 was detected by western blotting. H3 was used as control. *$p<0.05$. n=6.

2.3.4 The methylation of both H3K27 and H3K36 could coexist in the mouse brain with different methylation multiplicities

From MS results, two coexisting methylated sites, K27 and K36, on the histone H3 were observed (Fig.2.8a). A series of peaks separated by 14/15 Da at *m/z* 1446.696, 1460.709, 1475.802, 1489.898, 1503.892, 1518.881 were detected. These peptides emerged from the common sequence of ^{27}KSAPATGGVKKPHR^{40}. The individual peptide contained one to six methyl groups shared by the two lysine residues (K27 and K36). The original unmodified peak of the peptide ^{27}KSAPATGGVKKPHR^{40}, MH^+=1432.826, could not be detected from the MS spectra. By comparing the spectra of the four groups (Fig.2.8a), we found that hypermethylated forms of H3 increased in the old-aged groups (especially in P8-12M group). The abundance of tri-methylated H3K27 increased with aging while the abundance of tri-methylated H3K36 decreased (Fig.2.8b), which indicated tri-methylated H3K27 might contribute to the hypermethylated state of H3 at old-age stage.

a

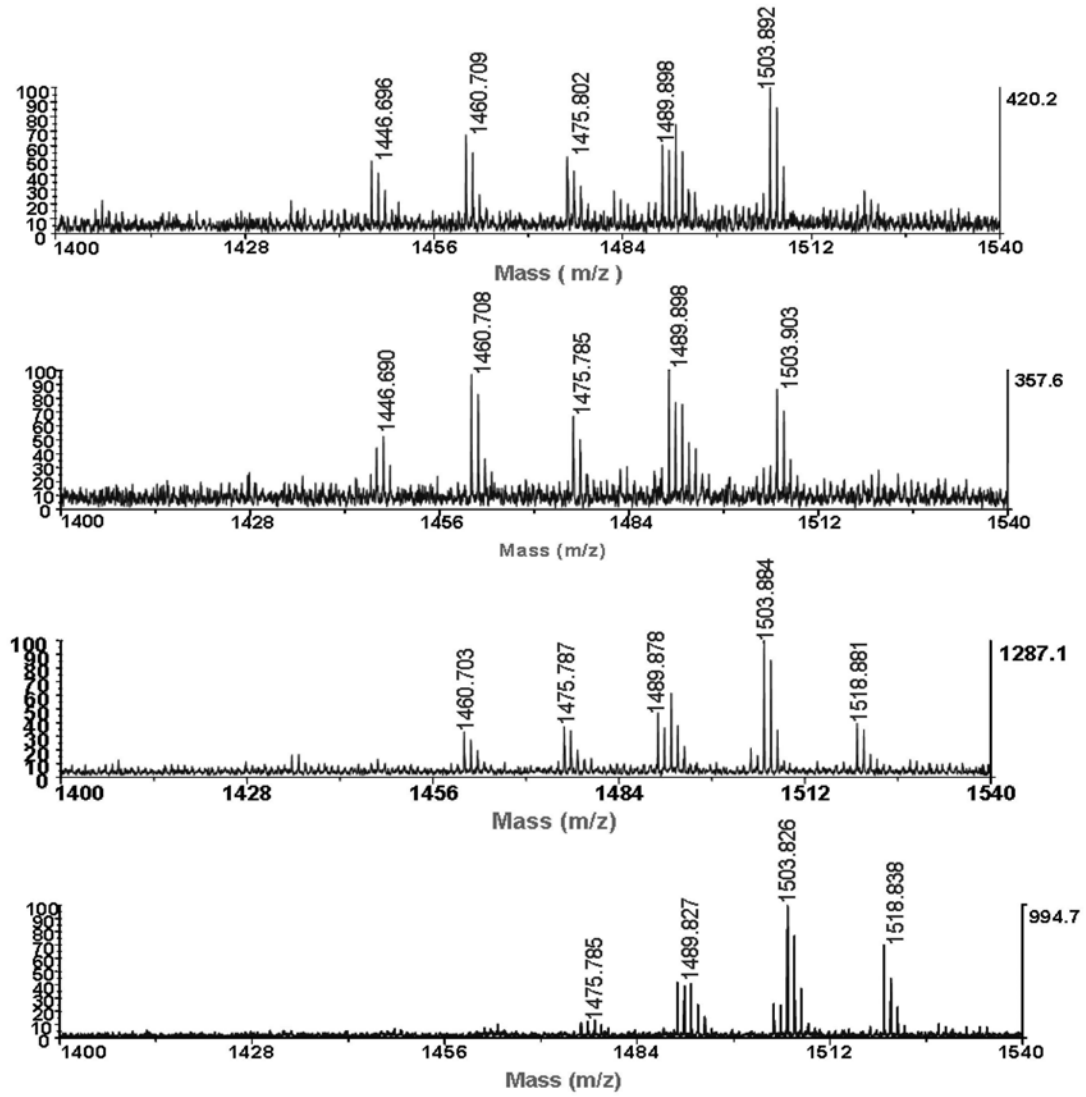

Fig.2.8 H3K27 and H3K36 methylation detection. a. H3K27 and H3K36 methylation sites coexisted. A series of the peaks separated by 14 Da at *m/z* 1446.696, 1460.709, 1475.802, 1489.898, 1503.892, 1518.881 indicated that 1 to 6 methyl groups were added on the original peak *m/z* 1432.826. The peptide ^{27}KSAPATGGVKKPHR^{40} could be deduced from MALDI-TOF/TOF MS/MS data, and the modification happened on the first lysine and the tenth lysine of the peptide, which were exactly the K27 and K36 on histone H3.

b

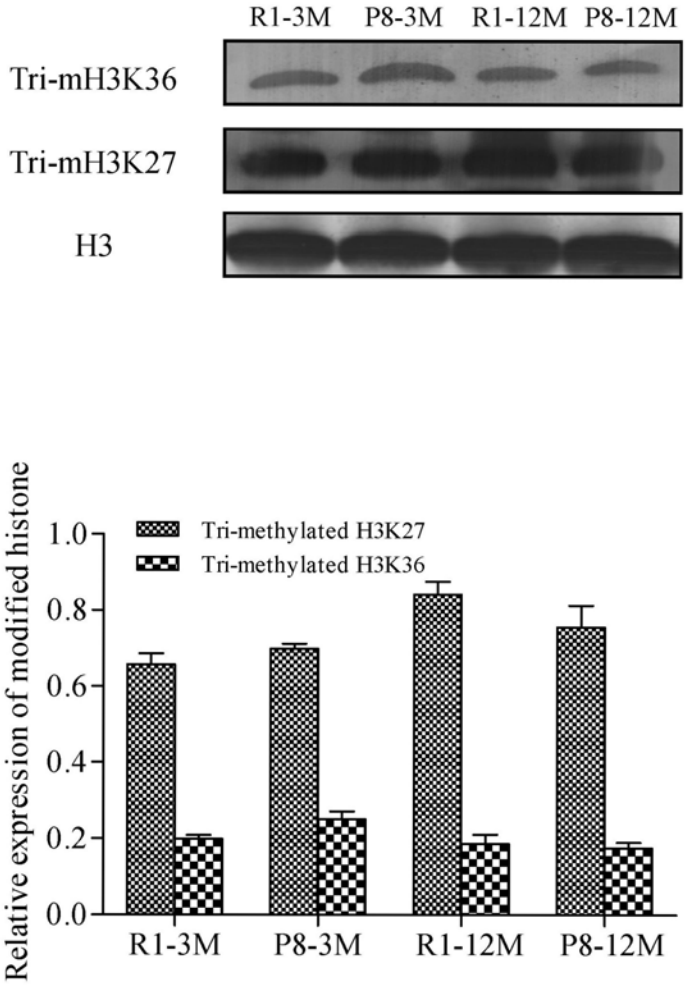

Fig.2.8 H3K27 and H3K36 methylation detection. b. Western blotting results of the expression of tri-methylated H3K27 and tri-methylated H3K36 in the mouse brain. H3 was used as control (n=6).

2.4 Discussion

Aging epigenetics is becoming an emerging discipline to disclose the mechanisms involved in aging process and histone modification maps could act as aging markers (Fraga and Esteller, 2007). However, no systematic investigations on the patterns of histone PTMs in the brain upon aging have been reported and the mechanisms of histone PTMs involved in aging are still unclear. In this study, we initiated the first analysis on the histone PTMs states, in particular methylation, in the brain of aged SAMP8 mice. MALDI TOF/TOF tandem mass spectrometry was used to decipher the specific PTMs in the aged SAMP8 mice brain. MS analysis can determine both the exact sites and types of PTMs along the polypeptide and yield comprehensive sub-sequence information with high mass accuracy and allow high sensitivity (Burlingame *et al.*, 2005; Cocklin and Wang, 2003; Huang *et al.*, 2002; Johnson *et al.*, 2004). Increasing PTMs sites and PTM types are being confirmed by utilizing this technology.

In brains of 12-month-old SAMP8, most PTM sites were found on histone H3 (Table 2.2). H3 has the longest N-terminal tails amongst other core histone molecules. Such N-terminal arm of H3 could protrude from the nucleosome and be modified at specific amino acids, which explained why more PTMs were found on histone H3. In addition to the N-terminal tails of histones, the globular C-terminal domain of the histone molecule (H2A and H3) could also be modified. Three methylated sites out of the N-terminal tails, H3K79, H3R128 and H2AR89, were detected in this investigation (Table 2.2). These modifications may control the binding of

non-histone proteins to nucleosome in the similar way to N-terminal tail modifications; they were also expected to have direct structural effects by influencing nucleosome-nucleosome interactions (Mersfelder and Parthun, 2006).

Methylation was thought to be stable and represent a heritable epigenetic mark compared with acetylation (Roopra *et al.* 2004). Five lysine (K) residues on the tails of histone H3 and H4 (H3K4, H3K9, H3K27, H3K36 and H4K20), as well as H3K79, were confirmed for methylation (Shi, 2007). Most of these methylations could be detected in the brain of 12-month-old SAMP8 mice (Table 2.2). Three new methylated sites, H3K24, H3K128 and H2AR89, were also detected in this study; however, no functional studies on these three sites had been reported.

In aged human brain, the genes involved in synaptic transmission, Ca^{2+} homeostasis/signaling and neuronal survival were down-regulated and the genes involved in stress response and inflammation were up-regulated (Bonneuil, 2007; Lu *et al.*, 2004). Previous researches had shown that methylated H3K36 and H3K79 were associated with increased gene transcription (Jin *et al.*, 2007), whereas the methylation of H3K27 and H4K20 were described as the sites for gene repression and/or heterochromatin (Klose and Zhang, 2007; Vakoc *et al.*, 2006). In the brains of 12-month old SAMP8 mice, the expression of methylated H3K27 increased while the expression of methylated H3K36 decreased in the aged mouse brain (Fig.2.8). And the coexisting methylations of H3K27 and H3K36 with different degree of methylation multiplicities were observed (Fig.2.8). It was suggested H3K27 methylation might inhibit the methylation of H3K36 in brain upon aging. Previous

researches had indicated that H3K27 could be methylated on transcriptional repressed regions such as inactivated homeobox loci or X-chromosome, while methylated H3K36 was linked to gene activation (Bannister *et al.*, 2005). H3K27 methylation may also played a vital role in transcriptional termination and/or early RNA processing in *Saccharomyces cerevisiae* and some higher eukaryotes, such as chicken, and methylated H3K36 was essential for normal growth and development in *Neurospora crassa* (Adhvaryu *et al.*, 2005). Therefore, hypermethylated H3K27 may maintain the state of transcriptional repression by preventing H3K36 methylation and partially contribute to the gene silencing during aging, thus the modification of these two sites demonstrated a modulating event. EED-EZH2 complex is the histone H3K27-specific methyltransferase and Set2 could specifically methylate H3K36 (Cao and Zhang, 2004; Krogan *et al.*, 2003). The methylation of H3K27 may inhibit the binding of H3K36-specific methyltransferase Set2 or block H3K36 site due to the re-structuring of histone or nucleosome after H3K27 methylation. But this hypothesis needs further investigation and confirmation.

During aging, brain cells were continuously exposed to reactive oxygen species which was generated from oxidative metabolism. DNA was a potential target upon oxidative damage. The decreased potential of DNA repair was one of the major factors contributing to the aging and the degeneracy of brain (Katyal and McKinnon, 2007; Vyjayanti and Rao, 2006). Both single and double strand breaks of nuclear DNA were found to be accumulated in rat neurons with age (Mandavilli and Rao, 1996; Rao, 2007). Methylations of H3K79 and H4K20 had been reported to link to

the DNA-damage response (Bostelman *et al.*, 2007; Sanders *et al.*, 2004). H3K79 methylation played important roles in the nucleotide excision, post-replication and recombination repair pathways, as well as RAD9-mediated checkpoint function during UV-damage repairing (Bostelman *et al.*, 2007). Methylated H4K20 was required for the recruitment of checkpoint protein Crb2 (Sanders *et al.*, 2004). Loss of Set9 (H4K20 methylation transferase) activity or marked mutation of H4K20 could impair the survival of cells after genotoxic challenge and compromise the ability of cells to maintain checkpoint mediated cell cycle arrest. Mono-methylated H4K20 was also needed in the maintenance of proper higher order structure of DNA and was consequently essential for chromosome condensation (Sakaguchi and Steward, 2007). In this study, these two modifications (H4K20 and H3K79 methylation) were detected. Their decrease indicated that DNA could not maintain the proper higher order structure and DNA repair potential ability was decreased in aged brain, which could induce cell death / apoptosis and consequently made the dysfunction of brain.

Other researchers had found that in kidneys and liver of aged rat, di-methylated H4K20 was the main methylation product; the amount of mono- and di-methylated forms did not effectively change whereas tri-methylated H4K20 significantly increased during aging (Sarg, 2002). In this study, tri-methylated form of H4K20 was the main methylation product among these three methylated forms. The amount of mono-methylatd H4K20 decreased significantly from young (3-month-old) to old (12-month-old) SAMP8 mice while no significantly change was detected on the two

other forms (Fig. 2.7b). Though the exact functions of each H4K20 methylated form was still unknown, different patterns of H4K20 methylation in the aged organ (brain, liver and kidneys) suggested the diverse functions of the H4K20 methylation multiplicities in different organs upon aging.

SAMP8's brains had increased abundance of amyloid precursor protein (APP) (Kumar *et al.*, 2000). APP could increase oxidative stress in the brain. Protein carbonylation, an index of protein oxidation, had elevated in pathological conditions and aging, which also increased in brains of 12-month-old SAMP8 mice (Poon *et al.*, 2004). Histones H1, H2B/H2A, and H3 could be modified by carbonyl groups (Wondrak *et al.*, 2000; Sharma *et al.*, 2006) and the carbonyl modification in rat liver histones was significantly lower in old (30-month-old) than in young (5-month-old) animals (Sharma *et al.*, 2006). C-terminal fragments of amyloid precursor protein induced the acetylation of H3 and H4 and enhanced the neurotoxicity caused by C-terminal fragments of APP was found by histone deacetylation inhibitors (Kim *et al.*, 2004). The cytoplasmic tail of APP could form a complex with the nuclear adaptor protein Fe65 and the histone acetyltransferase Tip60 which could potently stimulate transcription (Cao and Südhof, 2001). Therefore, the interaction of Fe65 with APP assisted the recruitment of Tip60-TRRAP to DNA damage sites (Stante *et al.*, 2009). But no report had been found on the relationship of increased APP with histone methylation, which needs to be investigated in future.

In this study, core histones (H2A, H2B, H3 and H4) extracted from the whole mouse brain at defined developmental stages were used. After obtaining the patterns

of such histone methylation in the aged brain, target-oriented approaches could be adopted to detect the concerted PTM activities in specific cell type (neuron or neuroglia cell) or specific brain region which was involved in defined biological functions.

Previously researches had demonstrated the alterations of the gene expression and/or protein abnormalities in the brain of SAMP8 mice (Butterfield and Poon, 2005), but few experiments had investigated the relationship between gene and/or protein abnormalities and histone PTMs. According to histone code theory (Jenuwein and Allis, 2001), the ability of one modification to antagonize or synergize the deposition of another modification can have important biological consequences, and dynamic transitions among various modification states could regulate the spatial and temporal behavior of proteins in general, histones in particular. Now, aberrant patterns of histone modifications in cancer have been well investigated. They are becoming the crucial parameters in cancer diagnosis and prognosis. Novel strategies for epigenetic therapy to cancer are developing based on these results (Herranz and Esteller, 2007; Smith *et al.*, 2007). In order to understand the physiological implications of the histone modifications in aged brain, other PTMs, such as acetylation, phosphorylation, ubiquitination, carbonylation, the aberrant patterns of different combinations of histone modifications combination, and further their functions on gene regulation and DNA repair should also be investigated in the future.

Chapter 3 The investigation of tissue distribution and localization of methylated H3K79 and its interaction proteins

3.1 Introduction

H3K79 methylation was the first modification site which was located outside the N-terminus of histones (Feng *et al.*, 2002). It occurred in a wide variety of eukaryotic species organisms (Ng *et al.*, 2002a; van Leeuwen *et al.*, 2002.). Three types of methylated histone H3K79, mono-, di- and tri-methylation, were generated by Dot1 (**d**isruptor **o**f **t**elomeric silencing), a family of methyltransferases (HMTases) without a SET domain (Feng *et al.*, 2002). This enzyme introduced one, two or three methyl groups to H3 lysine 79 via a nonprocessive mechanism and no specific functions of these three methylation states of H3K79 have been attributed so far to (Frederiks *et al.*, 2008). In *S. cerevisiae*, previous transient ubiquitination of H2B at lysine 123 could affect the tri-methylation of H3K79 by enhancing synthesis of all H3K79 methylation states (Frederiks *et al.*, 2008). Similar localization of all methylated states of H3K79 along the length of *GAL* gene cluster indicated that their functions might overlap (Shahbazian *et al.*, 2005).

Based on the published nucleosome structure (Luger *et al.*, 1997), lysine 79 was located in a loop connecting the first and the second α helixes in the H3 structure. This region was exposed and adjacent to the interface between H3/H4 tetramer and H2A/H2B dimmer which could influence the access of molecules to the interface. So the methylation on H3K79 might alter the properties of the nucleosome and plays an important role in regulating the access of other DNA binding factors to chromatin

(Feng *et al.*, 2002).

Previous researches demonstrated that arginine methylation of H3 and H4 was associated with transcriptional activation, while lysine methylation of histones might have either positive or negative effects on transcription, depending on the methylation site(s) (Kouzarides, 2002). Most methylations were generally associated with transcriptional repression, such as methylation of H3K9, H3K27 and H4K20, whereas methylation of H3K4, H3K36 had been implicated in the transcriptional activation process (Snowden *et al.*, 2002; Cao *et al.*, 2002; Kalakonda *et al.*, 2008; Shilatifard, 2008; Morris *et al.*, 2005). The methylation of H3K79 was also involved in transcriptional activation process (Steger *et al.*, 2008). It was a conserved marker of active chromatin regions (Im et al. 2003) and was enriched on H3.3, a histone variant found at transcriptionally active loci in *Drosophila* (McKittrick *et al.*, 2004). In mammalian cells, the recruitment of DOT1L/KMT4 to H3K79 was coupled with the regulation of gene transcription (Steger *et al.*, 2008). The silencing proteins could block the ability of Dot1 to methylated histone H3 and the level of H3K79 methylation was low at all Sir-dependent silenced loci (Ng *et al.*, 2002), whereas this phenomenon was not uniform throughout active chromatin domains (Im *et al.*, 2003).

Except for the chromatin activation, previous studies had suggested that H3K79 methylation was directly involved in the detection of DNA double strand break (DSB) (Game *et al.*, 2005; Giannattasio *et al.*, 2005; Huyen *et al.*, 2004; Wysocki *et al.*, 2005) and played overlapping roles within the nucleotide excision, post-replication and recombination repair pathways, as well as RAD9-mediated checkpoint function (Bostelman *et al.*, 2007). Binding of the conserved checkpoint protein 53BP1 to methylated H3K79 seemed to be an early event by which eukaryotic cells sense and respond to DSBs (Huyen *et al.*, 2004). In yeast, the loss of H3K79 methylation could

prevent phosphorylation of the 53BP1 homolog Rad9, which was required for recruitment and activation of Rad53 kinase (Giannattasio *et al.*, 2005; Wysocki *et al.*, 2005). Researchers found that activation of Rad53 was a key step in the signal transduction cascade during checkpoint activation and Rad53 could be regarded as a marker for DSB (Janzen *et al.*, 2006). Methylated H3K79 could also interact with chromatin assembly factor 1 (CAF-1) in the processes of gene silencing and DNA repair and this association mostly appeared in the late S phase (Zhou *et al.*, 2006). H3K79 methylation accompanied with H2A phosphorylation was required by stable Rad9 accumulation in foci, which correlated with late stages of DSB repair (Toh *et al.*, 2006).

The methylation of H3K79 was also associated with meiotic checkpoint regulation. It was found that H3K79 methylation level decreased during S phase, reached its lowest level in G2 phase, increased during M phase, and maintained at a high level during G1 phase (Feng *et al.*, 2002). Deletion of DOT1B resulted in di-methylation of K76 (corresponding to H3K79 in yeast and mammals) throughout the cell cycle and caused subtle defects in cell cycle regulation and impaired differentiation. The depletion of DOT1A by RNAi could disrupt a mitotic checkpoint, resulting in premature progression through mitosis without DNA replication, and generated a high proportion of cells with a haploid DNA content, an unprecedented state for *Trypanosoma brucei* (Janzen *et al.*, 2006b).

In chapter 2, mono- and di-methylated H3K79 was detected in brain of the 12-month old SAMP8 mice. Therefore, organ distribution, the abundance in the brains of SAMP8 mice and the localization in the cortex and hippocampus of methylated H3K79 were demonstrated in this chapter. At the same time, the proteins which have the interaction with methylated H3K79 were also investigated by

chromatin immunoprecipitation (ChIP) using specific anti-methylated H3K79 antibodies.

3.2 Materials and methods

3.2.1 Animal model

The 3- and 12-month-old senescence-accelerated mice (SAM), including SAMP8 and SAMR1 were housed in an animal room at 23°C with 12-12-h light-dark cycles. Each group included 3 males and 3 females. The mice were terminated via cervical dislocation. The brain samples were divided into four groups: 3-month-old SAMR1 (R1-3M); 3-month-old SAMP8 (P8-3M); 12-month-old SAMR1 (R1-12M); 12-month-old SAMP8 (P8-12M). Other organs, such as liver, stomach, lung, kidneys, intestine, muscle, spleen, heart, bladder, uterus, ovary, testis and eyeballs, were collected from 12-month old mouse. The Institutional Animal Care and Use Committee at the Chinese University of Hong Kong approved all animal procedures in this study. All the samples were stored at -80℃ before use.

3.2.2 Histone extraction

The samples was first homogenized in lysis buffer (10mM Tris-HCl, pH 7.6, 150 mM NaCl, 1.5 mM $MgCl_2$, 0.05 % NP40, and 1 mM phenylmethylsulfonyl fluoride (PMSF), 50 mM sodium bisulfite ($NaHSO_3$), 45 mM sodium butyrate), and nuclei were obtained by centrifugation (1,500×g for 10 min). For the preparation of histones, nuclei were incubated with 4 volumes of 0.2 N sulfuric acid (H_2SO_4) for 2 h at 4°C. The supernatant was precipitated with 20% trichloroacetic acid (TCA) (Final concentration) and followed by centrifugation (12,000×g for 20 min). The obtained pellet was washed with cold acetone and subsequently dissolved in MilliQ water.

2-mercaptoehanol was added into the sample at a final concentration of 0.1% before lyophilization. The samples were stored at -80°C before analysis. The quantity of histone protein was evaluated using PlusOne^{TM} 2D Quant Kit (GE Healthcare Life Sciences, Sweden).

3.2.3 Western blotting analysis

Histone mixture (10 μg) and the proteins precipitated from ChIP experiment were resolved on 15% SDS-PAGE gels. The proteins were transferred to a polyvinylidene difluoride membrane (Hybond ECL, Amersham Biosciences Piscataway, USA). The membrane was blocked in 5% non-fat skimmed milk and was immunoprobed with antibodies specific to mono-, di-methyl H3K79 (1:1000) (Upstate, Biotechnology, Inc, USA), and pbx1/2/3/4 (1:1000) (Santa cruz biotechnology, Inc, USA). Alkaline phosphate-conjugated rabbit IgG (Santa Cruz Biotechnology, CA) at 1:3000 dilutions was used as secondary antibody. The signal was detected by the NBT/BCIP tablet (Roche Applied Science, USA). The members were scanned and analyzed by Bio-Rad Quantity One 4.4.0 software (Bio-Rad, USA).

3.2.4 Tissue fixation and mounting

The brain samples taken from the mice were fixed by 4 % paraformaldehyde (PFA) overnight. The tissues were immersed subsequently by 70 % ethanol, 90 % ethanol and 100 % ethanol. Each step was repeated three times and each time lasted for 30 min. Finally the tissues were immersed in toluene three times for 20 min each.

All the above procedures were performed by the Leica TP1050 enclosed tissue processor (GMI, Inc., USA) automatically at room temperature. After processing, samples were embedded in paraffin wax. 5 μm thick tissue sections were cut using a rotary microtome (Wetzlar, Germany) and mounted onto histological slides with 3-aminopropyltriethoxysilane (Sigma, USA). The slides then were dried overnight at room temperature and stored for the next immunohistochemistry experiment.

3.2.5 Immunohistochemistry

Immunolocalization of di-methylated H3K79 in the cortex and hippocampus was investigated using the rabbit anti-histone H3K79 di-methylation antibodies. Sections were deparaffinized and rehydrated first before endogenous peroxidase was blocked by incubation in 3 % (v/v) H_2O_2 for 30 min. Non-specific antibody binding was blocked with normal goat serum for 1 h. The tissues were then incubated with the primary antibody (1:100) at 4°C overnight. Immunostaining was performed using biotinylated goat anti-rabbit immunoglobulin for 1 h using DAB (3, 3'-Diaminobenzidine) peroxidase substrate kit (Vector, CA) to detect positive signals. After detected by DAB peroxidase substrate, the sections were subsequently counterstained with hematoxylin. The slides were viewed using Nikon microscope system (Nikon Instruments Inc., USA), and the images were analyzed by the Spot software (Diagnostic instruments Inc. MI). Control sections were incubated with 5 % BSA (w/v) in PBS without the primary antibody and subsequently processed as described above.

3.2.6 Chromatin immunoprecipitation assay (ChIP)

Brain tissue was chopped into small pieces with a razor blade, ice cold PBS with 1% formaldehyde was added and incubated for 15 min at room temperature for cross-linking. The reaction was stopped by adding glycine to a final concentration of 0.125 M and rotated on the shaker for 5 min at room temperature. The sample was washed twice with PBS and centrifuged at 500×g. The pellet sample was grinded in 1 ml of 100 mM Tris/100 mM NaCl/30 Mm $MgCl_2$/0.1 % NP-40/0.1 mM PMSF before the centrifugation at 500×g for 5 min. Cell pellet was resuspended in 200 µl of SDS lysis buffer with protease inhibitors (1 mM PMSF, 1 µg/mL aprotinin and 1 µg/mL pepstatin A) and incubated for 10 min on ice. To shear DNA to lengths between 200 and 1000 bp, the pellet was sonicated with 10 pulses of 30 s each in ice cold water. Finally, the sample was centrifuged at 12,000×g for 15 min. The supernatant was kept at -80°C for immunoprecipitation experiment.

Chromatin immunoprecipitation (ChIP) assay kit (Upstate, USA) was employed to investigate the protein which could interact with the methylated H3K79. The supernatant was diluted 10 fold with ChIP dilution buffer including protease inhibitors (0.01 % SDS, 1.1% triton X-100, 1.2 mM EDTA, 16.7 mM Tris-HCl, 167 mM NaCl, pH 8.1 and 1 mM PMSF) and divided into aliquots for immunoprecipitation experiments. To reduce nonspecific background, each 1000 µl aliquot of supernatant was pre-cleared with 50 µl of protein A agrose / Salmon sperm DNA for 1 h at 4°C with agitation. The supernatant fraction was collected by brief centrifugation. 10 µl of anti-monomethyl- H3-lysine 79 antibody and anti- dimethyl-H3- lysine 79 antibody were added in the supernatant. Both antibodies were polyclonal (rabbit) and purchased from upstate biotechnology (USA). No-antibody added sample was used as negative control. The supernatant with specific antibody

incubated overnight at 4°C with agitation. After overnight incubation, the antibody/ histone complex was collected by incubating the supernatant fraction with 75 µl of protein A agrose/ Salmon sperm DNA for 1 h at 4°C with agitation. Protein A agrose was collected by gentle centrifugation at 200 g for 1 min at 4°C. The supernatant was removed carefully. Washed the protein A/protein / histone /DNA complex for 3-5 min on a rotating platform with 1 ml of low salt immune complex wash buffer (0.1 % SDS, 1 % triton X-100, 2 mM EDTA, 20 mM Tris-HCl , 150 mM NaCl, pH 8.1 and 1 mM PMSF) and high salt immune complex wash buffer (0.1 % SDS, 1 % triton X-100, 2 mM EDTA, 20 mM Tris-HCl , 500 mM NaCl, pH 8.1 and 1mM PMSF). Finally, the protein A/protein/histone/DNA complex was gotten by gentle centrifugation (200×g) for 1 min at 4°C. The proteins were further separated by SDS-PAGE gel electrophoresis and identified by mass spectrometry and western blotting.

3.2.7 SDS-PAGE gel electrophoresis

The obtained protein A/protein/histone/DNA complex was firstly denatured with 25 µl 1X Laemmli SDS sample buffer by boiling for 10 min. 20 µl of the denatured samples was loaded onto a 15% SDS-PAGE gel running at 120 V for 2 h in Tris-glycine running buffer.

3.2.8 Silver staining

After electrophoresis, the gel was removed from the cassette and placed into a tray containing appropriate volume of fixing solution (40 % ethanol containing 10 %

acetic acid and 0.05 % formaldehyde) for 1 h. The gel was washed in 20 % ethanol for 20 min after fixative solution was discarded. The gel was then sensitized for 10 min in 0.02 % (w/v) sodium thiosulfate ($Na_2S_2O_3$). After washed by MiliQ water for three times, the gel was stained with 0.25 % (w/v) silver nitrate (Sigma, USA) for 1 h. When staining was complete, the gel was rinsed with a large volume of MiliQ water for 1 min to remove the excess of unbound silver ions. Repeated the washing one more time. The gel was developed by developing solution (6 % (w/v) sodium carbonate (Na_2CO_3), 0.0004 % (w/v) $Na_2S_2O_3$, 0.05 % formaldehyde) for 2-5 min. The reaction was stopped by adding 10% acetic acid as soon as the desired intensity of the bands was reached. Finally the gel was scanned with an Image Scanner (GE healthcare life science, Sweden) at a resolution of 300 dots per inch.

3.2.9 In-gel protein digestion

The protein bands on the SDS-PAGE gel were excised, and cut into small pieces, The gel pieces were incubated in destaining solution (0.4 g potassium ferricyanide ($K_3Fe(CN)_6$) in 200 ml $Na_2S_2O_3$ solution (0.2 g/L) with gentle shaking until no bands were visible. Gel slices were washed 4-5 times for 15 min with plenty of MilliQ water until gel was transparent and has no background color. Then dehydrated by adding 100% ACN, and dried by speed vacuum. The gel slices were digested with 20 ng/μl trypsin in 25 mM NH_4HCO_3 for 14-16 h at 30°C. The peptides were extracted from the gel with the 2.5 % TFA in 50% ACN for MALDI-TOF/TOF tandem mass spectrometry analysis.

3.2.10 MALDI-TOF/TOF tandem mass spectrometry analysis

One microliter of enzyme digested sample was spotted on a MALDI plate followed by 0.5 μl α-cyano-4-hydroxycinamic acid (sigma, USA). Reflector positive ion mode of mass spectrometry was used to identify the protein. Peptides ranged from 700 m/z to 3500 m/z were acquired, signal intensity of peptides of each spectrum was accumulated with 1500-2500 laser shots at a fixed laser intensity of about 4000-4500. Monoisotopic peptides were detected with the mass tolerance of 30 ppm without smooth. Eight peptides with strong intensities (minimum s/n ratio was 50) were selected as precursor ions for further MS/MS analysis. Ion signals were accumulated with 4000-5000 laser shots at a fixed laser intensity of about 4500-4800. Then proteins were further identified by peptide-mass-finger printing (PMF) analysis using GPS Explore™ software v2.0 (Applied Biosystems Inc. CA) and Mascot search engine. NCBI nr protein database was selected and all species was tested. Partial modifications of oxidation on methionine were always taken into account. A mass tolerance of 50 ppm was used in the database searching. The candidate sequences which include the modification site were confirmed by *de novo* sequencing.

3.2.11 Statistical analysis

Data were expressed as mean ± SD. The data were analyzed by Statistical Package for the Social Science (SPSS) for Windows (version 11.5, Chicago, USA). Student-Newman-Keuls (SNK) test and Least-significant difference (LSD) test of one way analysis of variance (ANOVA) were used to compare the difference among mean values. Statistical significance was accepted at $p<0.05$.

3.3 Results

3.3.1 Tissue distribution of the mono- and di-methylated H3K79 in mouse

Previous reports showed that H3K79 methylation occurred in a wide range of organisms and conserved from yeast to human. However, there were no researches on the tissue distribution of H3K79 methylation in mammalian species. In chapter 3, the mono- and di-methylated H3K79 were detected to be expressed in 12-month-old SAMP8 mouse brain. Therefore, the distribution of methylated H3K79 in the different organs of 12-month-old SAMP8 mice was demonstrated by western blotting. At the same time, these two modification types which were identified by MS could be further confirmed using specific anti mono- and di-metylated H3K79 antibodies.

As shown in Fig 3.1, H3K79 mono- and di-methylation could express in various SAMP8 mouse tissues. It was not only expressed in brain, but also was highly expressed in small intestine, lung, liver, spleen, kidney, uterus, ovary, testis and eyeball. Little amount of methylation H3K79 was detected in heart and muscle, while no expression was found in stomach. However, the abundance of these two types of methylations was different in the same organ. It was found that the abundance of the di-methylation of H3K79 was higher than that of mono-methylation of H3K79 in brain, heart and bladder while lower than that in the testis.

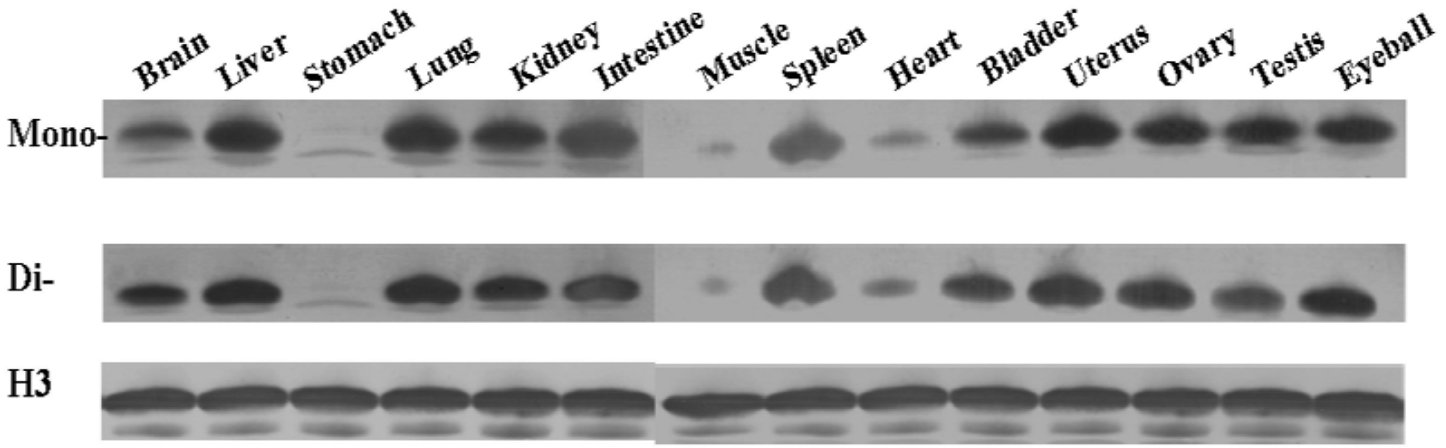

Fig 3.1 Distribution of and abundance of H3K79 mono-, and di-methylation in different mouse organs. 10 μg of total core histones from the different organs (brain, liver, stomach, lung, kidney, intestine, muscle, spleen, heart, bladder, uterus, ovary, testis and eyeball) was separated on 15% SDS-PAGE gels, transferred to a ployvinylidene difluoride membrane, and probed with anti-mono-methylated H3K79, anti-di-methylated H3K79 and anti-H3 antibodies (1:1000).

3.3.2 The changes of mono- and di-methylated H3K79 abundance in the brains of 3- and 12-month old SAMP8 mouse

Next, the abundance of mono- and di-methylated H3K79 in the brains of 3- and 12-month-old SAMP8 was investigated (Fig 3.2). In comparing with the young-aged mouse (3-month-old), the abundance of methylated H3K79 (mono- and di-) in the brains increased during aging process and the trend of such increase was the same in both SAMP8 and SAMR1 mouse models. No statistical difference of the mono-methylation level was found between 12-month-old SAMP8 mice group and 12-month-old SAMR1 mice. The abundance of di-methylated H3K79 in the 12-month-old SAMP8 mice was significant less than that of the 12-month-old SAMR1 mice, while no difference was observed in the brains of SAMR1 mice (Fig.3.2).

3.3.3 Expression of H3K79 methylation in the cortex and hippocampus of 12- month old SAMP8 brain

Due to the importance of the cerebral cortex in cognitive functions and the role of the hippocampus in learning and memory processes, the expression of di-methylated H3K79 in the cortex and the hippocampus of 12-month old SAMP8 mice and SAMR1 mice were detected by immunohistochemistry method (Fig.3.3). Di-methylated H3K79 could express in the cortex and the hippocampus (including CA1, CA2, CA3 and dentate gyrus). No positive signals were observed in the corpus callosum. Most of the brownish positive signals were observed in the nuclei of neuron cells, such as pyramidal cells in

CA1 and granule cells in dentate gyrus. The number of non-stained cells was higher in the cortex of 12-month old SAMP8 mice than that of age-matched control SAMR1 mice (Fig. 3.3 b and e).

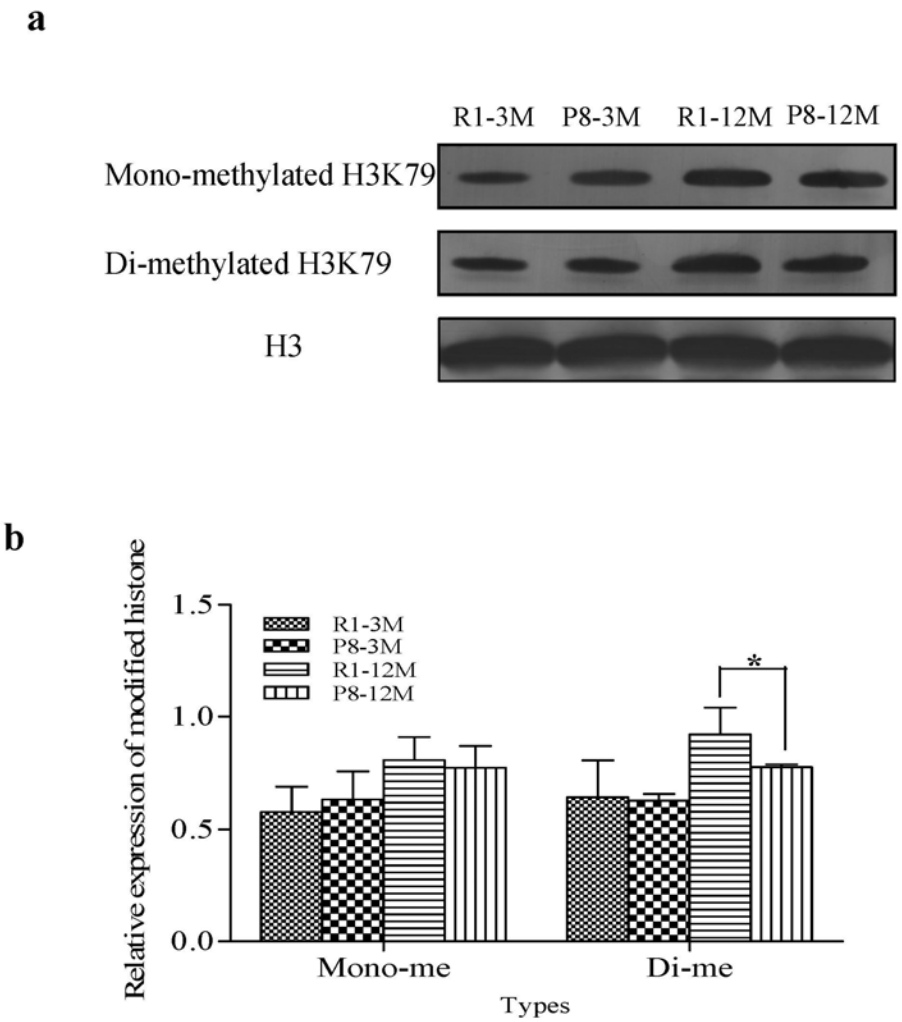

Fig. 3.2 The abundance of H3K79 mono- and di-methylation in the brain. a: Core histones mixture (10μg) of four groups were separated on 15% SDS-PAGE gels, transferred to PVDF membrane, and probed with anti-MeH3K79 and anti-Me2 H3K79 antibodies. b: The comparison of the abundance of the H3K79 mono-methylation in four groups. Asterisk indicated that $P<0.05$ (R1-12M vs P8-12M). R1-3M and R1-12M indicated the 3, 12-month old SAMR1mouse, respectively; P8-3M and P8-12M indicated the 3, 12-month old SAMP8 mouse, respectively.

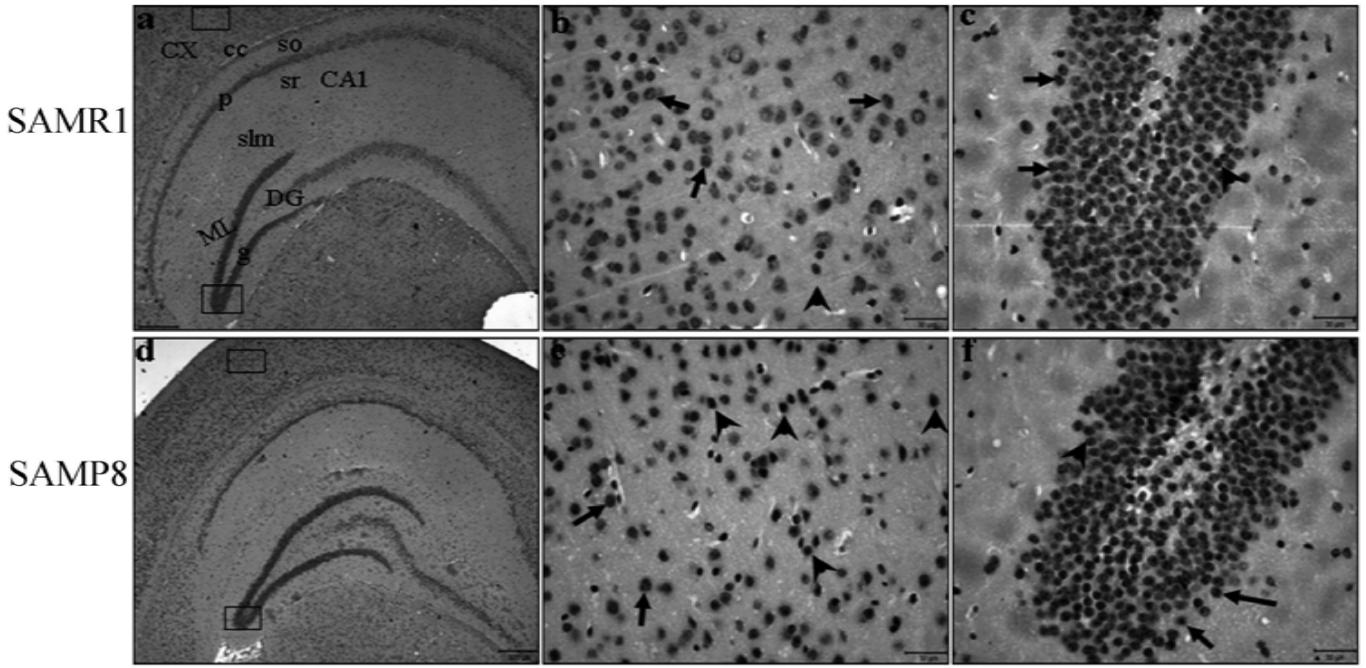

Fig 3.3 Expression of H3K79 methylation in cerebral cortex and hippocampus of SAMP8 mice brain. The brain sections from 12-month-old SAMP8 (d, e, f) and SAMR1 (a, b, c) mice were immunoprobed by specific anti-dimethylated antibodies before DAB detection. Brown color was the positive signal (arrow). And the blue color was the nucleus counterstained with the hematoxylin (arrowhead). Picture b, c, e and f were amplified images (40X) of the square area (4X). Scale bar:300 micron(a, d); 30 micron (b, c, e and f) . Abbreviations: CA1, hippocampal regions; DG, dentate gyrus; ml, molecular layer of DG; slm, stratum lacunosum moleculare; so, stratum oriens; sr, stratum radiatum; p, pyramidal neurons; g, granule cells; CX, Cortex; cc: corpus callosum.

3.3.4 Investigation of interaction proteins with methylated H3K79 by ChIP

Histone post-translational modifications can alter chromatin structure and/or serve as binding platforms for proteins that influence transcriptional activity. Molecular mechanisms underlying histone modifications can be summarized into 'cis' mechanisms and 'trans' mechanisms (Wang, et al. 2007). Previous researches indicated that methylated of H3K79 could involve in transcriptional activation process (Steger et al. 2008), whereas, no confirmed protein that could bind specifically to the methylated H3K79 has been identified (Botuyan et al. 2006; Kim et al. 2006). From ChIP result, several proteins could be immunoprecipitated using specific anti mono- and di-methylated H3K79 antibodies, and a few specific protein bands could be observed in SDS-PAGE gel after sliver staining (Fig 3.4). Three specific bands were observed in both lines 2 and 4. Among them, two bands (bands 1 and 5; bands 2 and 6) were the same in both mono-methylated H3K79 and di-methylated H3K79 groups. By mass spectrometry analysis, several candidate proteins were identified. Fig. 3.5 showed MALDI-TOF MS spectrum of band 1. Seven peptides, 1490.8187, 1701.8478, 1944.9586, 1956.9529, 1971.9407, 2103.9917 and 2232.1384, matched to a transcriptional regulator, TetR family. From the spectrum of band 1 (Fig 3.6), four proteins were also predicted by *de novo* sequence analysis. They were T-box isoform 20 (Tbx 20) (precursor 850.5087), bromodomain adjacent to zinc finger domain 2b (precursor 1704.8352), 50 ribosomal protein (precursor 1939.9489) and transcriptional regulator (precursor 2103.9917). Band 5 had the similar

spectrum with band 1. Fig 3.7a showed MALDI-TOF MS spectrum of band 2 (Band 6 had the similar spectrum with band 2). Seven peptides extracted from band 2 matched the protein which was similar to homeodomain transcription factor Pbx1 isoform 1 (864.4962, 1111.6042, 1283.6669, 1493.7307, 1588.7273, 1713.8073, and 2284.1853). Western blotting result showed that mono- and di-methylated H3K79 could interacted with pbx1 protein, especially di-methylated H3K79 (Fig 3.7b). However, no identified proteins could be deduced from the peptides extracted from band 3 and band 4.

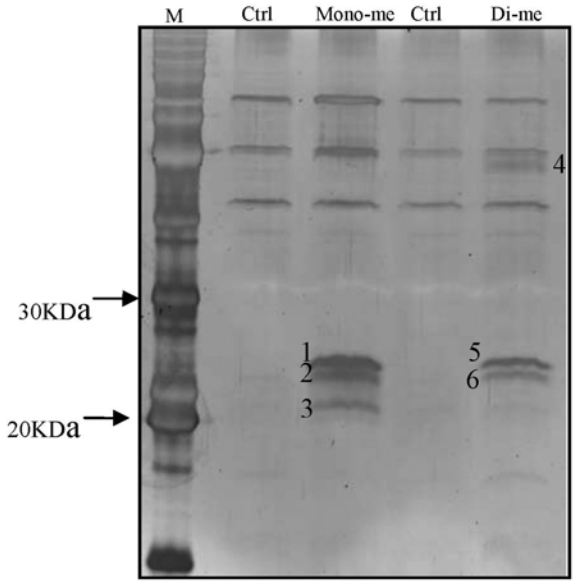

Fig 3.4 SDS-PAGE gel separation of the protein interacted with the methylated H3K79 site. The protein A/protein/histone/DNA complex obtained by ChIP kit was denatured by 1X Laemmli SDS sample buffer and separated by 15 % SDS-PAGE gel. The gel was stained by silver. Lines 1 and 3 were control samples in which no antibody was used. Lines 2 and 4 were the samples in which anti-mono-methylated H3K79 and anti-di-methylated H3K79 were added, respectively. The proteins of bands (labeled with 1, 2, 3, 4, 5 and 6) were digested, extracted and identified by mass spectrometry.

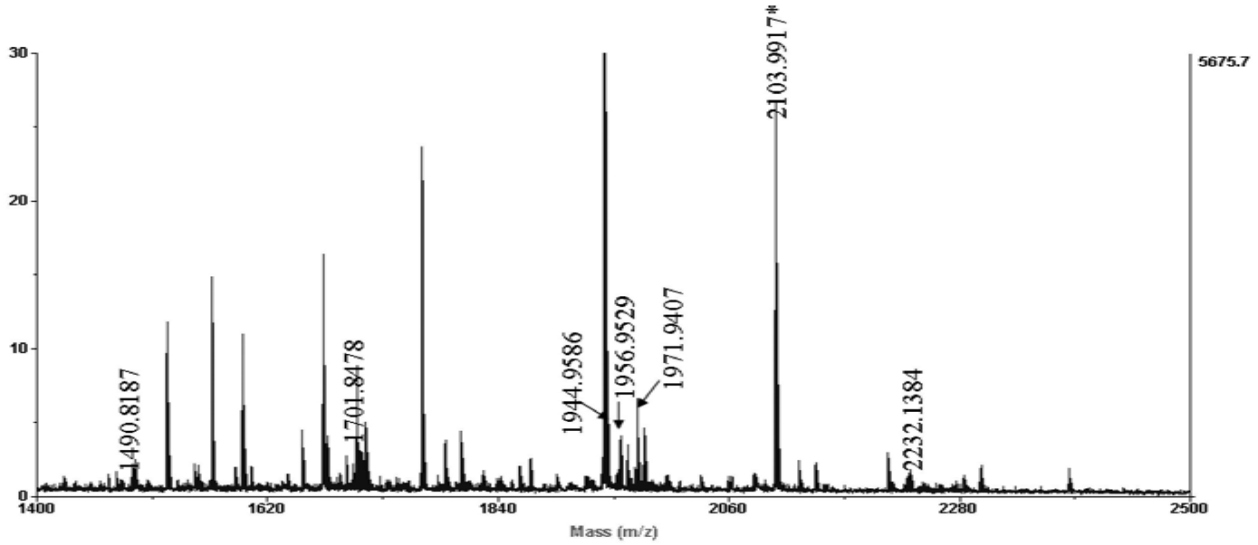

Fig 3.5 Part of MALDI-TOF MS spectrum of band 1. Tryptic digested peptides were extracted from band 1 and selected peptide (Indicated by asterisk) was further for MS/MS, *de novo* sequence and database searching. Seven peptides of band 1 matched to the transcriptional regulator, TetR family; their masses were 1490.8187, 1701.8478, 1944.9586, 1956.9529, 1971.9407, 2103.9917 and 2232.1384. The sequence of TVHNGLKVTPDY was deduced by the precursor 2103.9917.

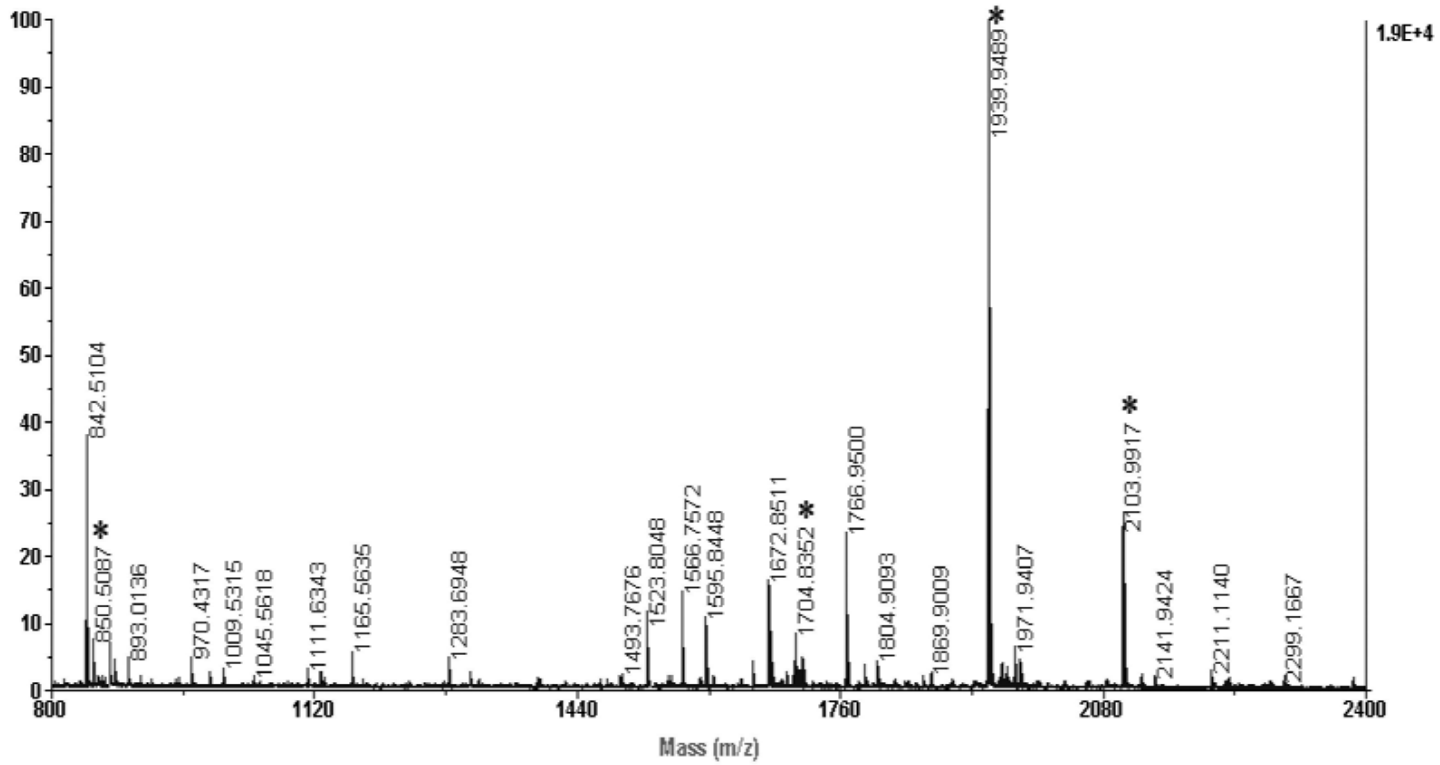

Fig 3.6 MALDI-TOF MS spectrum of band 1. Tryptic digested peptides were extracted from band 1 and selected peptides (Indicated by asterisk) were further for MS/MS, *de nevo* sequence and database searching. The candidate protein which ion score was higher than 50 was predicted. They were T-box isoform 20 (precursor 850.5087; deduced sequence: ATPIPHP), bromodomain adjacent to zinc finger domain 2b (precursor 1704.8352; deduced sequence: PHSAPHLHIS), 50 ribosomal protein (precursor 1939.9489; deduced sequence: EDMIKEGEIVDVRA) and transcriptional regulator (precursor 2103.9917; deduced sequence: TVHNGLKVTPDY).

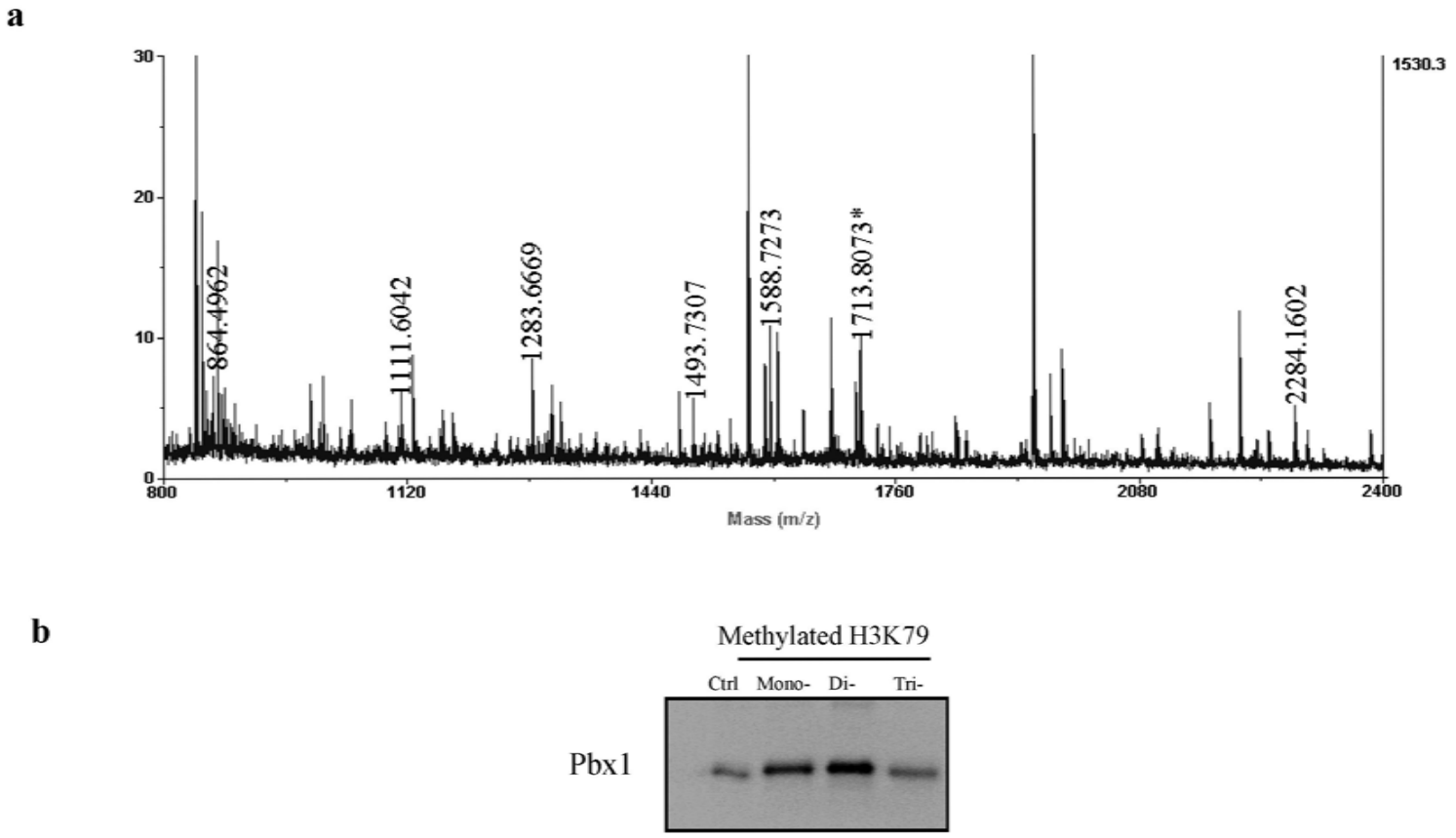

Fig 3.7 The identification of Pbx1 protein. a: MALDI-TOF MS spectrum of band 2. Seven peptides**,** precursor 864.4962, 1111.6042, 1283.6669, 1493.7307, 1588.7273, 1713.8073, and 2284.1853 were matched to the protein named similar to homeodomain transcription factor Pbx1 isoform 1. **b**: Western blotting result. Proteins precipitated by anti mono-, di- and tri-methylated H3K79 antibodies was detected by anti pbx1/2/3/4 antibody (1:1000)

3.4 Discussion

SAMP8 mouse was characterized by age-related learning and memory deficits, which were the first symptoms of AD. Studying histone modification in the aged SAMP8 mouse brain could provide us an opportunity to understand the fundamentally molecular mechanism upon brain aging.

H3K79 was the first methylation site which was found out of N-terminus of histone and evolutionarily conserved from yeast to mammals. But its functions have not been well characterized. The results from chapter 2 showed methylated H3K79 could be found in brain of the 12-month old SAMP8 mice. Actually, its expression was not only limited in the brain. It could also be expressed highly in other organs, such as liver, kidney, uterus, ovary, testis and eyeball (Fig. 3.1). However, little expression of methylated H3K79 could be found in heart and muscle, even no expression in stomach (Fig 3.1). This indicated the diversity functions of H3K79 methylation in different organs.

In aged human brain, the genes involved in synaptic transmission, Ca^{2+} homeostasis/signaling and neuronal survival were down-regulated and the genes involved in stress response and inflammation were up-regulated (Bonneuil 2007; Lu *et al*., 2004). The decreased potential of DNA repair was also found (Katyal and McKinnon, 2007; Vyjayanti and Rao, 2006). Abnormal gene expression and DSBs break contributed to the aging process and the degeneracy of brain. H3K79 methylation was one of methylations which are associated with increased gene transcription. It was also involved in the detection of DSBs and DNA repair. In the brain of 12-month old SAMP8, dimethylated H3K79 was significantly decreased compared with that of 12-month old SAMR1 (Fig 3.2). SAMP8 mouse do not

show the senescence accelerated aging characteristics at the early stage of life span, therefore, the expression change of methylated H3K79 in the brain during aging process showed its possibility in the brain aging. H3K79 methylation might have different functions depending on the number of methyl groups added on the same residues. In somatic cells and oocytes, di-methylated H3K79 was observed throughout the genome and was considered as an active gene marker (Ooga *et al*., 2008), while it was only detected during mitosis in *Trypanosoma brucei*. In the SAMP8 mouse brain, only the di-methylation of H3K79 was significantly decreased in 12-month-old SAMP8 mouse brain compared with normal age matched SAMR1 mouse (Fig 3.2), which indicated di-methylation of H3K79 may have more important roles than mono-methylated H3K79 during aging processing. How di-methylated H3K79 is involved into the brain aging needs further study because the functions of the different methylation states of H3K79 are currently unknown.

The hippocampus plays major roles in short term memory and spatial navigation, and it was the first attacked area in the brain of aging and AD patient. Cerebral cortex has the role in cognitive functions and global thinning was apparent in aging (Salat *et al*., 2004). Neurons and glial cells are the major constituent cells in brain. Neurons could send and receive electro-chemical signals to and from the brain and nervous system. Extensive neuronal loss and the dysfunction in the hippocampus and cortex could induce to the dysfunction of brain on learning, memory and cognitive function of aged brain. The number of methylated H3K79 positive cell decreased in the brain of old age SAMP8 compared with age matched normal SAMR1 mice (Fig 3.3), which might indicate that the expression change of H3K79 methylation regulated genes and the decrease of the ability of DSBs repair in neuron cells.

The association between proteins and DNA is crucial for many vital cellular functions, such as gene transcription, DNA replication and recombination, repair, segregation, chromosomal stability, cell cycle progression, and epigenetic silencing. It is important to know the genomic targets of DNA-binding proteins and the mechanisms by which they control and guide gene regulation pathways and other biological actions. Histone modification sites could provide a platform for the recruitment of DNA-binding proteins, which was also called non-histone 'readers', and lead to corresponding functions.

In this chapter, several candidate proteins which interacted with methylated H3K79 site were found. Pbx1 was one of indentified proteins. Pbx proteins were indicated as a DNA-binding protein which acted as a cofactor to modify the HOX/DNA binding specificity (Paraguison *et al.*, 2007). They were widely expressed in fetal and adult tissues and interacted preferentially with 3' HOX proteins (Phelan and Featherstone, 1997) and modulate the affinity and stability of DNA binding and regulate transcriptional activity. Pbx1 could also maintain stem cell quiescence (Ficara *et al.*, 2008). It could bind to the DNA sequence ATCAATCAA cooperatively with Hox homeodomain proteins, such as Hox-A5, Hox-B7, Hox-B8, Hox-C8 and Hox-D4 homeodomain protein, which suggested that Pbx1 might take part in the regulation of Hox target gene transcription and contribute to the process of anterior-posterior patterning and structural development in vertebrate (Lu *et al.*, 1995). HOX-PBX complexes were likely to achieve transcriptional repression or activation through differential association with coactivators and corepressors (Struhl, 1998). Histone acetyltransferases (HATs) and the histone deacetylases (HDACs) were one class of coregulators to HOX-PBX complexes and the other coregulator was protein kinase (PKA) which acted as a

signaling switch that converts HOX-PBX complexes from transcriptional repressors to activators (Saleh *et al.*, 2000).

Bromodomain adjacent to zinc finger domain 2b (BAZ2B) was also found. It could interact with ISWI and play a role in transcriptional regulation (Poot *et al.*, 2000). SWI/SNF chromatin-remodeling enzymes were generally recruited after the assembling of factors onto promoters (Martens and Winston, 2003; Salma *et al.*, 2004; Soutoglou and Talianidis, 2002; Spilianakis *et al.*, 2003). Therefore, BAZ2B might be recruited after the specific DNA sequence recognition by DNA-binding protein, such as Pbx1.

Tbx 20 was another detected protein. It was a protein which was not just required for development of the *Caenorhabditis elegans* hindgut and heart development (Woollard and Hodgkin 2000; Qian *et al.*, 2008). Tbx 20 orthologues also showed a role in motor neuron development (Pocock *et al.*, 2008). The detection of this protein in this study indicated the diversity functions of methylated H3K79 in different tissue might fulfill by recruiting different transcription factors.

Base on the review by Laurent (Laurent *et al.*, 2008) and the proteins identified in this ChIP experiment, a model of methylated H3K79 on transcriptional regulation was proposed (Fig 3.8). The methylation of H3K79 could recruit Pbx protein to the DNA binding site and help Pbx to recognize specific DNA sequence. At the same time, transcription factor or regulator, such as Tbx 20, TetR family precursor BAZ2B and ribosomal protein were also be recruited, finally chromatin-remodeling enzymes (CBP, HAT, HDAC and the SWI/SNF proteins). All the recruited protein formed a Pbx-containing transcription complex. The target genes were thus transcribed at a rate defined by the overall complex interaction with the basal transcriptional machinery.

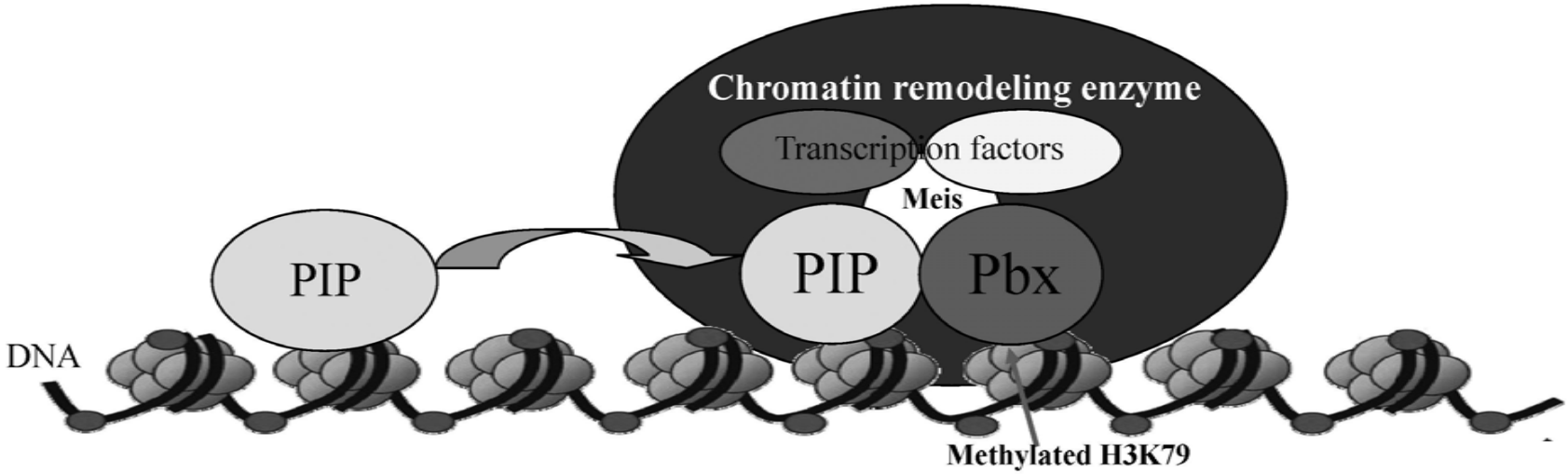

Fig 3.8 The model of methylated H3K79 on transcriptional regulation. PIP: Pbx interacting protein, such as Hox, Hox-like; Meis as DNA binding partner of Pbx; Chromatin-remodeling enzymes such as CBP, HAT, HDAC and the SWI/SNF proteins; Transcription factors and transcriptional regulator , such as Tbx 20 and TetR family precursor.

Though several candidate proteins interacting with methylated protein were found and a model of methylated H3K79 on transcriptional regulation was proposed, further confirmation is still needed and it will be a large challenge in future. Furthermore, two specific bands which interacted with mono- and di-methylated H3K79 respectively in ChIP experiment could still not be identified by mass spectrometry due to trace amount of protein pulling down by the antibodies. These proteins might provide the possibility to distinguish the diversity functions of different methylated states of H3K79. Therefore, a lot of work needs to be performed in future.

In this chapter, methylated H3K79's tissue distribution and localization in cerebral cortex and hippocampus were investigated. Moreover the change of its abundance during aging was also measured. Based on ChIP results, a model of methylated H3K79 on transcriptional regulation was supposed. All these results provide us more information to characterize the functions of methylated H3K79 in the brain upon aging. To clearly elucidate the function of the H3K79 methylation in the aged brain, siRNA transformation will be performed to detect the effect of the down regulation of H3K79 methylation on the neuron cells in next chapter.

Chapter 4 Comparative proteomic analysis of Neuro 2a cells in response to siRNA-mediated silencing of *Dot1*

4.1 Introduction

Posttranslational modification (PTM), the covalent modification of a protein after its translation, is one of the later steps involved in various protein biosynthesis. It is well known that the functions of proteins could be extended by the attachment of other biochemical functional groups such as methyl, acetyl, and phosphate groups. In 1964, Murray (Murray, 1964) first reported histone PTMs with the identification of ε-methyl-lysine in acid hydrolysates of calf thymus histones. Since then, reports on the modifications in the core histones were extended to phoshorylation, acetylation, ADP-ribosylation, ubiquitylation, deimination and proline isomerization (Keinsmith *et al*., 1966; Ord and Stocken, 1967; Gershey, 1968; Vidali, 1968; Ueda *et al*., 1975; Shiio and Eisenman, 2003; Hagiwara *et al*., 2002; Nelson, 2006). Over the last few years, more histone-modifying enzymes have been identified and demonstrated to catalyze the diverse PTMs of histones (Couture and Trievel, 2006).

In 2002, Dot1 (**d**isruptor **o**f **t**elomeric silencing) was found to specifically catalyze the methylation of H3 lysine 79 (H3K79), the first modification site located outside the N-terminus of histones (Feng *et al*., 2002). This enzyme is conserved from trypanosomes to humans and catalyzes mono-, di- and tri-methylation of histone H3K79 (Van Leeuwen *et al*., 2002). However, Dot1, which shares a similar

catalytic core region to class I arginine methyltansferases (Cheng *et al.*, 2005), dose not contain the SET (**s**uppressor of variegation, **e**nhancer of zeste and **t**rithorax) domain compared with other histone methyltransferases.

Dot1 genes were firstly identified by genetic screening in *Saccharomyces cerevisiae*. Overexpression of Dot1 not only disrupted telomeric silencing but also reduced silencing at other repressed loci such as HM loci and rDNA (Singer *et al.*, 1998). In addition, Dot1 was found necessary for pachytene checkpoint in *S. cerevisiae*, and was crucial for Sir protein-mediated heterochromatic gene silencing, meiotic checkpoint control and DNA damage response in budding yeast (San-Segundo and Roeder, 2000; Ng *et al.*, 2002; Okada *et al.*, 2005). Mutations on H3K79 or SAM binding motif of *Dot1* gene impaired telomeric silencing, which suggested that Dot1 could regulate telomeric silencing predominantly through H3K79 methylation by restricting the Sir protein at heterochromatic regions (Feng *et al.*, 2002; Ng *et al.*, 2002). In addition, hDot1L was involved in activation of Hox genes in certain types of leukemia (Okada *et al.*, 2005). Dot1a-AF9 complex could repress the aldosterone-induced gene expression (Zhang *et al.*, 2006). In mice model, Dot1L played important roles in the embryogenesis and was required for the integrity of constitutive heterochromatin (Jones *et al.*, 2008). Our previous study illustrated that the decreased of H3K79 methylation in the brain of senescence accelerated mouse prone 8 (SAMP8) compared with control senescence accelerated-resistant mouse R1 (SAMR1) brain (Fig 3.2). However, the biological functions of Dot1 or H3K79 methylation of neuronal cells remain largely unknown.

In this study, I established *Dot1* silencing Neuro-2a (N2a) cell line via transfection with *Dot1*-siRNA, and investigated the effects of Dot1 on cell growth, cell cycle, cell morphology and the associated proteomic changes.

4.2 Materials and methods

4.2.1 Cell culture

Neuro-2a (ATCC ® Number: CCL-131™) was purchased from American Type Culture Collection (ATCC, Manassas, VA). Cells were cultured in Dulbecco's Modified Eagle's Medium (DMEM) supplemented with 10% fetal bovine serum (FBS) (Gibco), penicillin G50 (100 U/ml) and streptomycin (100 µg/ml) at 37°C in a 5 % CO_2 incubator (HEPA Filter Water-Jacket CO2 Incubators, Forma Scientific, USA). Medium was changed every other day and cells were split every 3-4 days. The morphology of the cells was visualized using an inverted microscope (Nikon Eclipse TS-100 inverted microscope, Nikon Inc., USA).

4.2.2 Transfection of *Dot1*-siRNA

Gene interference study was performed using a *DOT1*-siRNA and *Control*-siRNA. The *DOT1*-specific siRNA corresponding to the sequence of CACGAGTGTTATATTTGTGAA (Gene secession number: NM_199322) was custom designed and purchased from Qiagen-Xeragon (Germantown, MD). The *ctrl*-siRNA sequence: 5'-CAGAGCUUUGGAGUCAGCA-dTT-3' was also designed such that non-silencing siRNA has no homology known to mammalian genes. The day before transfection, $1.5x10^5$ cells or 1,500 cells were seeded in each

well of 6-well plate (Nalge Nunc International, Naperville) or 96-well plate, respectively. The cells were incubated in DMEM containing serum and antibiotics under normal growth conditions (37°C in a 5 % CO_2 incubator). On the day of transfection, transfection complexes were prepared according to the manufacture's instruction with the ratio of siRNA to RNAiFect transfection reagent in 1:3 and incubated for 10-15 min at room temperature before it was added drop-wise into the wells. Cells were incubated with the transfection complexes under normal growth conditions and gene silencing efficiency was monitored at 24 h, 48 h and 72 h after transfection. The proliferation of cells was detected by MTT assay after 24 h, 48 h and 72 h incubation. 2-D gel electrophoresis and flow cytometry assay were performed after 48 h incubation.

4.2.3 Semiquantitative RT-PCR

Total RNA was isolated from transected N2a cells using Trizol reagent (Invitrogen, USA). First strand cDNA was synthesized as instructed by the manufacturer. PCR was preformed using 25 µl reaction mix which included 1 µl of total cDNA mixed with 1×PCR buffer, 1.5 mM $MgCl_2$, 0.2 mM dNTP, 0.5U *Taq* DNA polymerase (Roche, USA) and 1 µM of one of the following gene specific oligonucleotide primer pairs: *DOT1*: Forward: 5'GGAGTGGAGAAAGCGGA CATC3'; Reverse: 5'TCAAGTATGGTGCGGTCAATGG3'; β-actin: Forward 5'GGAGTGGAGAAAGCGGACATC3'; Reverse: 5'TTCATGAGGTAGTCTGTC

-AGGTCC3'. PCR amplifications were performed using the following conditions: 94°C for 5 min; 35 cycles of 94°C for 30 s, 50°C (*Dot1*) or 55°C (β-actin) for 30 s, 72°C for 90 s; 72°C for 10 min. The PCR products (10 μl) were visualized following electrophoresis on a 1.5 % agarose gel by ethidium bromide staining. The expected product sizes were 201 bp for β-actin and 400 bp for *Dot1*. The intensity of the bands was determined using Quantity One software 4.5.0 (Bio-rad, USA), and normalized to the band intensity with β-actin. Each experiment was repeated three times.

4.2.4 Histone extraction

The cells was first homogenized in lysis buffer (10 mM Tris-HCl, pH 7.6, 150 mM NaCl, 1.5 mM $MgCl_2$, 0.05 % NP40, and 1 mM phenylmethylsulfonyl fluoride (PMSF), 50 mM sodium bisulfite ($NaHSO_3$), 45 mM sodium butyrate), and nuclei were obtained by centrifugation (1,500×g for 10 min). For the preparation of histones, nuclei were incubated with 4 volumes of 0.2 N sulfuric acid (H_2SO_4) for 2 h at 4°C. The supernatant was precipitated with 20% trichloroacetic acid (TCA) (Final concentration) and followed by centrifugation (12,000×g for 20 min). The obtained pellet was washed with cold acetone and subsequently dissolved in MilliQ water. 2-mercaptoethanol was added into the sample at a final concentration of 0.1 % before lyophilization. The samples were stored at -80°C before analysis. The quantity of histone protein was evaluated using PlusOne^{TM} 2D Quant Kit (GE Healthcare Life Sciences, Sweden).

4.2.5 MTT assay

About 1,500 cells in 200 µl medium were seeded in each well of the 96-well plate and incubated for 24 h at 37°C in 5% CO_2 before transfection. On the day of transfection, transfection complexes (Ratio of siRNA: RNAiFect transfection reagent was 1:3) were added into each well. After incubation for 24 h, 48 h and 72 h, 20 µl MTT (5 mg/ml) solution was added and further incubated for 4h (37°C, 5% CO_2). 200 µl dimethyl sulfoxide (DMSO) was added into each well after the media was dumped off. Absorbance at 570 nm of each well was assayed on SPECTRAmax 250 microplate spectrophotometer (Molecular Devices, Sunnyvale, CA).

4.2.6 Hematoxylin and Eosin (HE) Staining

The day prior to transfection, cells were plated on 6-well plates containing glass coverslips coated with poly-L-ornithine (0.5 mg/ml), laminin (10 µg/ml) or fibronectin (50 µg/ml). After 48 h treatment of Dot1-siRNA, the specimens were fixed by 4 % paraformaldehyde (PFA) in PBS (pH 7.4) for 1 h at 15-25°C and processed for HE staining. Briefly, the specimens were washed with PBS and rehydrated with 100 % ethanol, 95 % ethanol and 75 % ethanol, subsequently. Then the cells were stained by hematoxylin for 1 min, and followed by eosin for 1-2 min. After staining, the samples were dehydrated with ethanol, cleared in xylene and were mounted with DPX mounting medium. The image was viewed with Nikon

microscope system (Nikon Instruments Inc. USA) and analyzed by the spot software 3.0 (Diagnostic instruments Inc., MI).

4.2.7 Flow cytometry

Flow cytometry was used to determine the effect of *Dot1* silencing on cell cycle and cell viability of N2a cells. The cells were harvested at 24 h, 48 h and 72 h after transfection with *ctrl*- and *Dot1*-siRNAs, and washed with cold PBS. Followed by incubation in propidium iodide solution (1 μg/mL) for cell cycle analysis or staining with AnnexinV- FITC apoptosis kit (R&D systems, USA) to detect the viability of cells. After incubation, the stained cells were quickly analyzed by flow cytometry (Beckman, USA). Three replicates of the specimens were examined.

4.2.8 2D Electrophoresis

All experiments of 2D gel electrophoresis were performed following the modified protocol of GE Healthcare life science. Cells lysates were prepared from N2a cells in lysis buffer (7 M urea, 2 M thiourea, 0.01 % TBP, 4 % CHAP, and 0.01 % NP 40) with protease inhibitors (GE Healthcare, Sweden). Lysates were incubated on ice for 30 min, and then centrifuged at 12,000×g for 15 min to remove all cell debris. The total protein concentration of the samples was determined using PlusOne^{TM} 2D Quant Kit (GE Healthcare life science, Sweden) according to the

manufacturer's instruction. Samples (120 μg) were loaded onto immobilized pH strips. IEF was performed on Ettan™ IPGphor™ Isoelectric Focusing System (GE Healthcare Life Sciences, Sweden) at 20°C. Passive rehydration was first carried out at 0 V for 6 h. To facilitate the entry of high-molecular-weight proteins into IPG strips, low voltage (30 V for 6 h) was applied afterwards. IEF was then performed with 150 V for 2 h, 500 V for 30 min, and 1000 V for 30 min, then progressively increase from 1000 V to 3500 V for 3500 Vh, 6000 V for 6000 Vh and 8000 V for 47000 Vh, with a total voltage hours (Vhs) of 57730 Vhs. Before the second dimension, IPG strips were subjected to two-step equilibration in buffer (50 mM Tris-HCl, 6 M urea, 30 % v/v glycerol, 2 % w/v SDS, 0.002 % w/v bromophenol blue) containing DTT (100 mg/10ml) and iodoacetamide (250 mg/10ml), respectively, each for 15 min. Afterwards, proteins on IPG strips were separated by 11 % SDS-PAGE gel at 75 V for 16 h. After silver staining (PlusOne™ Silver Staining Kit, GE Healthcare Life Sciences, Sweden), gels were scanned (resolution of 300 dots per inch) with an Image Scanner (GE Healthcare Life Sciences, Sweden). Image analysis was performed with ImageMaster™ 2D Platinum V. 5.0 software (GE Healthcare Life Sciences, Sweden). Differentially expressed proteins were excised from 2D gels. The excised gel pieces were destained with 30 mM potassium ferricyanide in 100 mM sodium thiosulphate, then digested with 8-10 μl (20 ng/μl) modified sequencing grade trypsin (Promega, USA) at 30 °C for 14-16 h. Tryptic peptides were extracted from gel pieces with 2.5 % TFA in 50 % acetonitrile (ACN) by sonication for 10 min.

4.2.9 Protein identification by MALDI-TOF/TOF mass spectrometry and database searching

Mass spectrometric analysis was carried out using a MALDI-TOF/TOF tandem mass spectrometer ABI 4700 proteomics analyzer (Applied Biosystems, USA). For acquisition of mass spectra, 0.5 µl samples were spotted onto a MALDI plate, followed by 0.5 µl matrix solution (4 mg/ml α-cyano-4- hydroxycinnamic acid in 35 % ACN and 1 % TFA). Mass data acquisitions were piloted by 4000 Series Explorer™ Software v3.0 using batched-processing and automatic switching between MS and MS/MS modes. All MS survey scan were acquired over the mass range 700-3500 *m/z* in the reflectron positive-ion mode and accumulated from 2000 laser shots with acceleration of 20 kV. The MS spectra were internally calibrated using porcine trypsin autolytic products (*m/z* 842.509, *m/z* 1045.564, *m/z* 1940.935 and *m/z* 2211.104) resulted in mass errors of less than 30 ppm. The MS peaks (MH^+) were detected on minimum S/N ratio ≥20 and cluster area S/N threshold ≥25 without smoothing and raw spectrum filtering. Peptide precursor ions corresponding to contaminants including keratin and the trypsin autolytic products were excluded in a mass tolerance of ± 0.2 Da. The filtered precursor ions with a user-defined threshold (S/N ratio ≥50) were selected for the MS/MS scan. Fragmentation of precursor ions was performed using MS-MS 1 kV positive mode with CID on and argon as the collision gas. MS/MS spectra were accumulated from 3000 laser shots using default calibration with Glu-Fibrinopeptide B from 4700 Calibration Mixture (Applied

Biosystems, USA). The MS/MS peaks were detected on minimum S/N ratio ≥3 and cluster area S/N threshold ≥15 with smoothing.

The MS and MS/MS data were loaded into the GPS Explorer™ software v3.5 (Applied Biosystems, USA) and searched against NCBInr database by Mascot search engine version 1.9.05 (Matrix science, UK) using combined MS (peptide-mass-fingerprint approach) with MS/MS (*DeNovo* sequencing approach) analysis for protein identification. The following search parameters were used: monoisotopic peptide mass (MH^+); 700-3500 Dalton; one missed cleavage per peptide; enzyme, trypsin; taxonomy, Mus ; p*I*, 0-14; precursor-ion mass tolerance, 50 ppm; MS/MS fragment-ion mass tolerance, 0.1 Dalton; variable modifications, oxidation for methionine. Known contaminant ions corresponding to keratin and trypsin were excluded from the peak lists before database searching. Top ten hits for each protein search were reported. Proteins with MOWSE score greater than 70 and at least four matched peptides were accepted as identified. Also, *DeNovo* Explorer™ software v3.5 was used to deduce the peptide sequence (sequence taq) of the selected peptide from MS scanning.

4.2.10 Western blot analysis

Histone mixtures (10 μg) or transfected N2a total proteins (30 μg) were resolved on SDS-PAGE gels (15% gel for histone and 12% gel for Rad23b, prohibtin, P53 and actin). Protein bands were transferred onto a polyvinylidene difluoride membrane

(Hybond ECL, Amersham Biosciences Piscataway, USA). The membranes were blocked in 5 % skimmed milk, then immunoprobed with antibodies (1:1000) to H3, mono- methylated H3K79, di- methylated H3K79 (Upstate, Biotechnology, Inc, USA), and anti-Rad23b, prohibtin, p53, β-actin (Santa Cruz Biotechnology, CA). Secondary antibody with HRP-conjugated to rabbit IgG (Santa Cruz Biotechnology, CA) at 1:3000 dilutions was used. The signal was detected by LumiGLO®* chemiluminescent detection kit (Cell signaling, USA). The members were scanned and analyzed by Bio-Rad Quantity One 4.4.0 software (Bio-Rad, USA).

4.2.11 Statistics

Data are expressed as mean ± SD. T test of SPSS 10.0 software was used to evaluate significant difference of compared groups. Differences were considered significant with p value < 0.05.

4.3 Results

4.3.1 *Dot1* expression could be down-regulated after *Dot1*-siRNA transfection

To determine the functions of Dot1 in N2a cells, we first established *Dot1* silencing N2a cell line. *Dot1* expression was unaffected when cells were transfected with *ctrl*-siRNA but it was significantly reduced upon the transfection with *Dot1*-siRNA. After 24 h, 48 h, and 72 h transfection, semiquantitative RT-PCR analysis revealed that *Dot1* gene was down-regulated and the expression could be silenced (~ 70 % after 24 h), and the silencing effect persisted for several days (Fig. 4.1 a and b). The expression of mono-methylated H3K79 was also concomitantly down-regulated with *Dot1* gene silencing (Fig. 4.1c). Thus, the change of methylated H3K79 expression was consistent with the change of *Dot1* expression. These results therefore confirmed previous studies in which H3K79 could be methylated by Dot1 and the functions of H3K79 methylation could be investigated by silencing *Dot1* gene.

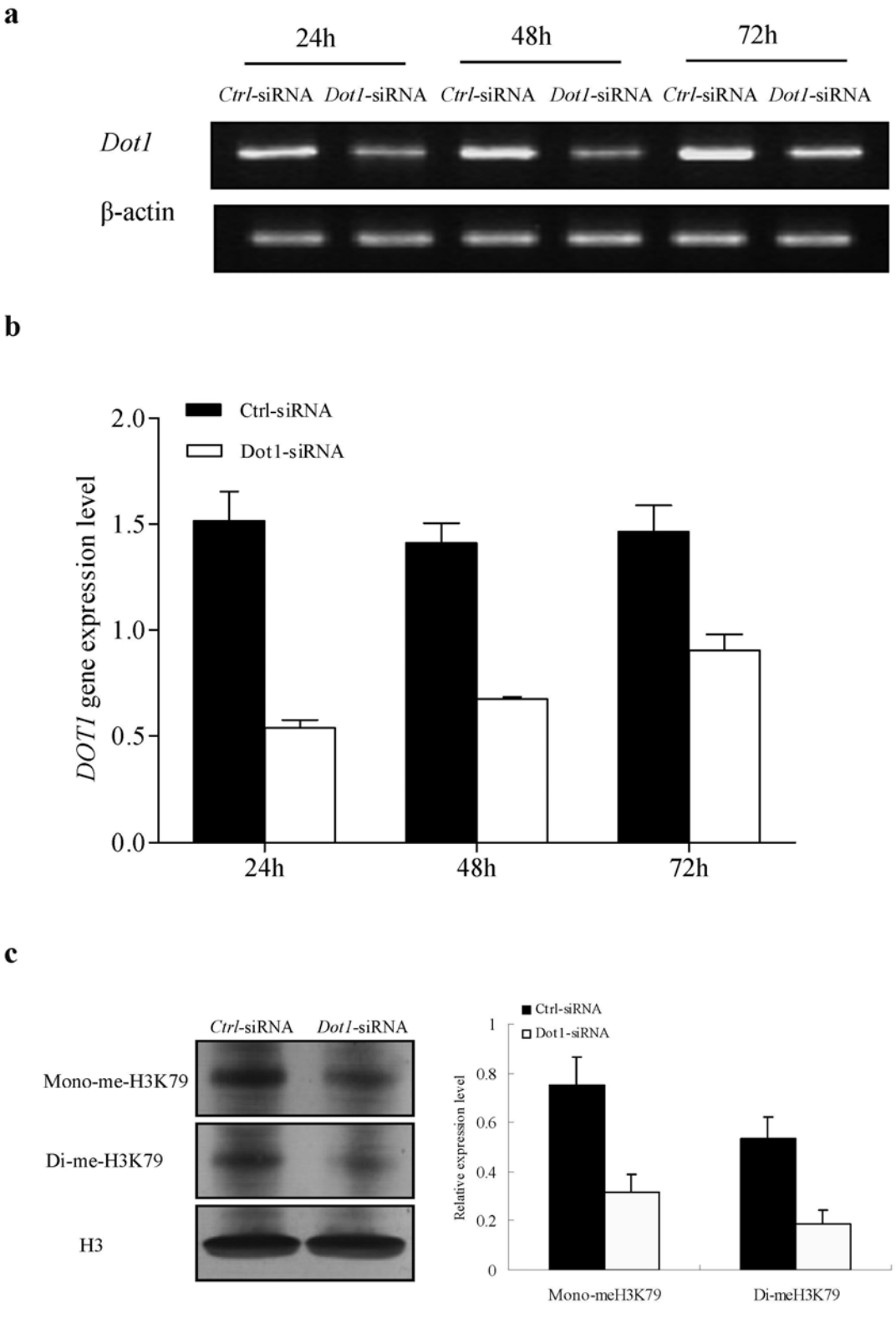

Fig 4.1.Transfection of *Ctrl*- and *Dot1*-siRNA into N2a cells. (a) RT-PCR analysis detected the expression of *Dot1* at 24 h, 48 h and 72 h; (b) The ratio of *Dot1*/β-actin expression derived from densitometric scanning of the images from three experiments; (c) The expression of mono-and di-methylated H3K79 after 48 h transfection. Three replicates were examined.

4.3.2 The effects of *Dot1*-silencing on N2a cell growth

MTT assay was performed to study whether *Dot1* silencing affected cell proliferation. Cells at 0 h, 24 h, 48 h, and 72 h after transfection were assayed, and the growth curve was showed in Fig.4.2a. Though the absorbance at 570 nm of Dot1 silencing group was higher than that of control group, no significant difference could be observed. In addition, the expression of proliferating cell nuclear antigen (PCNA), a cell proliferation indicator, was measured using Western blot after 48 h transfection. The expression of PCNA remained unchanged (Fig 4.2b). Taken together, the results clearly illustrated that the silencing of *Dot1* gene did not alter the growth of N2a cells.

a

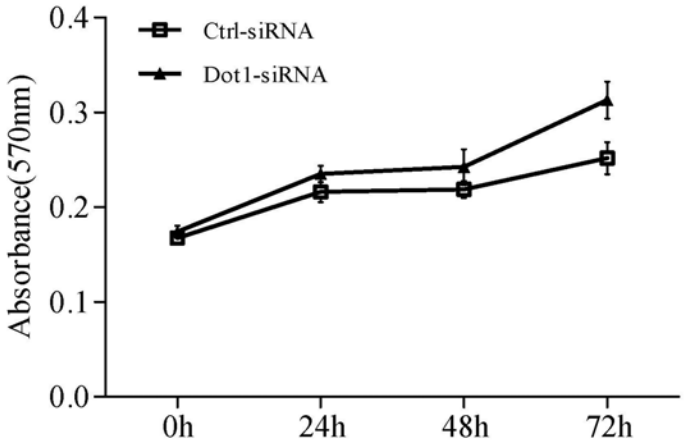

b

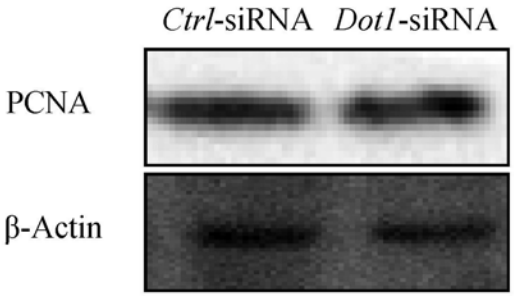

Fig 4.2 The effect of *Dot1* silencing on N2a cell growth. (a) MTT assay. 1,500 cells were seeded in 96-well plate and treated with *Dot1*-siRNA and *Ctrl*-siRNA. At 0 h, 24 h, 48 h and 72 h, viable cells were exposed to MTT, and the absorbance of each sample at 570 nm was read by SPECTRAmax 250 microplate spectrophotometer (n=6). (b) The expression of PCNA after 48 h transfection. 30 μg of extracted total protein from N2a cells was loaded on 12 % SDS-PAGE gel and probed with anti-PCNA antibody (1:1000). Three replicates were examined.

4.3.3 The morphological changes of N2a cells upon *Dot1* silencing

After transfection, significant morphological difference between the *Dot1*-siRNA-treated and *Ctrl*-siRNA-treated cells was observed under the phase contrast microscope (Fig.4.3). N2a cells are neuroblast cells with typical morphology of neuronal and amoeboid stem cells. After *Dot1*-siRNA treatments, the cells changed from the normal pyramid like or irregular shape to a more spherical shape (Fig.4.3e). In the HE staining sections (after 48 h treatment) (Fig.4.3 c and f), the number of cells extending neurodendrite in *Dot1*-siRNA group was less than that observed in *Ctrl*-siRNA group and the cells in *Dot1*-siRNA group had a much shorter neurite than that in *Ctrl*-siRNA group.

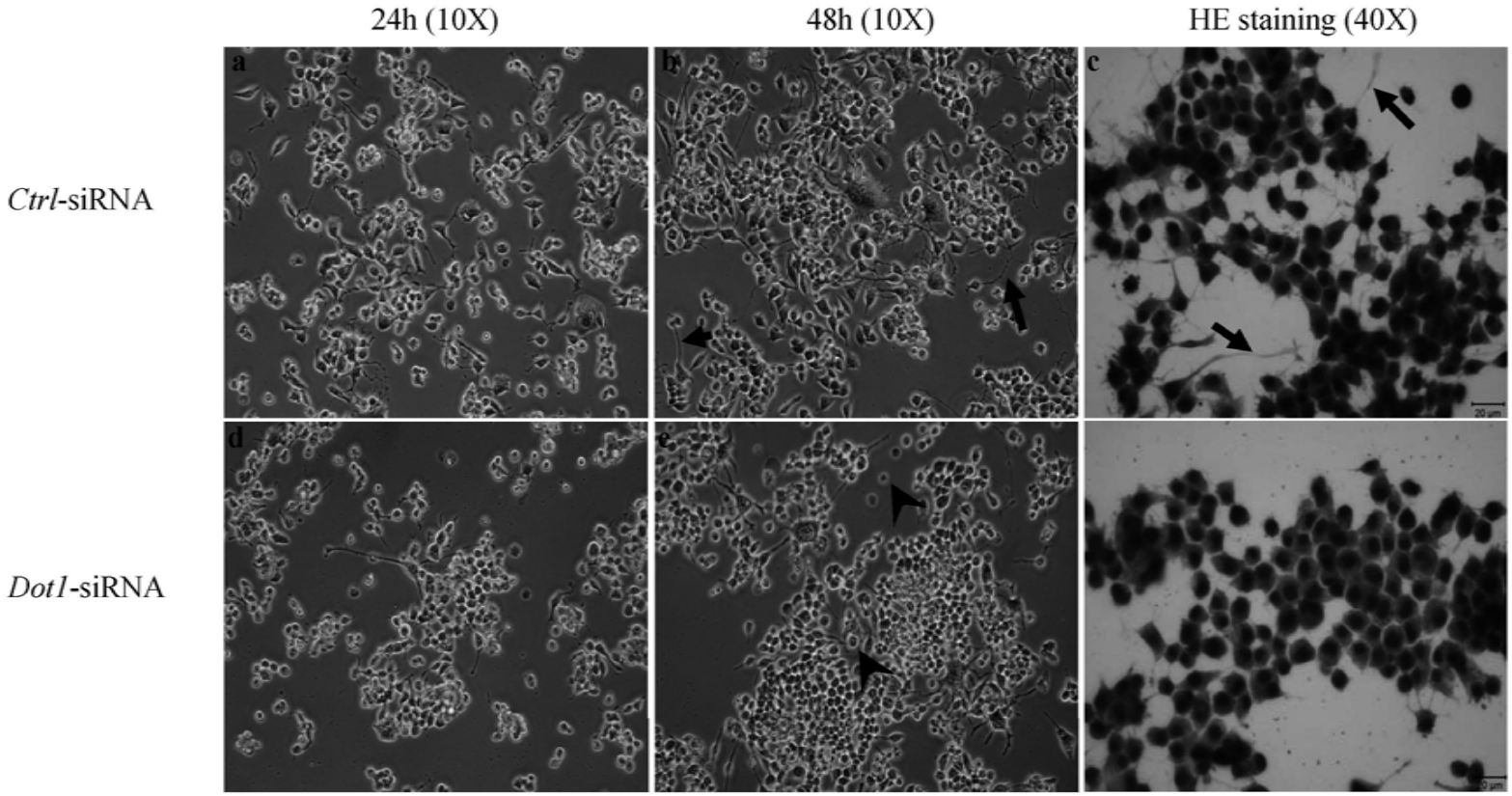

Fig 4.3 Cell morphology changes after *Dot1*-siRNA transfection. After *Dot1*-siRNA transfection (24 h and 48 h), cell morphology was detected under phase contact microscope (10X; a, b, d and e) .The neurite and dendrite of N2a cells (at 48 h) were observed by HE staining （40X; c and d）. After *Dot1* silencing the cells became deattached to the flask. Some cells changed their normal pyramid shape or irregular shape to the spherical shape (e; arrowhead). HE staining pictures showed that *Ctrl*-siRNA treated cells had abundant and long neurite (c; arrow), while *Dot1*-siRNA treated cells had much shorter neurite and less dendrite (f). Bar= 20 μm

4.3.4 *Dot1* silencing could neither induce cell cycle arrest nor cell death

The effects of Dot1 on N2a cell cycle was analyzed using flow cytometry (Fig.4.4). After being transfected for 24 h, 48 h and 72 h, N2a cells were harvested, stained with propidium iodide (PI), and the distribution of cells in each phase of cell cycle was evaluated. No significant difference on cell population distribution between different treatment time points was observed which indicated that *Dot1* down-regulation has no effects on cell cycle progression. For the detection of apoptosis, N2a cells were harvested and stained with Annexin V-FITC/propidium iodide (Fig.4.5). However, there was no difference on the number of viable cells between *Ctrl*-siRNA group (97.323 ± 0.065) and *Dot1*-siRNA group (97.770 ± 1.067). Few early stage apoptotic cells (the lower right quadrant) or late stage apoptotic cell and death cells (the upper right quadrants) could be detected. Altogether, *Dot1* silencing did not affect cell death or cell viability of N2a cells.

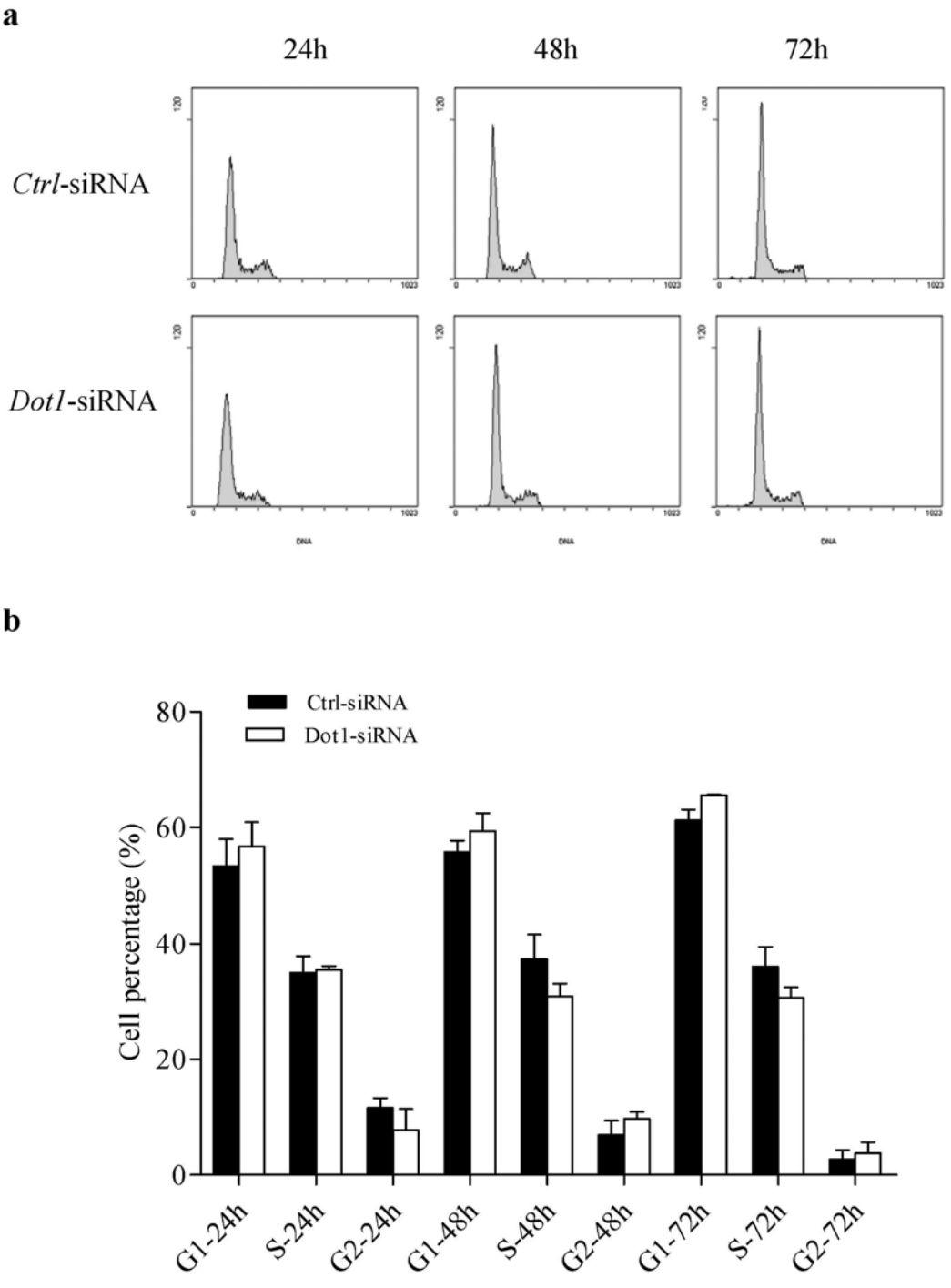

Fig 4.4 Flow cytometric analysis of N2a cell cycle after *Dot1* silencing. After continuously exposed to *Dot1*-siRNA for 24 h, 48 h and 72 h, N2a cells were stained for DNA content with propidium iodide, and then detected by flow cytometry. **a.** Representative flow cytometry histograms of each group. **b**. Effect of *Dot1* silencing on cell cycle distribution (n=3).

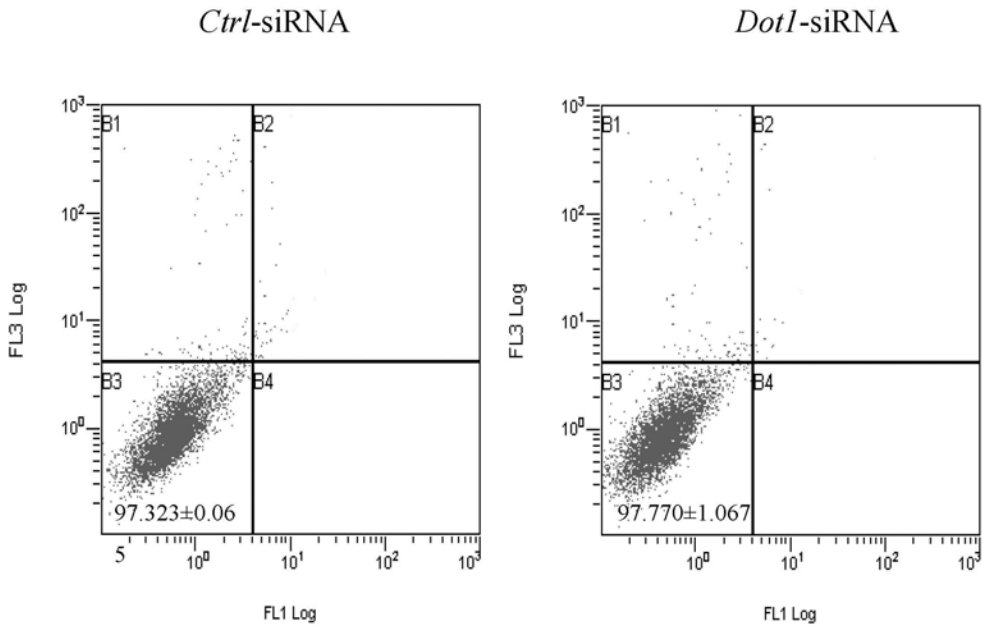

Fig 4.5 Apoptosis detection of N2a cells after *Dot1* silencing by flow cytometry. N2a cells were incubated in DMED supplemented with 10% FBS with *Ctrl*-siRNA (left) and *Dot1*-siRNA (right). After 48 h transfection, the cells were harvested, stained with Annexin V-FITC and propidium iodide, and analyzed by flow cytometry. The lower right quadrants represent the cells in the early stage of apoptosis; the upper right quadrants contain the cells in the late stage of apoptosis or necrosis; the lower left quadrants represent the viable cells. n=3.

4.3.5 Proteomic change of *Dot1* silenced N2a cells

Next, comparative proteomic approach was used to search for potential functions of Dot1 in N2a cells. 2-D electrophoresis was employed to establish the protein profiles of N2a cells transfected with *Ctrl*- and *Dot1*-siRNAs. The protein spots corresponded to up- or down-regulated by more than 1.5 folds in three independent gel analysis were chosen and identified by MALDI-TOF/TOF tandem mass spectrometry. Silver-stained gels were shown in Fig 4.6. MALDI-TOF/TOF tandem mass spectrometry analysis successfully identified eight different expressed proteins. Following *Dot1* knockdown, stress-induced-phosphoprotein 1 (Hop), RAD23b homolog and peroxiredoxin 1 were up-regulated whereas far upstream element-binding protein 1 (FBP-1), nucleosome assembly protein 1-like 1 (NAP1L1) isoform 2, eukaryotic translation initiation factor (eIF) 3, nascent polypeptide-associated complex (NAC) alpha subunit and prohibitin were down-regulated (Table 4.1). MS and MS/MS spectra of RAD 23b protein were demonstrated as the example of the protein identification (Fig 4.7). The functions of these identified proteins were summarized in Table 4.2. Western blotting also showed the up-regulated RAD 23b and the down-regulated prohibitin after Dot1 silencing, which was consistent with 2D results. In addition, down-regulation of p53, transcriptional activity of which could be induced by prohibitin, was detected in *Dot1* silencing N2a cells (Fig. 4.8).

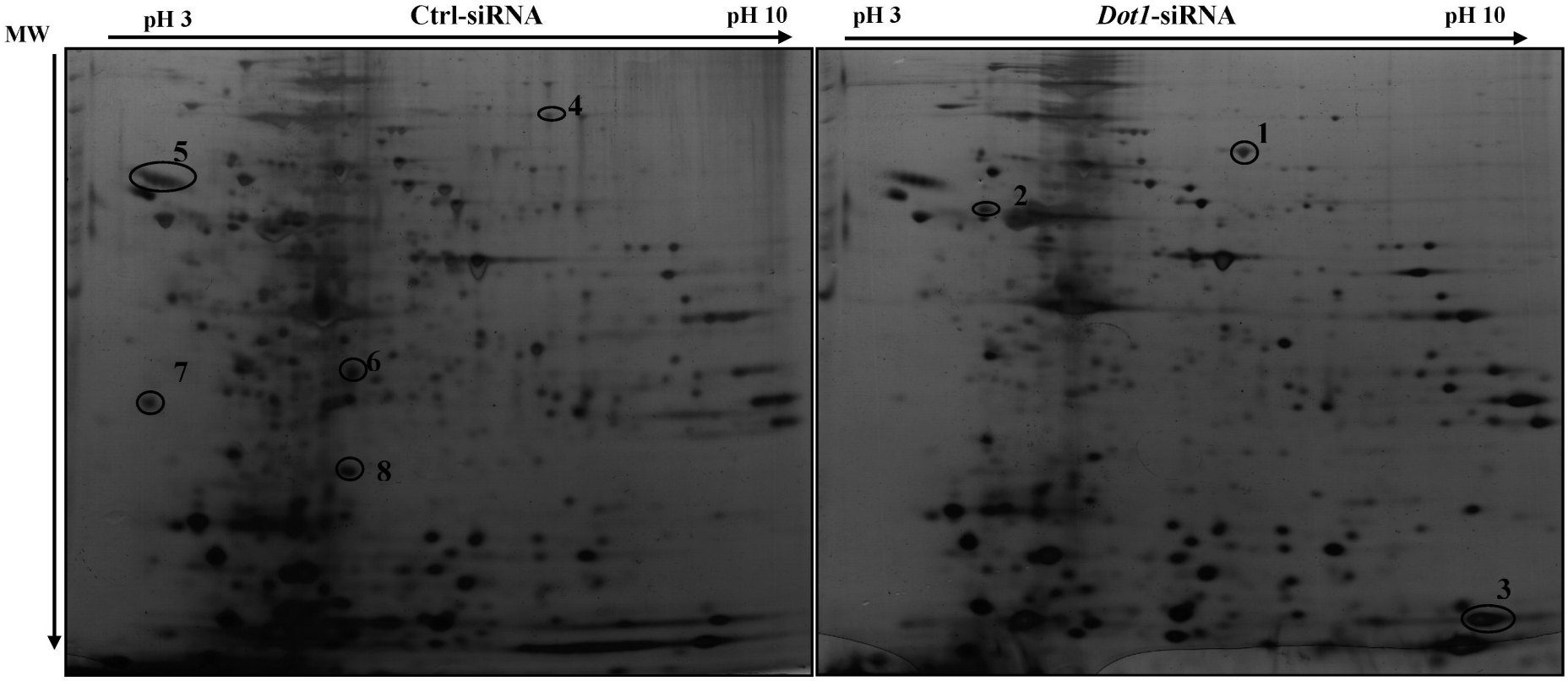

Fig 4.6 Representative 2-DE gel of protein extracts from N2a cells that had been transfected with *ctrl*- or *Dot1*-siRNA. 120 μg proteins which respectively extracted from *Ctrl*-siRNA treated (left) and *Dot1*-siRNA treated (right) N2a cells were used for IEF (total Vhs was 57730) with 13 cm strips (pH 3-10). 2D gels were stained by silver. Different expressed proteins (>1.5 fold) were labeled in gels. Fold decrease/increase was estimated from three replicates. Spots1-3 were up-regulated proteins, spots 4-8 were down-regulated proteins after *Dot1*-siRNA transfection, pI 3–10 (x-axis) and MW in kDa (y-axis).

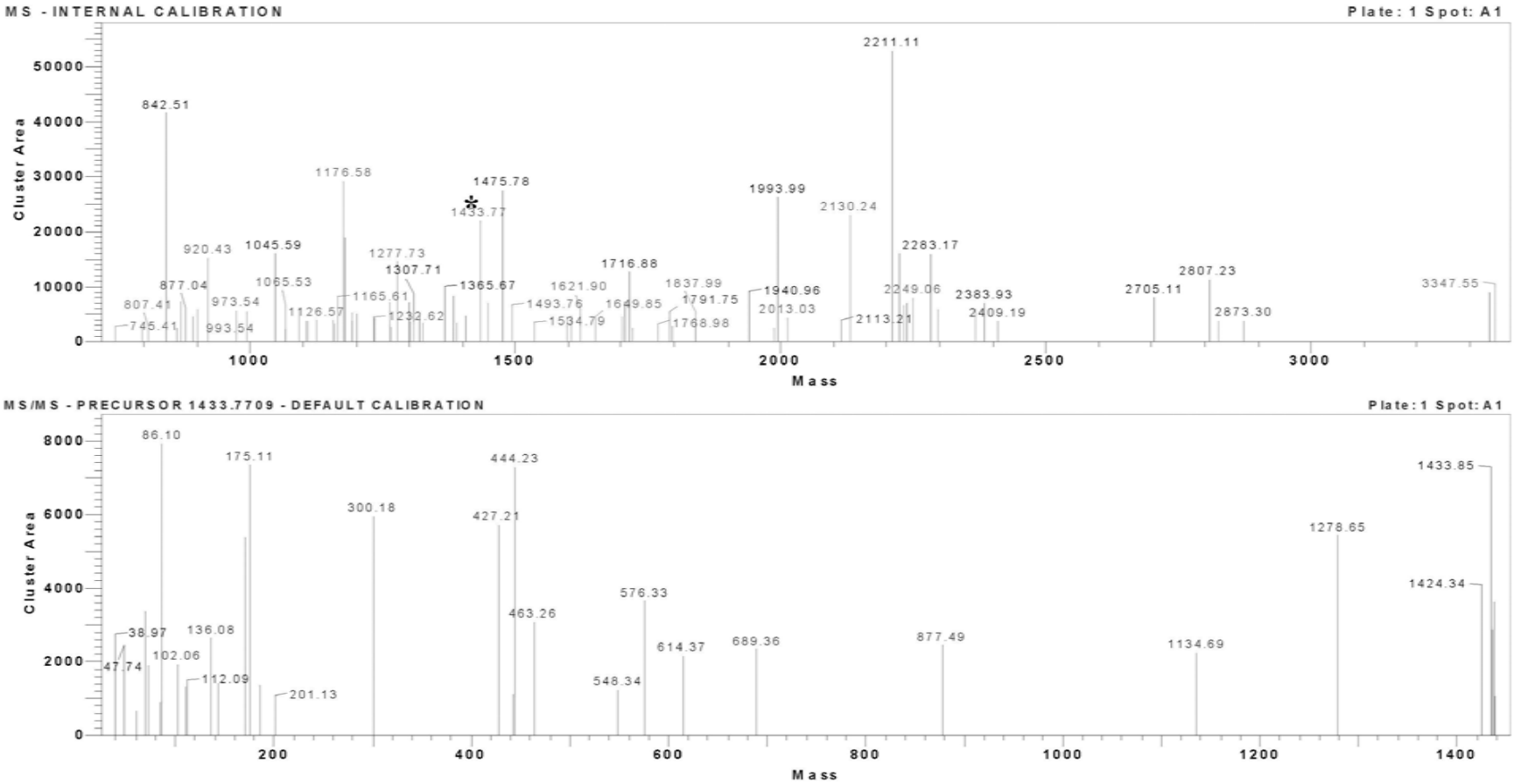

Fig 4.7 MS and MS/MS spectra and mass list of UV excision repair protein RAD23 homolog B (spot 2). The up panel was the MS spectrum of the spot; 9 match peaks of the sample were labelled using red colour. The low panel was the MS/MS spectrum of the mass precursor 1433.7709 (* in up panel) which induced the sequence of AVEYLLMGIPGDR.

Table 4.1 Identification of differentially expressed proteins in *Dot1*-siRNA transfected N2a Cells (cont.)

Spot	Protein name	Mean fold (up/down)[a)]	Acc. No.	Mass Da / pI	No. of matched peptides	Peptide coverage (%)	Protein score	Best ion score	Peptide sequence with the best ion score
1	Stress-induced-phosphoprotein1	1.90±0.51(Up)	gi|14389431	62542.4 /6.4	31	57	531	84	^{33}LDPQNHVLYSNR^{44}
2	RAD23b homolog	1.76±0.07(Up)	gi|6679607	43489.8 /4.77	9	25	187	68	^{221}AVEYLLMGIPGDR^{233}
3	Peroxiredoxin 1	2.29±0.30(Up)	gi|6754976	22162.3/ 8.26	17	75	406	75	^{129}GLFIIDDKGILR^{140}
4	Far upstream element-binding protein 1	5.75±0.13(Down)	gi|37078458	68497/ 7.74	12	21	321	49	^{260}CQHAAEIITDLLR^{280}
5	Nucleosome assembly protein 1-like 1 isoform 2	1.54±0.07(Down)	gi|7657357	45316.9 /4.36	4	11	76	51	^{95}FYEEVHDLER^{104}
6	Eukaryotic translation initiation factor3,subunit 1	3.80±0.14(Down)	gi|9055370	36437.6 /5.38	14	55	413	90	^{283}GHFGPINSVAFHPDGK^{298}

a) vol % of each spot was measured to calculate fold difference of spot in each group. The result was estimated from three replicates

Table 4.1 Identities of differentially expressed proteins in *Dot1*-siRNA transfected N2a Cells

Spot	Protein name	Mean fold (up/down)[a)]	Acc. no.	Mass Da / pI,	No. of matched peptides	Peptide coverage (%)	Protein score	Best ion score	Peptide sequence with the best ion score
7	Nascent polypeptide-associated complex alpha subunit	5.73±0.61(Down)	gi|41350312	23369.7/ 4.52	4	22	294	102	^{101}NILFVITKPDVYK^{113}
8	Prohibitin	1.55±0.03 (Down)	gi|6679299	29801.9/ 5.57	12	55	593	121	^{240}KLEAAEDIAYQLSR^{253}

a) vol % of each spot was measured to calculate fold difference of spot in each group. The result was estimated from three replicates

Table 4.2 The functions of identified proteins in 2D gel (Information from UniProtKB/Swiss-Prot)

Spot	Protein name	Functions
1	Stress-induced-phosphoprotein1	Mediates the association of the molecular chaperones HSC70 and HSP90
2	RAD23b homolog	Involve in Proteosomal degradation of misfolded proteins and DNA repair
3	Peroxiredoxin 1	Eliminating peroxides generation; Participates in the signaling cascades of growth factors and tumor necrosis factor-alpha by regulating the intracellular concentrations of H_2O_2
4	Far upstream element-binding protein 1	Acts both as activator and repressor of transcription; Regulate myc expression
5	Nucleosome assembly protein 1-like 1 isoform 2	Acts as a chaperone for histone; Required for chromatin remodeling; Plays a role in gene regulation
6	Eukaryotic translation initiation factor3,subunit 1	Component of the eukaryotic translation initiation factor 3 (eIF-3) complex and involve in the initiation of protein synthesis
7	Nascent polypeptide-associated complex alpha subunit	Prevents inappropriate targeting of non-secretory polypeptides to ER; Play roles in transcription
8	Prohibitin	Inhibits DNA synthesis. It has a role in regulating proliferation; May play a role in regulating mitochondrial respiration activity, maintenance of mitochondrial integrity and aging.

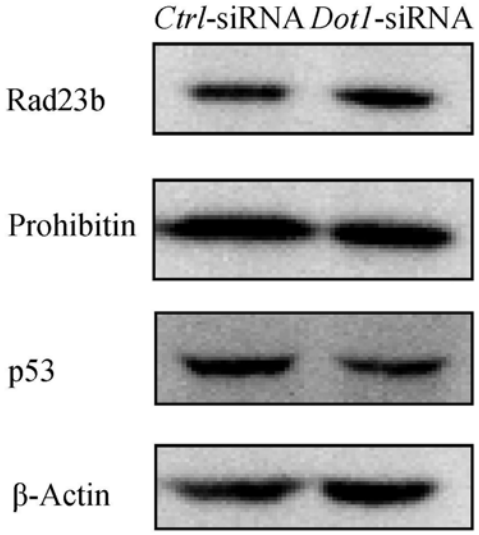

Fig 4.8 The expression of Rad23b, prohibitin and p53. The expression of Rad23b and prohibitin were detected by western blot to confirm the comparative proteomic results. At the same time, the expression of p53 was also detected after *Dot1* silencing. β-actin serves as internal control. 30 μg of extracted total protein was loaded on 12 % SDS-PAGE gel and probed with anti-Rad23b, anti-prohibitin, anti-p53 and anti-β-actin antibodies (1:1000). The signal was detected by LumiGLO®* chemiluminescent detection kit. The members were scanned and analyzed by Bio-Rad Quantity One 4.4.0 software (Bio-Rad, USA). Three replicates were examined.

4.4 Discussion

In the past, yeast was usually used to investigate the functions of Dot1 and H3K79 methylation. However, the biological functions of Dot1 or H3K79 methylation in mammalian cells are still largely unknown. Thus, I established *Dot1* silencing N2a cells line via transfection with *Dot1*-siRNA, and investigated in details the roles of Dot1 in N2a cells using the proteomic approaches.

Our results clearly illustrated that *Dot1* silencing procedures affected neither N2a cell growth nor cell viability with no detectable cell phase arrest or cell death (Fig. 4.2; Fig.4.4; Fig.4.5). However, *Dot1* gene silencing caused a loss of normal neuronal shape (changed from pyramid shape or irregular shape to the spherical shape) of N2a cells plus shorter extending dendrites of the cells and reduced connection between cells were observed (Fig.4.3). It is well known that nerve cells are connected to thousands of other nerve cells through axon or dendrites and organized as a network in the brain. Significant age related loss of dendrites in the cerebral cortex had been first reported by Scheibel and coworkers (Scheibel *et al.*, 1975). These age-related dendritic losses included both shortening and fewer dendritic branches (Dickstein *et al.*, 2007). Dendrites are important neuronal structures for synaptic contacts for signal transduction. Other groups had demonstrated that the massive nerve cell death and synaptic loss could be observed in the brain of late stage Alzheimer's disease (AD) patients (Samuel *et al.*, 1994). Although the detailed underlying mechanism remains to be determined, it showed

that synaptic plasticity was one of the biologically relevant modules conserved between AD and aging (Miller *et al.*, 2008b). Results from our previous study illustrated the decrease of H3K79 methylation in the brain of SAMP8 mouse (Fig.3.2). In fact, the SAMP8 mice model showed significant age-related impairments in learning and memory which were similar to the symptoms of the early stage of AD. In this study, the morphological changes of N2a cells after *Dot1* silencing such as a decrease of the connection between cells suggested that *Dot1* gene might play an important role in the neuronal processes of axon and dendrites which induced the communication between the near-by neuron cells through synapses. Previous studies indicated that histone modifications regulated plasticity and memory formation in the adult rat hippocampus (Miller *et al.*, 2008a). For example, H3K4-specific methyltransferase, MLL1 (mixed lineage leukemia 1), was essential for hippocampus' synaptic plasticity which might be involved in cortical dysfunction of some schizophrenia cases (Akbarian and Huang, 2009). Taken together, histone modifications may provide a new research clue for a better understanding of the pathogenicity of aging and neurodegenerative disease, especially on the dendrite processes and the plasticity of synapses.

In this study using the proteomic approaches, the expression of three proteins (far upstream element-binding protein 1 (FBP-1), prohibitin and nucleosome assembly protein 1-like 1 (NAP1L1) involved in the gene transcription were decreased after *Dot1* silencing (Fig.4.6 and Table 4.1). Previous studies reported that Dot1 or H3K79 methylation was involved in gene activation. Moreover, H3K79

hypermethylation accompanied with hyperacetylated H3 and H4 and hypermethylated at H3K4 were detected at active genes (Schübeler *et al.*, 2004). At heterochromatic mating-type, ribosomal DNA and telomeric loci, H3K79 methylation was markedly depleted (Ng *et al.*, 2003; Pokholok *et al.*, 2005). In our study, the proteins which were identified suggested that Dot1 and H3K79 methylation are probably important in specific gene activation pathway.

FBP-1 binds to an upstream element of the c-myc promoter and regulates the c-myc mRNA level which encodes an important member of transcription factors. Human fibroblasts or endothelial cells with the reduction of c-myc expression switched with an increased frequency to a senescent state by a telomere-independent mechanism involving the polycomb group repressor Bmi-1 and the cyclin-dependent kinase inhibitor p16INK4a. The same regulatory circuit was triggered upon exposure to mild oxidative stress (Guney *et al.*, 2006; Guney and Sedivy, 2006). Myc, one of the c-myc products, was a transcription factor that binds a multiple of genomic sites. Myc binding promoted acetylation of multiple lysines, and dimethylation of H3K79 was also selectively induced at target promoters (Martinato *et al.*, 2008). From our results, *Dot1* silencing decreased H3K79 methylation and induced a down-regulation of FBP-1 (Fig.4.6; Table 4.1) suggesting that Dot1 or H3K79 methylation could be involved in c-myc regulated transcription and then lead to organismal aging.

In addition, prohibitin and p53 were simultaneously down-regulated after *Dot1* silencing (Fig.4.6; Fig.4.8; Table 4.1). Prohibitin was localized in the nucleus and modulated transcriptional activity by interacting with various transcription factors or

inhibiting DNA synthesis (Mishra *et al.*, 2006). In addition, prohibitin could induce p53-mediated transcription by enhancing its recruitment to various promoters. Previous studies reported that protein arginine methyltransferases CARM1 and PRMT1 acted as co-activators of p53 mediated transcription, via a direct interaction with p53 and its associated co-activator partner p300 (An *et al.*, 2004). Methylation of histones H3 and H4 were catalyzed by arginine methyltransferases and facilitated p53-mediated transcription (Scoumanne and Chen, 2008). Dot1 shared a similar catalytic core region to class I arginine methyltansferases (Cheng *et al.*, 2005), which suggested that Dot1 might also have the important functions on controlling p53-mediated transcription. p53 could regulate the expression of multiple antioxidant genes and protected the genome from oxidation by reactive oxygen species (ROS), a major cause of DNA damage and genetic instability. Down-regulation of p53 resulted in excessive oxidation of DNA, increased mutation rate and karyotype instability (Sablina *et al.*, 2005). The results from previous researches and this study indicated that Dot1 might involve in the signaling networks and coordinately manage the levels of ROS within N2a cell by regulating the expression of p53.

Besides the down regulation of gene promoter binding proteins, NAP1L1, one of chromatin interaction protein (NAP) family proteins, was also down-regulated after *Dot1* silencing (Fig. 4.6; Table 4.1). NAP1L1 was a histone-binding factor required for the maintenance of cumulative nucleosome formation *in vivo* and involved in regulating mitosis in yeast (Ohkuni *et al.*, 2003; Mortensen *et al.*, 2002). Study also proposed it was a genetic marker for small intestinal carcinoid malignancy

(Kidd *et al.*, 2006). Though it was high expressed in cerebral cortex (Kato, 1990), there have been no reports demonstrating its roles in neuronal cell so far. Nucleosome assembly protein 1-like 2 (NAP1L2), another NAP family protein, was associated with chromatin and interacted with histones H3 and H4 to regulate neuronal cells proliferation. The deletion of neuronal NAP1L2 gene in mice caused neural tube defects (Rogner *et al.*, 2000). Other study also indicated that loss of NAP1L2 could result in a decreased histone acetylation activity (H3K9/14), leading to transcriptional changes in differentiating neurons or affected neurogenesis and neuronal survival (Attia *et al.*, 2007). Whereas, whether NAP1L1 shares the similar function in neuronal cell or not needs further investigation.

From above, it was concluded that Dot1 played an obligatory role in gene expression either by changing the chromatin state or by controlling the expression of gene promoter binding protein. Furthermore, I also discovered the roles of Dot1 in N2a were not just restricted to gene regulation from the comparative proteomic data. Two proteins eukaryotic translation initiation factor (eIFs) 3, subunit 1 and nascent polypeptide-associated complex (NAC) protein were down-regulated after *Dot1* gene silencing (Fig. 4.6; Table 4.1). It was reported that eIFs could bound directly to 40S ribosomal subunit and stimulate the assembly of the translation initiation complex (Asano *et al.*, 2000; Mayeur et al., 2003), whereas NAC protein prevented mis-targeting of nascent polypeptide chains to the endoplasmic reticulum membranes. The decrease of alpha-NAC resulted in mis-targeting, mistranslation, and proteolysis of proteins, which was important in the pathology of neurodegenerative diseases

(Kim *et al.*, 2002). The formation of toxic protein aggregates was a common denominator of various neurodegenerative diseases and aging, and aggregated protein could lead to oxidative stress and finally cause cell death (Mattson and Magnus, 2006). Therefore, it was proposed that *Dot1* silencing might contribute to the brain senescence via mis-targeting, mistranslation and proteolysis of the nascent polypeptides.

In addition, the expression of several stress related proteins such as the stress response protein, stress induced phosphoprotein 1, and antioxidant enzymes of peroxiredoxin 1 were down-regulated after *Dot1* silencing of N2a cells. Whereas, RAD23 homolog B, one of nucleotide excision repair (NER) proteins, was up-regulated. Stress induced phosphoprotein 1, also called Hsp70/Hsp90-organizing protein, was a co-chaperone for Hsp70 and Hsp90 which is implicated in the negative regulation of apoptosis and in folding protein substrates by binding to heat shock protein (Bredemeyer *et al.*, 2006). Peroxiredoxin proteins were an important antioxidant enzyme in human brain defenses and peroxiredoxin 1 had negative role in ASK1-induced apoptosis. In Prx-1 knockdown cells, ASK1, p38, and JNK were quickly activated and leaded to apoptosis in response to H_2O_2 (Kim *et al.*, 2008b). Previously studies demonstrated that histone H3K79 methylation had different displays under different stress conditions. For example, shear stress (SS) treatment induced H3K79 methylation and influenced cell differentiation of mouse embryonic stem (ES) cells (Illi *et al.*, 2005), but di-methylation of H3K79 decreased after ER stress induction (Donati *et al.*, 2006). In this study, the change of stress related

proteins in N2a cells after *Dot1* silencing suggested its role on neuron cells' stress responses.

Altogether, I established *Dot1* silencing N2a cell line and investigated the effects of *Dot1* silencing on cell morphology, cell growth, cell cycle arrest in this chapter. At the same time, proteomic maps were also generated from *Dot1* silencing N2a cells. The identified differentially regulated proteins demonstrated the multiple functions of Dot1 in neuron cells. Dot1 could involve in axon and dendrite outgrowth, gene transcriptional regulation, protein translation and folding, even in the stress response of N2a cells. These results highlighted the complexity of the interconnected molecular networks between Dot1 and other molecules and suggested the possibility of Dot1 on the contribution to brain dysfunction in the neurodegenerative disease or aging. However, the detail mechanisms and how H3K79 methylation acts as the functional executant of Dot1 involving in its multiple functions need further studies.

Chapter 5 General discussion and prospects

Aging is characterized by the progressive functional decline of multiple organs and tissues, eventually culminating in death and such process is accompanied by an impairment of the physiological systems. Therefore aging became the major risk factor for age-related diseases, such as arthritis, osteoporosis, heart disease, cancer and AD. Nowadays, many countries including China are experiencing aging populations. The aging problem has already become a global headache.

Many previous researches have been performed trying to elucidate aging process and many mechanisms of aging have been proposed, such as free radical theory, mitochondrial theory, genetic control theory, and so on. However, most theories are incomplete，and they are often challenged by the opposite results or new discoveries. Many researches have been performed in an attempt to elucidate mechanisms of brain aging and the neurodegenerative disease from various aspects. For example, the investigations on mitochondrial dysfunction and oxidative stress, the morphological and biochemical features of apoptosis in aged neurodegenerative brain, transcriptional profiling defined a set of genes with reduced or increased expression in aged brain. Comparative proteome analysis was also used to identify aging-related brain proteins in brains from mouse model or AD patient. These investigations could provide the clues to elucidate the pathology of brain aging and neurodegenerative diseases. However, the mechanisms of aging and neurodegenerative diseases still remain unknown.

Except for biological function declination and gene expression alternation in aging human brain (Blennow et al., 2006; Doudet, 2007), increasing findings demonstrated the importance of epigenetic regulation in brain physiology and pathology (Shi, 2007). Scattered experimental evidences have suggested that epigenetic changes could be critical determinants for cellular senescence and organismal aging (Bandyopadhyay and Medrano, 2003). The researches on the role of epigenetics in the aging process have grown tremendously in recent years and epigenetics changes were proposed as the targets and marks of aging (Fraga and Esteller, 2007). However, many researches focused on DNA methylation state during aging, no systematic investigations have described the patterns of histone PTMs in the aged brain, and the underlying mechanisms of histone PTMs involved in aging are still unknown. In this study, I initiated the first analysis on the histone PTMs states, in particular methylation, in the brain of aged SAMP8 mice.

In aged human brain, the genes involved in synaptic transmission, Ca^{2+} homeostasis/signaling and neuronal survival were down-regulated and the genes involved in stress response and inflammation were up-regulated (Bonneuil, 2007; Lu *et al.*, 2004). The decreased potential of DNA repair was one of the major factors contributing to the aging and the degeneracy of brain (Katyal and McKinnon, 2007; Vyjayanti and Rao, 2006). In chapter 2, seven methylated sites (H3K24, H3K27, H3K36, H3K79, H3R128, H4K20 and H2A R89) were detected in the brain of 12-month-old SAMP8 mice. At the same time, the acetylation sites, such as K14, K18 of histone H3, and one phosphorylated site, S38 on histone H2B, were also

found. Among the detected modifications, mono-methylated H4K20, di-methylated H3K79 were decreased during aging and a modulating relationship between the methylation of H3K27 and H3K36. Previous researches showed that methylated H3K36 and H3K79 were associated with increased gene transcription (Jin *et al.*, 2007), whereas the methylation of H3K27 and H4K20 were described as the sites for gene repression and/or heterochromatin (Klose and Zhang, 2007; Vakoc *et al.*, 2006). Furthermore, methylations of H3K79 and H4K20 were reported to link to the DNA-damage response (Bostelman *et al.*, 2007; Sanders *et al.*, 2004). Therefore, the result indicated that mono-methylated H4K20, di-methylated H3K79 and hypermethylated H3K27 might be the major modifications during brain aging and neurodegeneration. They could regulate the gene expression, maintain the proper higher order structure of DNA and contribute to DSB repair in aged brain.

The results from chapter 3 proposed a model of methylated H3K79 on transcriptional regulation, which indicated that the signal of H3K79 methylation could be recognized and read by pbx1 protein, at the same time, other transcription factor or regulator were also recruited. Pbx1 could participate in the normal regulation of Hox target gene transcription *in vivo* and therein contribute to aspects of anterior-posterior patterning and structural development in vertebrate (Lu *et al.*, 1995). Moreover, HOX-PBX complexes could involve in transcriptional repression or activation through differential association with coactivators and corepressors (Struhl, 1998). Therefore, methylated H3K79 could

involve in diversity biological process via its interacting protein- pbx1.

siRNA silencing experiment in chapter 4 showed that Dot1/H3K79 methylation could involve in axon and dendrite outgrowth, gene transcriptional regulation, protein translation and folding, even in the stress response of N2a cells, which indicated the complexity of the interconnected molecular networks between Dot1/H3K79 methylation and other molecules. The change of cell morphology and proteomic pattern in N2a cell after *Dot1* silencing suggested the contribution of decreased H3K79 methylation to brain dysfunction in the neurodegenerative disease or aging.

All these results could help us to better understand the machinery of histone PTMs during aging progression and the pathogenesis of brain aging and neurodegenerative disease, especially H3K79 methylation. Moreover, they could not only help us to establish a platform for the exchange of comprehensive information related to aging and neurodegenerative disease but also provide an opportunity for the development of epigenetic therapeutic drugs to neurodegenerative diseases.

According to histone code theory (Jenuwein and Allis, 2001), the ability of one modification to antagonize or synergize the deposition of another modification have important biological consequences, and dynamic transitions among various modification states could regulate the spatial and temporal behavior of histone in general. In order to understand the physiological implications of the histone modifications in aged brain, other PTMs, such as acetylation, phosphorylation,

ubiquitination, carbonylation, the aberrant patterns of different combinations of histone modifications combination should be investigated by MS in the future. ChIP-on-chip technique will be applied to identify the genomic sequences undergoing these PTMs events in aged brain. Furthermore, basing on the results from this study, the molecular mechanisms of how Dot1 and H3K79 methylation involve in the aging process, and how H3K79 methylation acts as the functional executants of Dot1 will be investigated by the establishment of mutation model. Moreover, decreased mono-methylated H4K20 and the modulating event between H3K27 and H3K36 in aged brain also need in-depth study.

In this project, MALDI TOF/TOF tandem mass spectrometry was used to identify the specific PTMs in the aged SAMP8 mice brain. MS analysis allow high sensitivity in determining both the exact sites and types of PTMs along the polypeptide and yield comprehensive sub-sequence information (Burlingame *et al.*, 2005; Cocklin and Wang, 2003; Huang *et al.*, 2002; Johnson *et al.*, 2004). Increasing PTMs sites and PTM types are being confirmed by utilizing this technology. Nevertheless, MALDI TOF/TOF tandem mass spectrometry has its limitation. Matrix used could affect the detection of the peptides which mass were below 700. This might be the reason why some modification sites could not be found, such as H3K4 and H3K9. At the same time, some modifications which have similar mass value, such as tri-methylation and acetylation, could not be distinguished due to mass accuracy limitation of MALDI TOF/TOF tandem mass spectrometry. Therefore, Fourier transform mass spectrometry (FTMS) combined

with different enzyme digestion could be used as a supplemental approach for giving us more information on the PTMs patterns in aging brain.

Nowadays, accurate quantification of protein expression in biological systems is an increasingly important issue in proteomics research. MALDI TOF/TOF tandem mass spectrometry analysis can yield qualitative data but cannot account for quantitative measurement on histone PTMs. Though equal amount of samples were loaded, many factors could influence the peptides intensity, such as matrix quality or concentration, laser intensity, sample spot position effect. Incorporation of differential stable isotopes (deuterium, carbon-13, nitrogen-15, and oxygen-18) in samples for relative protein quantification has been widely used, such as isotope coded affinity tag (ICAT) and multiplexed isobaric tagging technology (iTRAQ) (Gevaert *et al.*, 2008; Vermeulen *et al.*, 2008). ICAT labeling is specific to cysteine residues, and non-cysteine containing peptides are not applicable. iTRAQ labeling tags N-termini and lysines of all peptides which makes the spectrum complexity and difficult to identify the modified peptides. However, the incorporation process may probably affect the existing modification or increase the risk of uncontrollable variations in the samples. Beside the incorporation of differential stable isotopes, using an internal standard peptide to quantify the modified histone peptides was also attempted in my study. However, it is difficult to find a suitable standard peptide which should have a similar mass to the peptides being quantified and have a MALDI-TOF ion that was similar in intensity to that of the distinguishing peptides being quantified. Therefore the change of identified PTMs in the brain of different

aged SAMP8 and SAMR1 could not be provided by MS analysis alone. To delineate the changes of these modifications in the different aged brain, Western blotting analysis was used to detect the abundance of modified histone. For the modification sites which have no commercial antibodies available, such as H3R128 and H2A R89, peptide synthesis and rising antibody will carry out for confirmation and quantification. Furthermore, how to quantify PTMs peptide using MALDI TOF/TOF MS needs more exploration.

Some studies had shown that gender could affect the oxidation of brain proteins during aging (Kayali *et al*., 2007; Uzun *et al*., 2009). Female sex was associated with increased risk of the development of AD (Azad NA *et al*., 2007), while the overall gender differences in prevalence of cognitive dysfunction were minimal (Badgio and Worden, 2007). In this study, both male and female mice were selected. However, there are no significant differences of histone methylation patterns were observed between the male and female mice. Whether the same modifications have the different readout in different gender environment or not needs further investigation.

Senescence accelerated mouse model was selected in this study, at the same time, murine neuroblastoma cells (N2a) was employed to investigate the effect of H3K79 down-regulation by siRNA transformation. Mouse and human cells are endowed with a similar molecular apparatus that regulates differentiation and death. The cells are also similar in the molecular mechanisms by which they execute basic cellular processes. They even share organs and systemic physiology

and show a certain consistency in disease pathogenesis. Therefore, the prevalence of mouse models in the analysis of age-related diseases and the rate of aging in humans has its biological rationale. Whereas, mice and humans with a maximum life-span potential of 4 years and 120 years, respectively. They also show striking dissimilarities in disease pathogenesis, such as cancer incidence and susceptibility (Holliday, 1996; Rangarajan and Weinberg, 2003). Therefore, exploiting murine systems to elucidate human aging or the human disease process must take into account the vast differences between these two species. Most of researchers used laboratory inbred mouse, yeast, *C. elegans*, or cultured cell such as fibroblast cell for the experiment. However, these animal models not only have life histories quite dissimilar to those of humans. Moreover, almost all the experiments we performed were mainly focused on the aging process. Therefore, nature long-lived animals should also be adopted and do the comparison with result getting from the senescence accelerated models.

In this study, the whole brain homogenate was used to analyze histone PTM patterns in aged SAMP8 mice brain, which made it difficult to distinguish PTMs in specific cells types. The most important reason of using whole brain to extract histones was cell type's separation before the histone extraction might increase the artificial PTMs or induce the loss of some PTMs, which could make the false PTMs identification. Based on the histone PTMs information gotten from MALDI TOF/TOF MS investigation, immunohistochemistry was used to further detect the expression of these identified PTMs in the different cell types and different brain

parts in this study. The corresponding functions of the specific modification were further deciphered in special cell type. In this study, N2a cell line was selected to study the function of H3K79 methylation. Actually, non-neuronal cells, which are named glial cells, also have the important roles in the nervous system. They could provide the support and nutrition, maintain homeostasis, form myelin, and participate in signal transmission. In aged brain, microglia displayed a dystrophic phenotype, with shorter cellular processes and large gaps between adjacent cells, and more astrocyte reactivity (Wasserman *et al*., 2008). The internode lengths significantly decreased as a function of age (Lasiene *et al*., 2009).Therefore, the dysfunction of glial cells could result in impaired neuronal function in AD, as well as in many progressive neurodegenerative disorders (von Bernhardi, 2007). In future, the change of histone PTMs in glial cells during aging process should also be investigated.

Now, aberrant patterns of histone modifications in cancer have been characterized. They are becoming the crucial parameters in cancer diagnosis and prognosis. Novel strategies for epigenetic therapy to cancer are developing based on these results (Herranz and Esteller, 2007; Smith *et al*., 2007). Therefore, the studies on the aberrant patterns of histone modifications in aged brain will definitely contribute to diagnosis and prognosis of neurodegenerative diseases, even benefit for setting up the strategies for epigenetic therapy. However, there are still many questions needed to be answered. For example, do the epigenetic phenomena of aging apply in the same manner to all cell types in an organism? Are

there epigenetic drugs that by changing histone modification patterns accelerate or slow the aging process? Therefore, it seems there still has a long way to go.